ABSTRACT

Title of Document: TOWARDS AN INTEGRATED SYSTEM FOR VEGETATION FIRE MONITORING IN THE AMAZON BASIN

Wilfrid Schroeder, Doctor of Philosophy, 2008

Directed By: Professor Christopher O. Justice
Department of Geography

Biomass burning is a major environmental problem in Amazonia. Satellite fire detections represent the primary source of information for fire alert systems, decision makers, emissions modeling groups and the scientific community in general. Those various users create a growing demand for good quality fire data of higher spatial and temporal resolution that can only be achieved via integration of multiple satellite fire detection products. The main objective of this dissertation was to develop an integrated fire product capable of improved monitoring and characterization of fire activity in Brazilian Amazonia.

Two major active fire detection algorithms based on MODIS and GOES data were used to meet the users demand for fire information. Large differences involving the performance of the MODIS and GOES fire products required the quantification of omission and commission errors in order to allow for appropriate treatment of individual detections produced by each data set.

Relatively small omission errors due to cloud obscuration were estimated for Brazilian Amazonia. Regional climate conditions result in reduced cloud coverage in areas of high fire activity during the peak of the dry season, therefore minimizing the effects of cloud obscuration on fire detection omission errors.

Clear sky omission and commission errors were largely dependent on the vegetation and background conditions. Relatively large commission errors occurring in high percentage tree cover areas suggested that fire detection algorithms must either be regionalized or incorporate additional tests to provide more consistent fire information across a broader range of surface conditions.

Integration of MODIS and GOES fire products using a physical parameter describing fire energy (i.e., fire radiative power) was proven difficult due to limitations involving the interplay between sensor characteristics and the types of fires that occur in Amazonia. As part of this research, a new integrated product was generated based on binary fire detection information derived from MODIS and GOES data, incorporating adjustments to reduce commission and omission errors and optimizing the complementarities among individual detections.

These findings made a significant contribution to fire monitoring science in Amazonia and could play an important role in the development of future fire detection algorithms for tropical regions.

TOWARDS AN INTEGRATED SYSTEM FOR VEGETATION FIRE MONITORING IN THE AMAZON BASIN

By

Wilfrid Schroeder

Dissertation submitted to the Faculty of the Graduate School of the
University of Maryland, College Park, in partial fulfillment
of the requirements for the degree of
Doctor of Philosophy
2008

Advisory Committee:
Professor Christopher O. Justice, Chair
Dr. Ivan A. Csiszar (Co-advisor)
Professor Ruth S. DeFries
Professor Zhanqing Li
Dr. Jeffrey T. Morisette
Professor John R. J. Townshend

Preface

The material contained in Chapters 2 and 3 of this dissertation was published in a peer reviewed journal and is for exclusive use in this document in compliance with the copyright terms that apply.

Acknowledgements

I thank Dr. Jeffrey Morisette, Douglas Morton, Dr. Ivan Csiszar, Prof. Chris Justice and Prof. Ruth DeFries for the unconditional support given to me from the very first moment I embarked in this project, and for all the fruitful discussions that followed. I thank Dr. Louis Giglio, Elaine Prins and Chris Schmidt for providing numerous positive feedbacks and for making large volumes of data easily accessible during various phases of my analyses.

I thank the Brazilian counterparts at the National Institute for Space Research (INPE), at the Brazilian Institute for the Environment (IBAMA), and at the System for the Protection of Amazonia (SIPAM) and Brazilian Air Force for providing essential data and support for this project. I thank Dr. Alberto Setzer, Luis Maurano, Dr. Luiz Augusto Machado, Dr. Juan Ceballos, Dr. Carlos Frederico Angelis and Dr. Yosio Shimabukuro from INPE for helping with numerous data requests. I thank Geraldo Lucatelli, João Raposo Pereira, Alexandre Perotto, Joaquim Toledo, Antonio Cattaneo and so many others from the PROARCO and PREVFOGO forest fire monitoring and management programs at IBAMA for helping with the field campaigns conducted in the early stages of the research. I am grateful to the late Dr. Alexandre Santos for collecting valuable field data and for making many difficult moments during the field campaigns seem so fun.

I thank the Large Scale Biosphere-Atmosphere Experiment in Amazonia (LBA), the Earth System Science Interdisciplinary Center (ESSIC) at the University of Maryland, NASA's Earth and Space Science Fellowship Program, and the

National Environmental Satellite, Data and Information Service (NESDIS) at NOAA Camp Springs for providing financial support for this research project.

I thank my wife Renata, my daughter Amanda and my son Daniel for their love and patience, and for adding so much joy to the entire process. I also thank all my relatives for their constant support despite the long geographic distances involved.

Table of Contents

List of Tables

List of Figures

Chapter 1: Introduction

1.1 BACKGROUND

Biomass burning is a major environmental phenomenon influencing the global climate, with important effects on the surface energy flux and atmospheric composition, and on the Earth's radiation budget [IPCC, 1995]. Vegetation fires are a major source of greenhouse gases including CO_2 and CH_4, and of chemically reactive constituents including CO and NO_x [Andreae and Merlet, 2001; van der Werf et al., 2004; Crutzen, 1979; Delany *et al*., 1985]. Bond *et al*. [2004] estimated that total global emission of black carbon from biomass burning is comparable to that produced from the use of fossil fuel, whereas Penner *et al*. [1992] showed that carbonaceous aerosols produced during biomass burning could result in comparable radiative forcing to that of anthropogenic sulfates.

Important feedbacks between forest fragmentation and the use of fire occur at the regional level, increasing the susceptibility of altered forests to larger and more destructive fires [Cochrane *et al*., 1999; Nepstad *et al*., 1999b]. Vegetation fires can impact biodiversity through large scale tree mortality, change forest composition and affect faunal populations and alter soil nutrient pools, thereby influencing secondary forest re-growth [Barlow and Peres, 2006; Barlow *et al*., 2003; Cochrane and Schulze, 1999; Hughes *et al*., 2000; Moran *et al*., 2000; Peres *et al*., 2003]. Vegetation fires are also found to have important social implications in tropical areas,

including significant economic losses as a consequence of property damage and impacts on industry, and increased health problems among local populations [Mendonça *et al*., 2004; Reinhardt *et al*., 2001]

In the last two decades Brazilian Amazonia has been under significant pressure as a result of high annual rates of deforestation [Laurance *et al*., 2004; PRODES, 2008]. Large areas of exceptionally high fire activity resulted from the wide spread use of vegetation fires to convert evergreen tropical forests into pastures or croplands or to maintain previously deforested areas [Alencar *et al*., 1997; Nepstad *et al*., 1999a; Sorrensen, 2004]. Human activities associated with those land use processes are in turn largely influenced by the regional climate conditions, characterized by high rainfall rates occurring during a relatively long wet season when fire use is rarely possible. However, during the dry season months, when there is a noticeable reduction in precipitation fires are used extensively [Schroeder *et al*., 2005].

Vegetation fires in Brazilian Amazonia are spatially concentrated in the major areas of deforestation [Cochrane and Laurance, 2002; Alencar *et al*., 2004]. Those areas often coincide with the agricultural frontiers, where investments in sustainable land use practices are scarce [Morton *et al*., 2006; Nepstad *et al*., 2001; Sorrensen, 2004]. Conservation areas serve as an important mechanism to reduce fire occurrence across large areas of tropical forest in Brazilian Amazonia [Arima *et al*., 2007; Nepstad *et al*., 2006]. However, the increasing pressure from the surrounding areas and the limited control exerted by park administration and law enforcement groups

can greatly reduce the efficacy of those areas to prevent fire spread [Ferreira *et al*., 1999; Laurance and Williamson, 2001; Pedlowski *et al*., 2005].

Brazilian Amazonia covers an area of approximately 5 Million km^2 characterized by a sparse road network and limited infrastructure. *In situ* monitoring of fire activity is very limited and usually constrained to the immediate vicinity of a few environmental law enforcement offices [Ferreira *et al*., 2007]. Satellite active fire detection data represent the primary source of information on fire occurrence for county, state and federal environmental agencies, Non-Governmental Organizations (NGOs), civil society and for the scientific community.

Fire detection data can be obtained from different satellite sensors covering the region [CPTEC, 2008]. However, most users only have access to limited information describing the location and timing of detections derived from individual products. Differences among fire products and the lack of information describing data quality create major difficulties for end users [Schroeder *et al*., 2005]. As a result, law enforcement activities and the decision making process are significantly compromised, state and federal strategic plans to assign resources to control fire activity at the county level are negatively affected, and scientific studies based on fire detection data become subject to large uncertainties (Figure 1.1).

This dissertation investigates the performance of satellite active fire detection data for Brazilian Amazonia and analyzes the potential for integration of the different products. The main objective is to improve fire monitoring in the region by properly identifying and quantifying the major sources of error affecting individual products

and by optimizing the use of multiple remote sensing fire products through data integration.

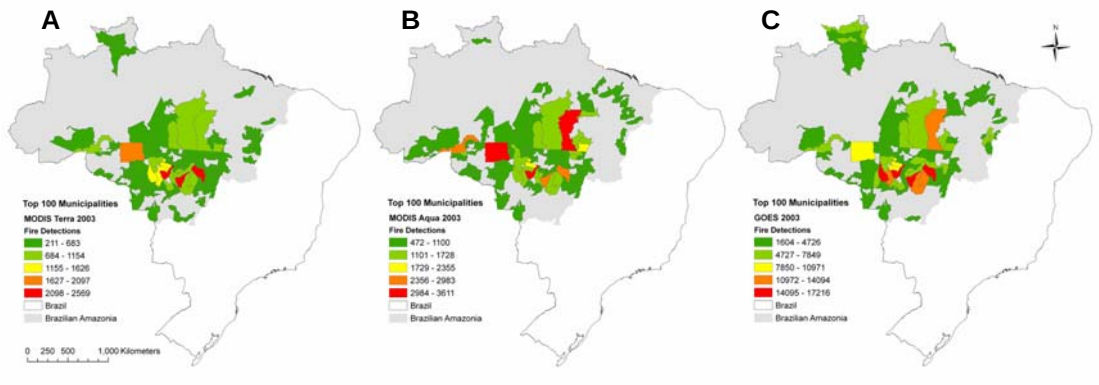

Figure 1.1: Top 100 municipalities showing the largest numbers of fire detections in Brazilian Amazonia using MODIS Terra (A) and Aqua (B) *Thermal Anomalies* and the WF-ABBA GOES (C) data for 2003.

1.2 SATELLITE ACTIVE FIRE DETECTION IN BRAZILIAN AMAZONIA

Satellite remote sensing data have been used extensively to detect vegetation fires in Brazilian Amazonia over the past two decades. The first program incorporating routine monitoring of vegetation fires in the region was implemented by the National Institute for Space Research (INPE) in Brazil in response to the Amazon Boundary Layer Experiment (ABLE-2A) which documented the occurrence of large smoke plumes spreading over forest areas [Setzer and Pereira, 1991]. Since then, awareness about the importance of biomass burning in the tropics has increased significantly among the scientific community [IPCC, 1995]. In response to the large demand for

routine fire information for the region, the number of satellite fire detection products increased rapidly over the years [CPTEC, 2008].

Early satellite active fire detection methods were primarily based on the use of simple threshold tests applied to mid-infrared image data of the Advanced Very High Resolution Radiometer (AVHRR) aboard the NOAA series of polar orbiting environmental satellites [Matson and Holben, 1987; Setzer and Pereira, 1991]. In this spectral region, the fire radiative energy peaks above the regular surface background (e.g., green vegetation) making pixels with active fires distinguishable [Matson and Dozier, 1981]. However, solar contamination in the mid-infrared spectral interval often limits the utility of simple threshold algorithms to small geographic regions where problems such as false alarms can be managed with the use of conservative regionally adjusted tests [Li *et al*., 2000; Morisette *et al*., 2005b]. To overcome those limitations, alternative fire detection techniques were proposed for continental and global remote sensing fire products incorporating the use of contextual approaches applied to the mid-infrared channels, complemented by multi-channel filters to reduce in particular the commission errors in those products [Giglio *et al*., 1999; Kaufman *et al*., 1998b; Prins and Menzel, 1992].

The Wildfire Automated Biomass Burning Algorithm (WF-ABBA) applied to the Geostationary Operational Environmental Satellite (GOES) imager data has been generating 30 min active fire detections at 4 km resolution for Brazilian Amazonia since the mid 1990's [Prins and Menzel, 1992, 1994; UW Madison CIMSS, 2008]. The WF-ABBA data have been applied to regional fire alert systems and biomass

burning emissions models, with a large and diverse user community currently depending on that product.

With the launch in late 1999 of the Moderate Resolution Imaging Spectroradiometer (MODIS) on board the Terra satellite, a new phase in active fire monitoring began. The addition of a fire detection channel enabled for the first time the systematic characterization of sub-pixel vegetation fires at 1 km spatial resolution [Giglio *et al*., 2003a; Justice *et al*., 2002]. The lower saturation of the sensor and higher geolocation accuracy of the *Thermal Anomalies* fire detection product helped the MODIS data gain popularity over data from previous instruments, including the AVHRR series.

Previous case study analyses have assessed the detection performance of WF-ABBA and MODIS *Thermal Anomalies* products over Brazilian Amazonia [Morisette *et al*., 2005b; Prins *et al*., 1998]. However, detailed characterization of those products was missing and differences in sensor characteristics and unexplained differences between WF-ABBA and MODIS *Thermal Anomalies* fire detections were common [Foster Brown, personal communication; Schroeder *et al*., 2005]. The lack of a large set of good quality ground truth data was one of the major obstacles limiting a comprehensive characterization of those products.

1.3 OBJECTIVES OF THE RESEARCH

Vegetation fires in Brazilian Amazonia are largely caused by humans. The strong synergy between human activities and the fuel conditions determined by regional

climate regimes create unique patterns of fire use across the region. As a result, the physical characteristics describing vegetation fires become highly influenced by the different land use and land cover types that occur in Brazilian Amazonia. The main objective of this dissertation is to quantify errors and evaluate the potential for integration of WF-ABBA and MODIS *Thermal Anomalies* fire detection products with attention to the regional conditions that lead to different fire regimes. The complementarities among those products are explored in order to generate improved fire detection rates with higher confidence levels.

The main hypothesis developed for this research is:

By integrating data from multiple sensors we can resolve differences between active fire detection products and increase the accuracy of vegetation fire spatial and temporal distribution

Given the considerations listed above, this dissertation is focused on the effects of cloud obscuration on detection omission errors, on the commission and omission rates associated with different land cover conditions, and on the effects of sensor characteristics which can lead to variations in detection rates and fire characterization. The dissertation is composed of the following research themes:

i) Quantify the impact of cloud coverage on fire detection and create mechanisms to adjust the detection numbers to reflect actual fire occurrence without creating spurious fires;

ii) Quantify commission and omission errors of WF-ABBA and MODIS *Thermal Anomalies* data for fires with different vegetation-background conditions;

iii) Evaluate fire characterization as defined by Fire Radiative Power (FRP) as a means to integrate the WF-ABBA and MODIS *Thermal Anomalies* products;

iv) Quantify scan angle effects on fire detection rates of MODIS;

v) Develop a strategy to integrate fire data from different sensors to generate an improved fire data record for Brazilian Amazonia.

1.4 RESEARCH OUTLINE

This dissertation is composed of five chapters. Chapter 1 covers the topic of biomass burning in Brazilian Amazonia and introduces the main scientific question, providing the rationale for this dissertation. In Chapter 2[1], the effects of cloud obscuration on the detection rates of WF-ABBA over Brazilian Amazonia are quantified. A new cloud mask product is derived for the GOES imager data to identify pixels containing opaque clouds that could prevent fire detection. A pixel based approach is implemented using all daytime and nighttime GOES data at full temporal resolution. The cloud obscuration omission error estimates produced are compared to the approaches used by previous authors to account for the same problem [Cardoso *et al*., 2003; Giglio *et al*., 2006; Roberts *et al*., 2005]. The comparative analysis is substantiated by 20 m resolution burnt area classification data from the China-Brazil Earth Resources Satellite (CBERS) used to validate the results.

Chapter 3[2] addresses the detection performance of WF-ABBA and MODIS *Thermal Anomalies* products over Brazilian Amazonia. The two products are

[1] Chapter 2 is a replica of Schroeder *et al*. [2008a] with only small changes applied to conform with the format of this dissertation

[2] Chapter 3 is a replica of Schroeder *et al*. [2008b] with only small changes applied to conform with the format of this dissertation

validated using "ground truth" information derived from 30 m resolution Advanced Spaceborne Thermal Emission and Reflection Radiometer (ASTER) and Landsat Enhanced Thematic Mapper Plus (ETM+) data. In addition to those data sets, *in situ* and airborne data are used to provide information on the different types and dynamics of the fires sampled. Commission and omission errors are derived for four major regions characterized by distinct intervals of percentage tree cover. The primary factors influencing the commission error rates are identified, and an alternative method is proposed to reduce the high number of false detections produced by the WF-ABBA and MODIS *Thermal Anomalies* products near forested areas.

In Chapter 4 the potential for integrating WF-ABBA and MODIS *Thermal Anomalies* is investigated. Two different approaches are tested. First, FRP estimates generated from GOES and MODIS data are used. Major sources of error in FRP values are identified and quantified using simulated data. Secondly, the relationship between WF-ABBA and MODIS *Thermal Anomalies* fire detections is established for Brazilian Amazonia. Finally, the variation in detection performance of the MODIS fire product as a function of scan angle is quantified using area averaged daily sum statistics of fire detections for a subset region in southern Brazilian Amazonia.

A new integrated fire product based on the WF-ABBA and MODIS *Thermal Anomalies* products is presented in Chapter 5, incorporating adjustments to correct for detection errors in both products.

The synthesis of results is presented in Chapter 6, followed by a discussion of the implications for satellite fire monitoring in Brazilian Amazonia. The flow diagram summarizing the main components of this dissertation is shown in Figure 1.2.

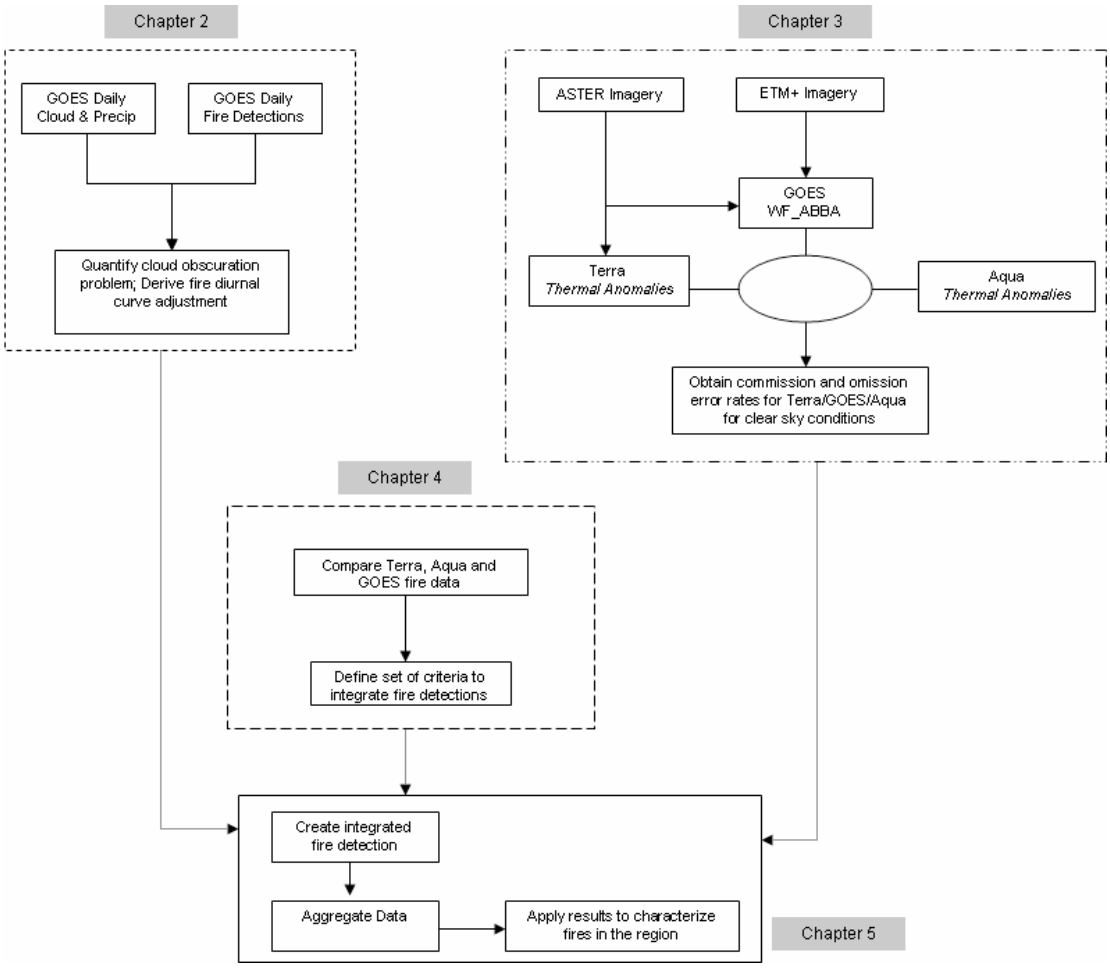

Figure 1.2: Flow diagram of dissertation.

Chapter 2: Quantifying the Impact of Cloud Obscuration on Remote Sensing of Active Fires in Brazilian Amazon[1]

2.1 INTRODUCTION

Vegetation fires play a significant role in land and atmospheric processes globally. Their occurrence is particularly important in tropical regions where human activity is still heavily based on the use of fires for land use management and land cover change. In the latter case, deforestation and fires are found to be closely related eventually leading to important feedback processes that favor faster and more destructive depletion of the local forests [Cochrane *et al*., 1999; Nepstad *et al*., 1999b]. In contrast, at higher latitude regions a greater percentage of fires are caused by lightning or are accidental in nature and are highly influenced by the local weather and climate conditions [Kasischke *et al*., 2002]. Fires in the tropics are influenced by local conditions too but will also present an equally important component due to the influence of human activities which are reflected in the spatial and temporal distributions observed across regional to global scales [Barbosa *et al*., 1999; Scholes *et al*., 1996].

Correct quantification of fire events is needed primarily for understanding the dynamics of land use and land cover change and therefore subsidize regional environmental programs, as well as for providing information for modeling of

[1] The material presented in this Chapter is part of Schroeder *et al*. [2008a]

emission estimates from biomass combustion [Korontzi *et al*., 2004; Van der Werf *et al*., 2003]. Consideration of the fire diurnal cycle is also required for biomass burning transport models, making high observation frequency a particularly important characteristic on active fire monitoring systems [Freitas *et al*., 2005; Giglio *et al*., 2006].

Satellite sensors have been used to monitor vegetation fire activity for many years now, providing greater insight on the processes associated with fire dynamics at different scales [Bucini and Lambin, 2002; Carmona-Moreno *et al*., 2005; Di Bella *et al*., 2006; Dwyer *et al*., 2000; Giglio *et al*., 2006]. In fact, the use of satellite data is the only way to assess fire activity at spatial and temporal scales required for land surface and atmospheric modeling studies. However, the remote sensing methods used for monitoring fires have limitations that tend to cause important biases in the final products [Boles and Verbyla, 2000; Cardoso *et al*., 2005; Eva and Lambin, 1998; Kasischke *et al*., 2003; Schroeder *et al*., 2005].

A major factor influencing fire numbers derived from remotely sensed data is the effect caused by cloud obscuration. Because fires have their highest spectral emission located in the mid-infrared band, active fire products exploit that part of the spectrum to distinguish biomass burning events from the surrounding background [Giglio *et al*., 1999; Justice *et al*., 2002]. The presence of optically thick clouds along the atmospheric path between the target (fire) and the satellite sensor will, however, greatly reduce the ability to detect a fire due to severe attenuation of the spectral signal emitted by either flaming or smoldering phases of biomass combustion.

Current methods used to compensate satellite active fire detection to account for fires missed due to cloud obscuration tend to rely on the assumption that fires occur with the same frequency under cloud covered areas as they do in the open [Cardoso *et al*., 2003; Giglio *et al*., 2003b, 2006; Roberts *et al*., 2005]. Despite being an attractive approach for its simplistic assumption, the adoption of such procedures becomes problematic in areas where fires are unevenly distributed in space. Under such conditions, the resulting adjustment numbers will be potentially influenced by the cell size selected to extrapolate the applicable clear sky fire density to the complementary cloud covered area. The major implication of such an approach is associated with the assumption of fires in areas with no burning activity which would lead to an overestimation of fire numbers.

Here we present an approach that uses precipitation data and land use information to more precisely quantify the potential omission error associated with the cloud obscuration affecting satellite active fire detection products. The proposed approach is applied to a geostationary satellite fire data set, in order to characterize the cloud effect on fire detection over the entire diurnal cycle. The analyses are focused on Brazilian Amazonia where intense fire activity and frequent cloud cover are prevalent (Figure 2.1). In the sections to follow we describe the data sets used and the method developed and present the results produced for 2005.

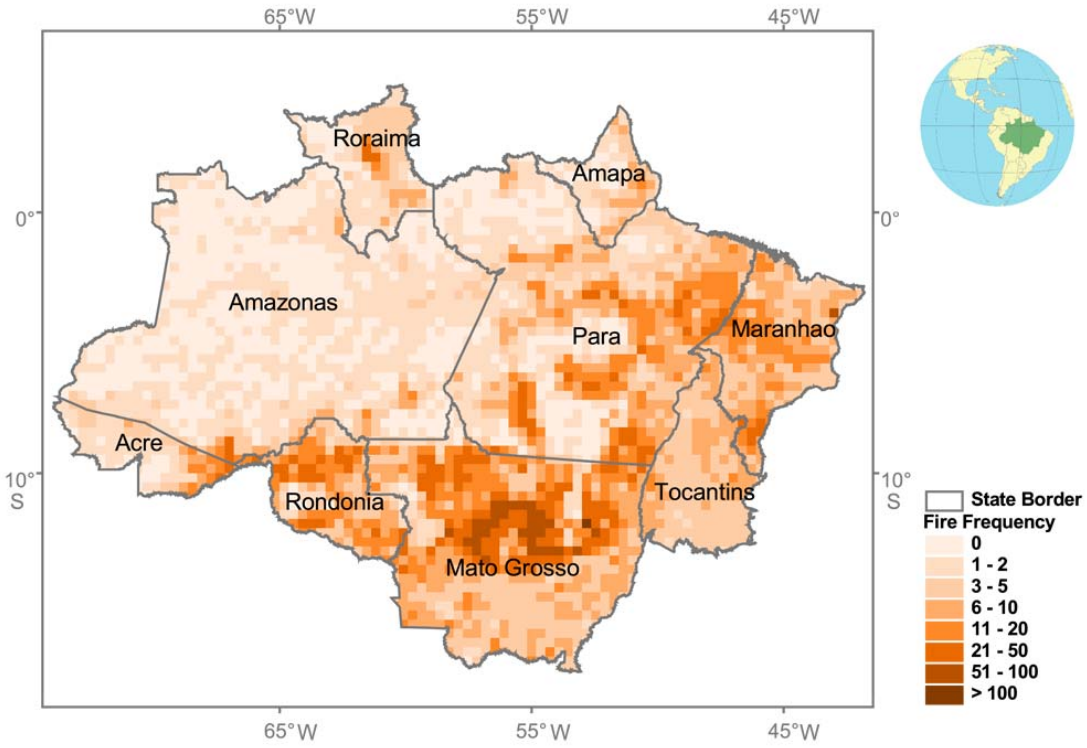

Figure 2.1. Fire frequency (fires 10^{-2} km^{-2} year^{-1}) across the nine Brazilian States in Amazonia. Values based on 3-year average (2003–2005) GOES WF-ABBA fire detection data using all observation hours available.

2.2 DATA

2.2.1 Active Fire Product

In the past two decades multiple satellite-based active fire products have been designed using a variety of sensors [Elvidge *et al*., 1996; Giglio *et al*., 2000; Kaufman *et al*., 1990, 1998a; Menzel *et al*., 1991]. The performance of individual products is found to be strongly dependent on the sensor's spectral characteristics and on the algorithm used, as well as on the imaging characteristics (e.g., pixel size, observation geometry) provided by the instruments and the orbital platforms on which they are

mounted [Morisette *et al*., 2005b; Schroeder *et al*., 2005]. Despite their usual coarser spatial resolution, geostationary satellites are extremely interesting for fire monitoring as they provide high observation frequency. High frequency observations are important for deriving the diurnal cycle of fire activity at the regional to basin-wide level as well as for modeling time dependent transport of biomass burning emissions [Freitas *et al*., 2005].

Data from the Geostationary Operational Environmental Satellite positioned at 75° longitude (GOES-East) are used in this study. The GOES-East satellite is located over the study area selected, thereby offering near optimal observation conditions (i.e., near nadir viewing geometry) for fire detection. The nominal 4×4 km pixel resolution at sub-satellite position remains stable throughout most of the region with less than 25% increase in pixel area being observed near the far most corners of the study area.

Two major GOES-based operational active fire products are available for the study area. The Wildfire Automated Biomass Burning Algorithm (WF-ABBA) is produced by the University of Wisconsin — Madison and uses a contextual approach for detecting active fires [Prins and Menzel, 1992; Prins *et al*., 1998]. This product is available for the period of 2000–present and covers the entire study area. The other product is generated by the Weather Forecast and Climate Studies Center in Brazil (CPTEC) and combines fixed threshold and contextual tests for detecting fires [CPTEC, 2008]; data are available from July 2004 to present. Because of limited temporal coverage found with the latter, we used WF-ABBA's active fire product in this study. The data set selected for use covers the period of January 2003–December

2005 and is composed of 17,520 half hourly files per year. Each file contains information on fire location and acquisition date along with the temperature and area estimates and the assigned confidence for each detection. The latter is divided into five categories ranging from high (0) to low (5) confidence. Category 5 was rejected here as in some cases it was found to be strongly associated with spurious detections composed of large clusters of pixels with no similar detections from other sensors. Previous validation of WF-ABBA's fire product performed during the Smoke, Clouds and Radiation-Brazil (SCAR-B) experiment, showed that forest conversion fires as small as 1 ha could be detected by that algorithm [Prins *et al*., 1998]. WF-ABBA's active fire detection product was selected as the source data to which the cloud obscuration adjustments were implemented based on the methodology described in Section 2.3. The necessary WF-ABBA product files were made available by the University of Wisconsin — Madison.

2.2.2 Precipitation Data

The second set of data used in this study was the satellite derived precipitation estimates. Brazilian Amazonia is still only partially covered by meteorological and hydrological surface stations from which precipitation data can be extracted. Rainfall is generated primarily within localized convective systems leading to potential effects on the quality of the precipitation estimates based on spatially interpolated surface station data from the region [Costa and Foley, 1998]. Availability of meteorological radar data is also scarce due to limited spatial and temporal coverage. Consequently, the use of radar data was not considered as a viable alternative for this study. Because

of these limitations, satellite derived precipitation products were used for assessing rainfall conditions throughout Brazilian Amazonia. As with the remote sensing of active fires, precipitation estimates are provided by different sensors using different algorithms that can be based on single instrument or on multi-sensor multi-data approaches [Bellerby *et al*., 2001; Kummerow *et al*., 1998; Rudolf *et al*., 1996]. Consideration of the spatial and temporal resolutions and the accuracy of the precipitation products that have achieved operational mode led to the use of GOES-based precipitation estimates for this study. CPTEC currently generates daily GOES-based precipitation estimates for most of South America at the nominal spatial resolution of 4×4 km. CPTEC's product is a revised version of the Hydro-estimator method [Vicente *et al*., 1998], which uses improved coefficients for the specific conditions observed over Brazil [Vila and Lima, 2004; Carlos Frederico Angelis — personal communication, 2005]. CPTEC's GOES-based precipitation estimates data production was initiated in January 2004 providing daily files with total accumulated precipitation at nominal 4 km resolution. The data set used in this study covers January 2004–December 2005.

Prior to the application of CPTEC's Hydro-estimator precipitation data to the proposed methodology, an evaluation was performed using point precipitation data obtained from 19 automated surface weather stations available across the basin [URL: http://tempo.cptec.inpe.br/PCD/]. Figures 2.2A–C show the results for all stations selected using three different time integration periods — 1, 7, and 30 days, respectively. The correlation between the two data sets is seen to improve significantly with the total number of days used in the sampling process.

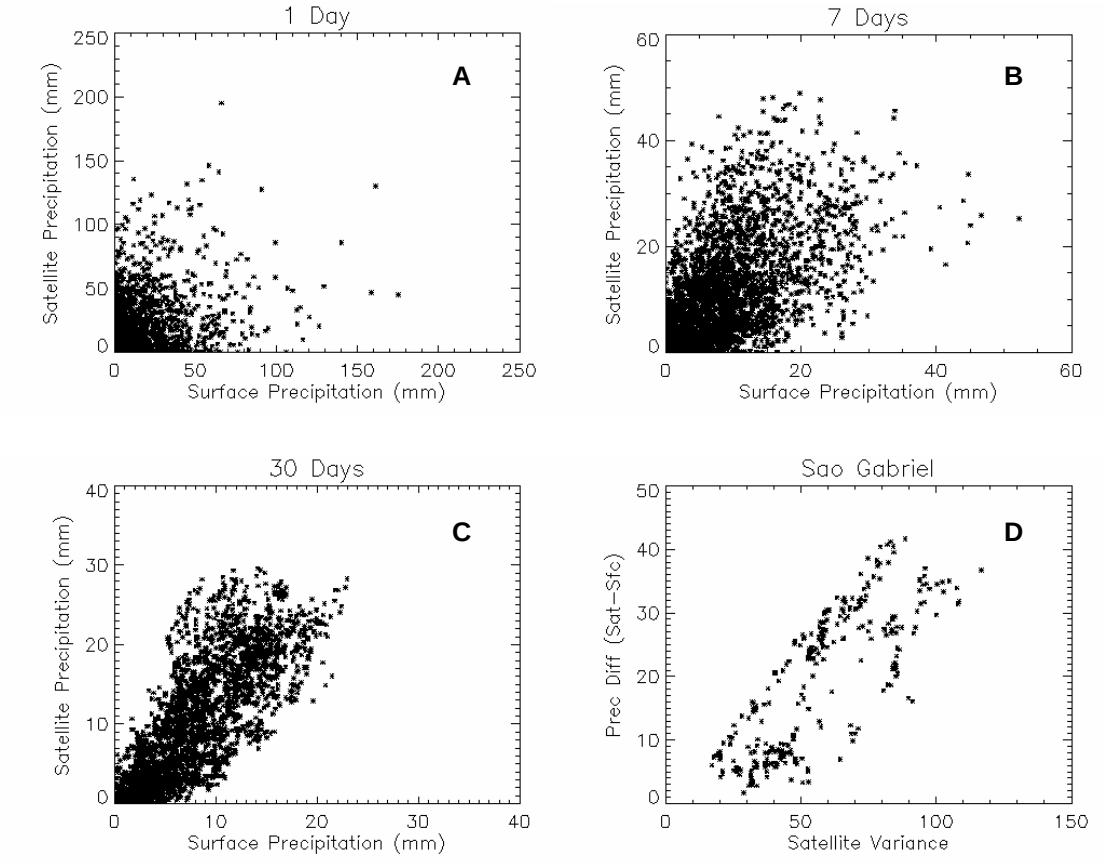

Figure 2.2. Scatter plots of the satellite precipitation estimates and the surface precipitation observations using 1 (A), 7 (B) and 30 (C) day average values and of the difference between the satellite precipitation estimates and the surface precipitation data and the satellite variance (D) calculated for the 9 pixels centered at the Sao Gabriel weather station in Amazonas state.

Two major factors were believed to contribute to the dispersion seen in all three graphs. First, there is the natural difficulty in relating the surface station's point data to the 4×4 km pixel footprint as obtained with the GOES data. The large rainfall spatial heterogeneity mentioned above will cause significant impact on the area averaged estimates produced from the satellite data. The effect of the spatial variability in precipitation patterns in the region is exemplified in Figure 2.2D, where the absolute difference calculated for the satellite and surface station precipitation

values is plotted against the satellite precipitation variance (σ^2) based on 9 pixels centered at one surface station location.

Another important factor contributing to the dispersion seen in Figures 2.2A–C is related to the inherent deficiencies in the precipitation product that are associated with the use of passive remote sensing data from GOES and empirical relationships that tend to impact the accuracy of the precipitation estimates produced [Boi *et al*., 2004; Ebert *et al*., 2007; Rozumalski, 2000; Vicente *et al*., 2002]. Despite these limitations, the high observation frequency of the GOES precipitation estimates allows for improved integration of the 24 h precipitation totals thereby providing valuable information for use in this study. Also, as will be described in Section 2.3.1, our approach will be based on relative differences between precipitation estimates making absolute accuracy of the product of less significance.

2.2.3 Cloud Mask

The WF-ABBA fire product consists of a list of fire detections, but no cloud mask is included. However, a cloud mask is needed for identifying cloud obscured pixels that require processing for potential fire omission. Therefore we developed a new cloud mask product at the 4 km spatial and 30 min temporal resolution of the original active fire data, which is the basis of the cloud obscuration processing scheme. The cloud mask was designed based on the use of the Global-Merged Infra-Red Brightness Temperature (from here on designated simply as BT) product generated by the Climate Prediction Center [CPC, 2008]. The BT data are a single band global product derived from multiple geostationary satellite imagery and gridded to nominal 4×4 km

resolution. In the case of Brazilian Amazonia the BT product is primarily derived from GOES-East imagery.

The unique conditions of the Amazon region in terms of daily BT trends were explored to derive a method that uses fixed and dynamic thresholds to distinguish between clouds and land surfaces in the BT images. Daily variation of BT is small for clear sky pixels as surface temperature remains much constant within a 30 day period [Alvalá *et al*., 2002]. The stability of surface conditions is demonstrated in Figure 2.3B in which a typical pattern of BT values extracted from a 30 day profile obtained from the same pixel and observation hour is presented. The set of empirically defined tests used in the production of the cloud masks is summarized bellow:

$$BT_i \leq 237\ K \quad \rightarrow \quad Super\ Cold\ Cloud \tag{i}$$

$$BT_i > 237\ K \quad and \quad BT_i \leq 278\ K \rightarrow \quad Cold\ Cloud \tag{ii}$$

$$BT_i > 278\ K \quad and \quad BT_i < \overline{BT_{n=30}} - 1.5 \times \sigma_{n=30} \quad \rightarrow \quad Warm / Subpixel\ Cloud \tag{iii}$$

$$BT_i > 278\ K \quad and \quad BT_i \geq \overline{BT_{n=30}} - 1.5 \times \sigma_{n=30} \quad \rightarrow \quad Clear\ Sky. \tag{iv}$$

Where BT is evaluated for each individual pixel imaged during the i^{th} observation hour. Conditions (iii–iv) use information from the previous 30 days to calculate the mean ($\overline{BT}$) and the standard deviation (σ) for observation hour *i*. Only pixels having BT values greater than 278 K are considered in the calculation of $\overline{BT}$ and σ. The cloud mask processing also requires that a minimum of 10% of the BT data available during the 30 day sampling period be greater than 278 K. The threshold of 278 K was

found to work well for this specific data set as it provided the dividing line between unambiguous cloudy pixels and other surfaces. Having a minimum of 10% of all values observed within a 30 day period above 278 K was then required to estimate the approximate clear sky BT value and therefore allows for proper classification of the pixels. For those cases where this criterion is not met, the pixels are classified as *undetermined* and thereby not used in the cloud obscuration processing. Approximately 1.5% of the pixels analyzed were classified as *undetermined*.

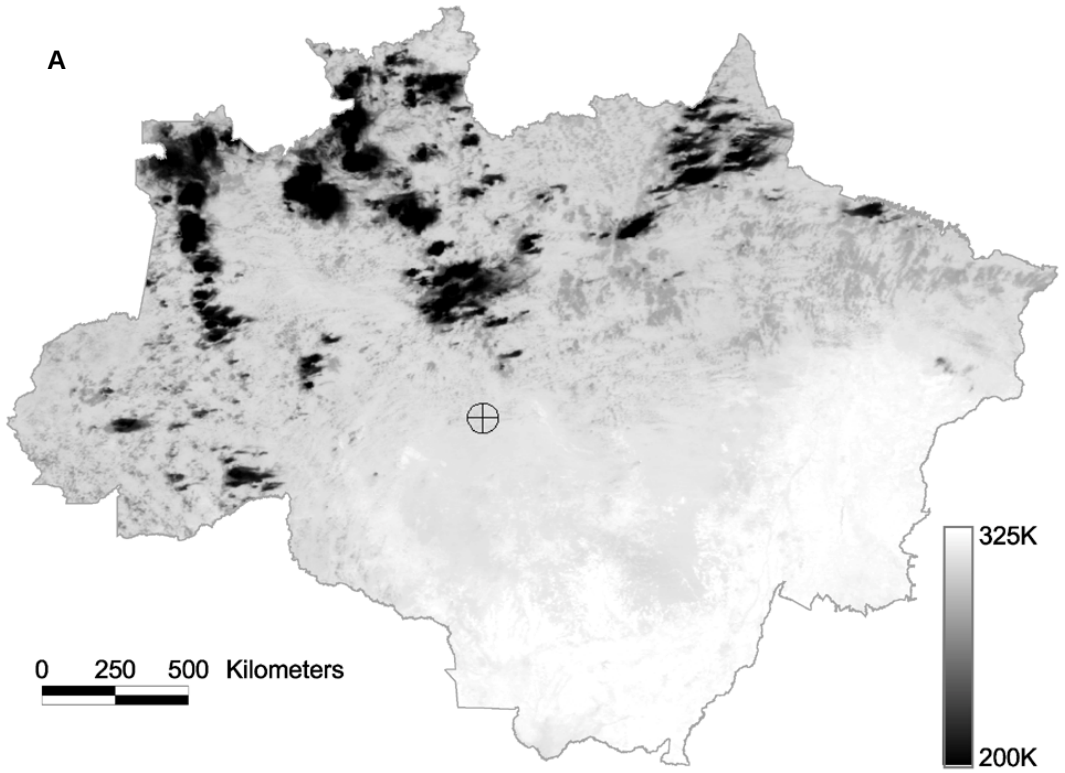

Figure 2.3. Brightness temperature (BT) image for 15 August 2004 1815 h UTC (A) and the 30 day (July 16→August 15 2004) temporal profile (B) for the pixel marked as "⊕" on the image. Solid line represents the observed BT values, the dotted line represents the 30 day mean value, and the dashed lines the 30 day standard deviation.

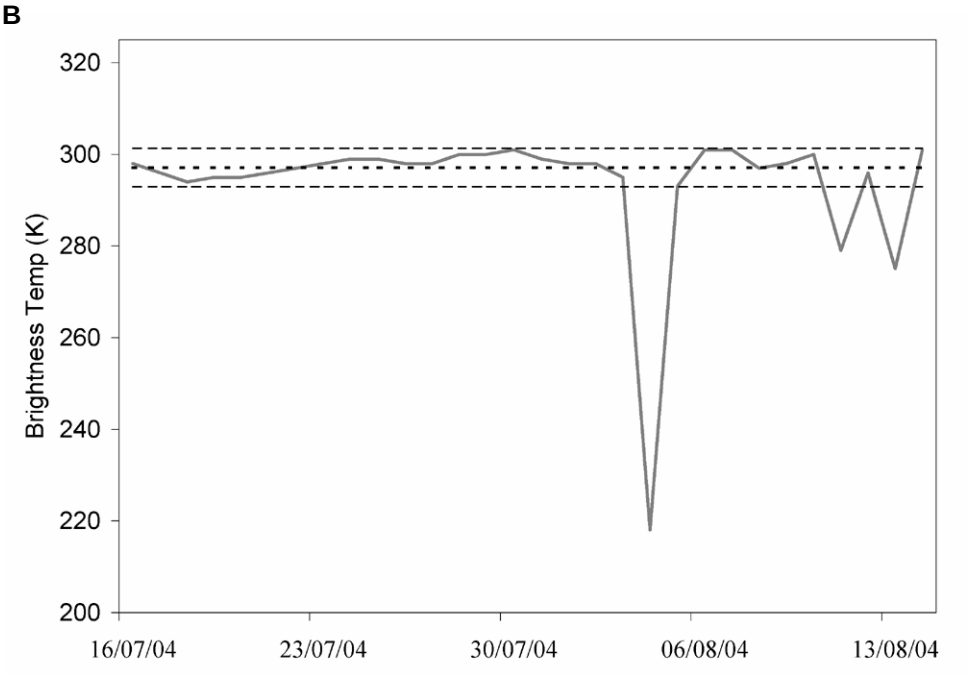

Figure 2.3. *continued*

The performance of the cloud mask product was tested against another source (CPTEC's GOES-based operational multi-band daytime-only cloud classification method; http://satelite.cptec.inpe.br) to check for consistency. Two 20 day periods were analyzed: one in the wet season (February 2005) and one in the dry season (September 2005). The results showed the two products to be in good agreement and proved the cloud mask to be effective in identifying cloudy pixels (>95% correspondence with CPTEC's classification during both wet and dry seasons). Pixels classified as cloud-free by the cloud mask product showed a less significant agreement with CPTEC's product (23% during the wet season and 56% during the dry season). To help explain the differences between the two products we randomly selected approximately 20 cases from the wet and dry seasons for which GOES 1 km

and MODIS 1 km and 500 m bands were visually inspected. The visual analysis suggested that sub-pixel cumulus clouds that are routinely observed in the Amazon basin as well as other sorts of contaminants (e.g., thin cirrus clouds, smoke plumes) are more frequently classified as clouds by the more conservative method used by CPTEC resulting in the differences found.

Half hourly global BT files were obtained from the NASA's Goddard Space Flight Center Distributed Active Archive Center (DAAC) covering years 2004 and 2005 (17,520 files per year) and the cloud mask algorithm was applied for Brazilian Amazonia spatial subset. Analysis of the BT data showed that pixels having confirmed measurable precipitation (based on precipitation observations derived from the same surface station network used to evaluate the hydro-estimator product above) had a mean value of 237 K (σ = 22 K). This result corroborates the findings of Arkin [1979] who obtained a 0.75 correlation coefficient between surface precipitation data and three month-average satellite rainfall estimates for brightness temperature values lower than 235 K. Based on this finding, the cloud obscuration analysis was only carried for pixels showing BT values greater than 237 K during the 24 h period between the last satellite precipitation estimate available and the following one.

2.3 METHODS

In order to predict whether there are fires present under clouds, we need to determine the conditions under which fires are likely to occur. In the case of Brazilian Amazonia, both physical and social factors play important roles in defining where and when fires occur. The methodology presented here uses precipitation estimates to

determine the physical conditions of the environment, along with previous active fire data to derive the spatial and temporal distributions of fires that are known to be influenced by specific land use patterns observed throughout the region. Given that the extent of Brazilian Amazonia is over 5 million km^2, the conditions leading to vegetation fires can vary significantly across the region. The existence of vegetation cover types ranging from grasslands to closed canopy evergreen forests requires that the area be divided into smaller parts in order to represent local characteristics of fire occurrence. Consequently a 40×40 km grid covering the study area (3358 cells total) was used to stratify the entire basin into smaller subparts. The grid size selected was meant to preserve the small scale phenomena represented in the analyses while balancing the need for reasonable sample sizes required to produce the summary statistics described below. In addition, the selected grid size allowed for easier association with the nominal 4×4 km GOES pixel distribution. Analysis of the physical conditions and spatial and temporal dynamics was undertaken for each one of the 48 daily GOES observation hours (30 min interval). In the following sections we describe the approach used to determine potential fire omissions due to cloud.

2.3.1 Fire Dynamics and Precipitation

Precipitation will have a great impact on the conditions of the local environment, influencing the mechanisms that control vegetation moisture content and temperature and the latent and sensible heat fluxes that affect land surface and atmospheric humidity and temperature conditions [Betts *et al*., 2002; Bruno *et al*., 2006; Nepstad *et al*., 2002]. WF-ABBA active fire data from 2004–2005 were used in conjunction

with the GOES precipitation estimates for the same period to derive the physical conditions that facilitate fire development. Precipitation amounts during the 30 day period preceding each fire detection were extracted for every observation hour and the information aggregated into the 40×40 km grid following:

$$RT_{i,n,z} = \left[\sum_{day=-1}^{day=-1} r_n, \sum_{day=-1}^{day=-2} r_n, \ldots, \sum_{day=-1}^{day=-30} r_n \right]. \quad (1)$$

Where RT is a 30 element array containing the accumulated precipitation r during a 30 day period preceding fire n [n = 1,…, N] detected during observation hour i [i = 1,…, 48] and located in grid cell z [z = 1,…, 3358]. A third degree polynomial was adjusted to the mean values representing the group of data found in each one of the 40×40 km grid cells for each observation hour using:

$$\overline{R}_{i,z} = \left(\frac{\sum_{n=1}^{n=N} RT_{i,n,z}[1]}{N}, \frac{\sum_{n=1}^{n=N} RT_{i,n,z}[2]}{N}, \ldots, \frac{\sum_{n=1}^{n=N} RT_{i,n,z}[30]}{N} \right) \quad (2)$$

$$M_{i,z} = \left\{ \left(1, \overline{R}_{i,z}[1]\right), \left(2, \overline{R}_{i,z}[2]\right), \ldots, \left(30, \overline{R}_{i,z}[30]\right) \right\}. \quad (3)$$

$$f_{i,z}(x) = a_0 + a_1 x + a_2 x^2 + a_3 x^3. \quad (4)$$

Where $\overline{R}$ is the 30 element array with the mean accumulated precipitation for N fires detected during observation hour i at cell z, and M is the resulting array of data for which the coefficients in Eq. (4) are calculated for. Eq. (4) is the function defining the

relationship between the number of days (x) preceding a fire and the respective mean accumulated precipitation for that period. Interestingly, M assumes a strong linear distribution when N grows larger (typically for $N > 50$) (Figure 2.4). The application of a third degree polynomial proved a good fit with most conditions observed. The resulting curve coefficients were stored in individual look up tables (LUT, one for each observation hour) and were to be used in the final code as a reference value describing the mean precipitation conditions preceding fires at each 40×40 km grid cell.

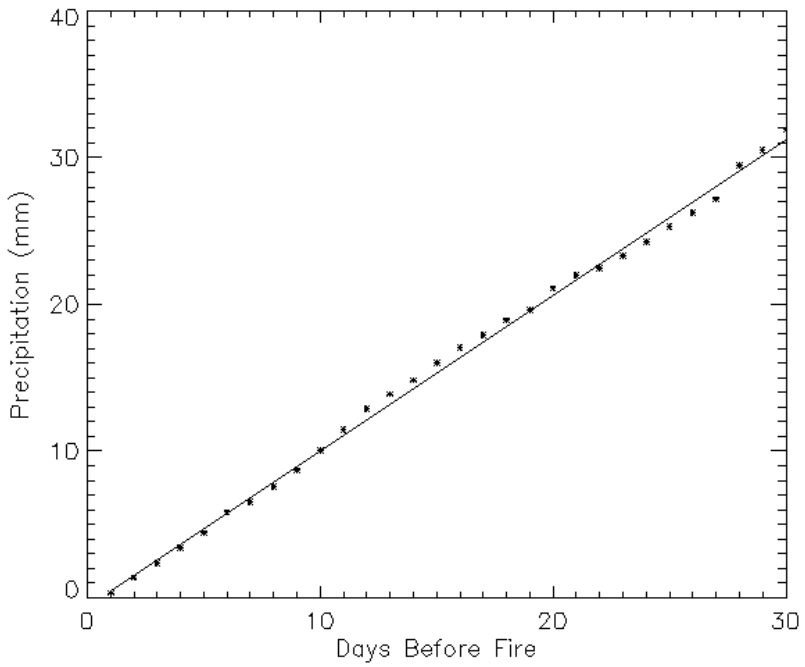

Figure 2.4. Mean precipitation values calculated for a single 40×40 km cell (approx. location: 60.10° W 12.50° S) based on N=151 active fire detections observed during 2004–2005. R^2=0.9974.

The information provided by the polynomial curves was used to set the probability ranges that describe the potential occurrence of fires based on the physical condition of the environment as defined by the precipitation data. The criteria used to determine the probability of fire occurrence as a function of precipitation were the following:

$$\sum_{day=1}^{day=30} RA_{i,z} \le \int_{1}^{30} f_{i,z}(x)dx \quad \rightarrow \quad P_R = 1 \tag{5}$$

$$\left\{ \begin{array}{c} \sum_{day=1}^{day=30} RA_{i,z} > \int_{1}^{30} f_{i,z}(x)dx \\ and \\ \sum_{day=1}^{day=30} RA_{i,z} \le 2\int_{1}^{30} f_{i,z}(x)dx \end{array} \right\rangle \quad \rightarrow \quad P_R = \int_{1}^{30}(x)dx - \frac{\sum_{day=1}^{day=30} RA_{i,z}}{\int_{1}^{30} f_{i,z}(x)dx}. \tag{6}$$

Where *RA* is the actual precipitation data that is accumulated over the 30 day period for a particular pixel at observation hour *i* and grid cell *z*, $\int dx$ is time integral (30 days) calculated for the polynomial curve *f(x)*, and P_R is the assigned probability of fire occurrence related to precipitation. According to Eqs. (5) and (6), *RA* must be less than two times the area defined by the LUT curve covering the 30 day period for a particular location and observation hour for the pixel to be considered for the cloud obscuration analysis. Additionally, a third test was implemented to avoid particular conditions when the actual precipitation is concentrated in the most recent period (day-1→day-7). This test is based on anecdotal evidence, which suggests that land owners in the region normally wait for approximately one week to burn following a

rainfall episode. In this case, a more conservative approach is applied using the criterion:

$$\sum_{day=1}^{day=7} RA_{i,z} \geq \int_{1}^{30} f_{i,z}(x)dx \quad \rightarrow \quad P_R = 0. \tag{7}$$

From the above test, for the pixel to be considered for the cloud obscuration processing, the actual precipitation recorded during the 7 day period preceding an observation cannot be greater than the 30 day mean precipitation associated with fires for that same location and observation hour.

2.3.2 Fire Spatial and Temporal Dynamics

Fire activity in tropical areas tends to follow very specific patterns as a function of land use and land cover change. In those areas, the systematic use of fires for land clearing and maintenance creates reasonably consistent spatial and temporal patterns in satellite active fire detection from year to year [Giglio *et al*., 2006]. To establish the mean annual fire activity in time and space over Brazilian Amazonia, we used active fire records derived from GOES during 2003–2004. The 40×40 km grid used to extract the fire and precipitation relationship was also applied in this analysis.

In order to derive the temporal distribution of fires, the year was divided into 26 14-day periods. We used 14 day period intervals to properly represent the seasonal curves of fire activity. Fire seasons were usually constrained to approximately 2–3 months, thereby 14 day periods allowed for a good representation of the progress in fire activity throughout the season while keeping our samples for each cell to a

reasonable size. The probability distribution of fires detected during each one of the 14-day periods in relation to the 2003–2004 totals was calculated for all 40×40 km grid cells according to:

$$P_{Tz}(t) = \frac{\sum_{\substack{t \\ 2004}} fires_z}{\sum_{2003} fires_z}. \quad (8)$$

Where P_T is the active fire probability distribution for grid cell z, the numerator represents the number of fires detected during a 14 day period t, and the denominator represents the total number of fires observed in grid cell z during the entire period analyzed (2003–2004). A LUT containing the results for each grid cell was produced for every observation hour to be used in the final code. To reduce the effects of the inter-annual variability in fire activity on the adjustment factors produced, we used information from the year for which the processing was implemented (in this case 2005) to account for departs from the mean values described by the LUTs containing the P_T data described above. For this we used a metrics P_{14} describing the sum of fires detected during the preceding 14 day period for each 40 km grid cell that was systematically updated during processing. Therefore, any increase or decrease in fire activity for a particular grid cell would be considered in the calculation of the cloud obscuration adjustment produced by either increasing or decreasing the contribution from the term P_T in Eq. (8) relatively to P_{14}.

In addition to the annual distribution of fires observed with the active fire data record from 2003–2004, evaluation of fire's return frequency was also conducted. Vegetation fires are usually associated with a high return frequency in tropical

regions [Cochrane and Schulze, 1999]. The analysis of GOES active fire data during the period of 2003–2005 including all observation hours showed that approximately 66% of the areas under the influence of fires in one year also exhibited some activity in the following year (Table 2.1). However, the likelihood of observing a fire in a particular area during the same observation hour over sequential years becomes much less evident. Multiple factors were believed to contribute to the latter, including but not limited to changes in the hour of the day a fire is ignited, changes in the fuel load affecting fire intensity and duration therefore impacting detectability, changes in land use, etc. Modeling these factors and the interactions among them is difficult and was not attempted here. In order to account for this greater variability when analyzing observation hours individually a random function (ξ) was used with the cloud obscuration analysis to represent fire return probability at every hour. This random function was adjusted to uniformly represent the average ranges of return probabilities at the individual observation hour from Table 2.1.

Table 2.1: Fire return rate based on GOES ABBA active fire product using a 4×4km grid covering Brazilian Amazonia.

Years with Detection	*1745UTC**	*All Hours Included**
2003 & 2004	33%	68%
2004 & 2005	40%	65%
2003 & 2005	33%	66%
2003 & 2004 & 2005	19%	52%

* Values represent the percentage of all cells with fire activity in one year that also showed detections in subsequent years based on (i) the observation hour of 1745UTC and (ii) all observation hours.

Complementing the analysis of the land use influence in the establishment of fire patterns across the study area, the spatial distribution of fires was determined with

the implementation of a 4×4 km grid nested in the previous 40×40 km grid. This finer grid was created to represent the GOES pixel map at nominal resolution. It was intended to distinguish between areas under the influence of fires where the cloud obscuration evaluation would be performed from areas with no fire activity recorded in the most recent years where no intervention was to be conducted. All 4×4 km cells showing fire activity during years 2003 and 2004 were identified and the information stored as binary values (0 — no fire history; 1 — fire prone) in individual LUTs for every observation hour. These LUTs were updated during the actual processing to account for areas of fire expansion by adding new fire prone pixels to the existing list.

2.3.3 Implementation and Accuracy Assessment

The methodology implemented during this study was designed to use the information derived from the previous steps for compensating year 2005 GOES-East fire data for the cloud obscuration of fires. GOES data were processed sequentially for every acquisition hour during year 2005 totaling 17,520 observations. For a particular observation date and time the code would initially search for all 40×40 km grid cells that, according to the temporal LUTs, are likely to show fire activity for that particular bi-week (Figure 2.5). Following this first selection, all 4×4 km areas contained by the grid cells (i.e., the nominal GOES pixels) with a history of fire activity are identified. The cloud mask product that was produced for the same year (2005) is then used to search for cloudy pixels among the previously selected ones. Two major scenarios were considered during processing, each representing distinct cloud coverage conditions.

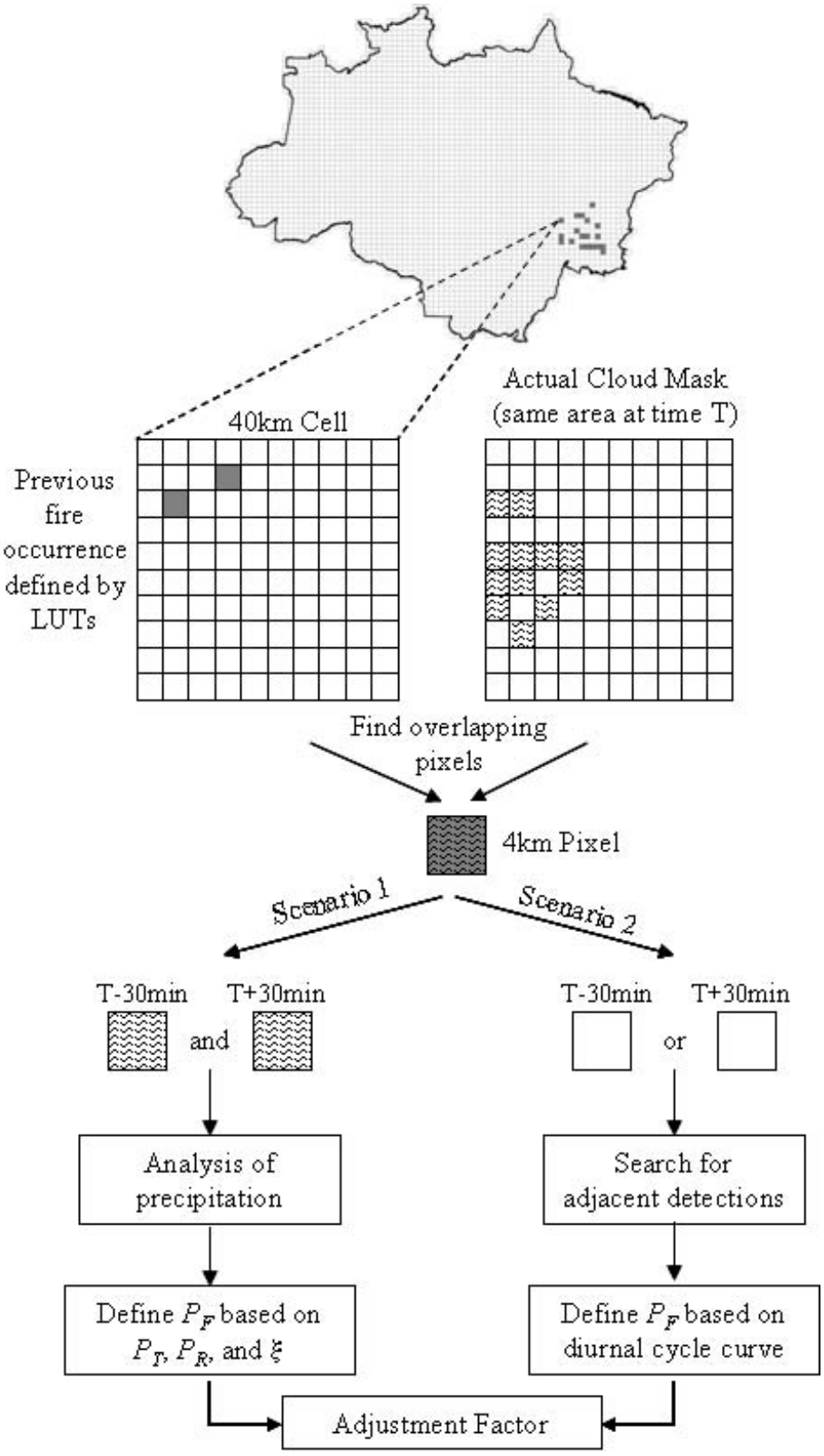

Figure 2.5. Cloud obscuration processing diagram.

In scenario one, a cloud covered pixel is selected for observation hour *T* and both adjacent detections (*T*−30 min and *T*+30 min) are also obscured by clouds. In this case, the actual precipitation data is assessed and compared against the values obtained from the LUT defining the mean precipitation curve associated with fire occurrence for that area (i.e., the 40×40 km cell). Having cleared the tests established in. (5), (6) and (7), the probability of fire omission (P_F) will be derived for that pixel using (5), (6) and (8) and the random function (ξ), assuming the form:

$$P_F = P_R \times P_T \times \xi.$$

In scenario two, a cloudy pixel detected in time *T* has either the preceding (*T*−30 min) or the succeeding (*T*+30 min) observation hour cloud free. Under these conditions the code will use information from the current WF-ABBA fire product (searching for adjacent detections), the pixel's local time and from a general fire diurnal cycle curve. For this particular application, the curve chosen to represent the fire diurnal cycle in the region had its peak located at 1500 h local time in order to coincide with the normal hour of maximum air temperature – or inversely, minimum air humidity – [da Rocha *et al*., 2004] as temperature and humidity will be strongly related to fire spread conditions. The diurnal cycle curve was divided into three parts, each describing a particular trend in fire progress over time (Figure 2.6).

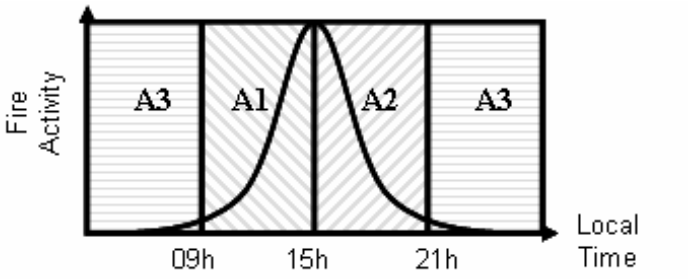

Figure 2.6. Stratification of the diurnal cycle of fire activity into three major areas, A1, A2, and A3.

In area A1 of Figure 2.6, a cloudy pixel observed at local time T_{local} will be likely to omit a fire if an actual detection exists for $T_{local-30\ min}$, since fire continuation will be favored by the usual increase in temperature followed by a decrease in relative humidity. The likelihood of a fire being omitted at local time T_{local}, when detection is observed during hour $T_{local+\ 30\ min}$ will depend on the potential fire occurrence during hour T_{local} for that time of the year. Based on these considerations, cloudy pixels observed during local hour T_{local} and falling within area A1 will be evaluated according to the following criteria:

Actual fire detection at $T_{local\text{-}30\ min} \rightarrow P_F = 1$ (i)

Actual fire detection at $T_{local+30\ min} \rightarrow P_F = P_T$. (ii)

In this case, if both $T_{local\ -\ 30\ min}$ and $T_{local\ +\ 30\ min}$ observations are cloud free, condition (i) will prevail. For area A2 in Figure 2.6, a cloudy pixel observed during local hour T_{local} will have the trend in fire progress being inversely described according to the following criteria:

Actual fire detection at $T_{local\text{-}30\ min} \rightarrow P_F = P_T$ (i)

Actual fire detection at $T_{local+30\ min} \rightarrow P_F = 1$. (ii)

In this case, condition (ii) will prevail when both $T_{\text{local}\ -30\ \text{min}}$ and $T_{\text{local}\ +\ 30\ \text{min}}$ observations are cloud free. Lastly, for area A3 in Figure 2.6 a cloudy pixel detected during local hour T_{local} will receive a nominal probability P_T if either $T_{\text{local}-30\ \text{min}}$ or $T_{\text{local}\ +\ 30\ \text{min}}$ observations are cloud free and a fire detection exists for any of those two observations.

To verify the consistency of the outputs produced we tested the cloud obscuration processing described above using simulated cloud coverage data in combination with the actual fire detection data from WF-ABBA. We used year 2005 cloud mask product to simulate the presence of clouds over randomly selected clear sky pixels found across the study area. The cloud obscuration analysis was then performed for those pixels selected in order to obtain the predicted number of fires missed due to clouds. For each pixel analyzed the actual fires detected by WF-ABBA were identified. The results were aggregated using the 40×40 km grid and the relationship between predicted fires versus observed fires assessed. The simulations demonstrated the predicted fires to be highly correlated with the observed fires (R^2 =0.82) (Figure 2.7). The sum of all fires produced by the cloud obscuration processing was able to represent the actual fires missed due to clouds to within 1.5% on an annual basis and to within 5% on a monthly basis.

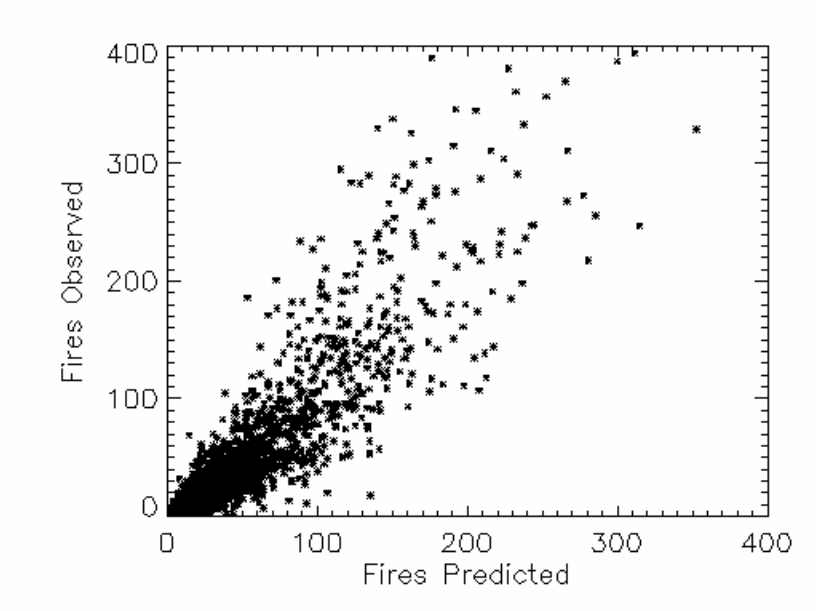

Figure 2.7. Relationship between fires produced by the cloud obscuration processing based on simulated data and observed fires for the same locations using 2005 data.

2.4 RESULTS AND DISCUSSION

The main processing code was used to process year 2005 data and the results are presented below. The numbers produced represent those cases where a cloud obscured pixel was identified and at least one of the criteria established above was met for any of the 17,520 annual GOES observations over an area of 5.4 million km^2 (335,800 pixels at 4×4 km spatial resolution) covering Brazilian Amazonia. The probability of fire omission derived for each pixel was accumulated over multiple hours and days of observation resulting in a total number of fires potentially missed due to the presence of clouds equivalent to 59,650, or approximately 11% of the actual GOES fires detected during 2005 (545,286 total — representing WF-ABBA's fire types 0–4 only; category 5 associated with low probability fires not considered) (Figure 2.8).

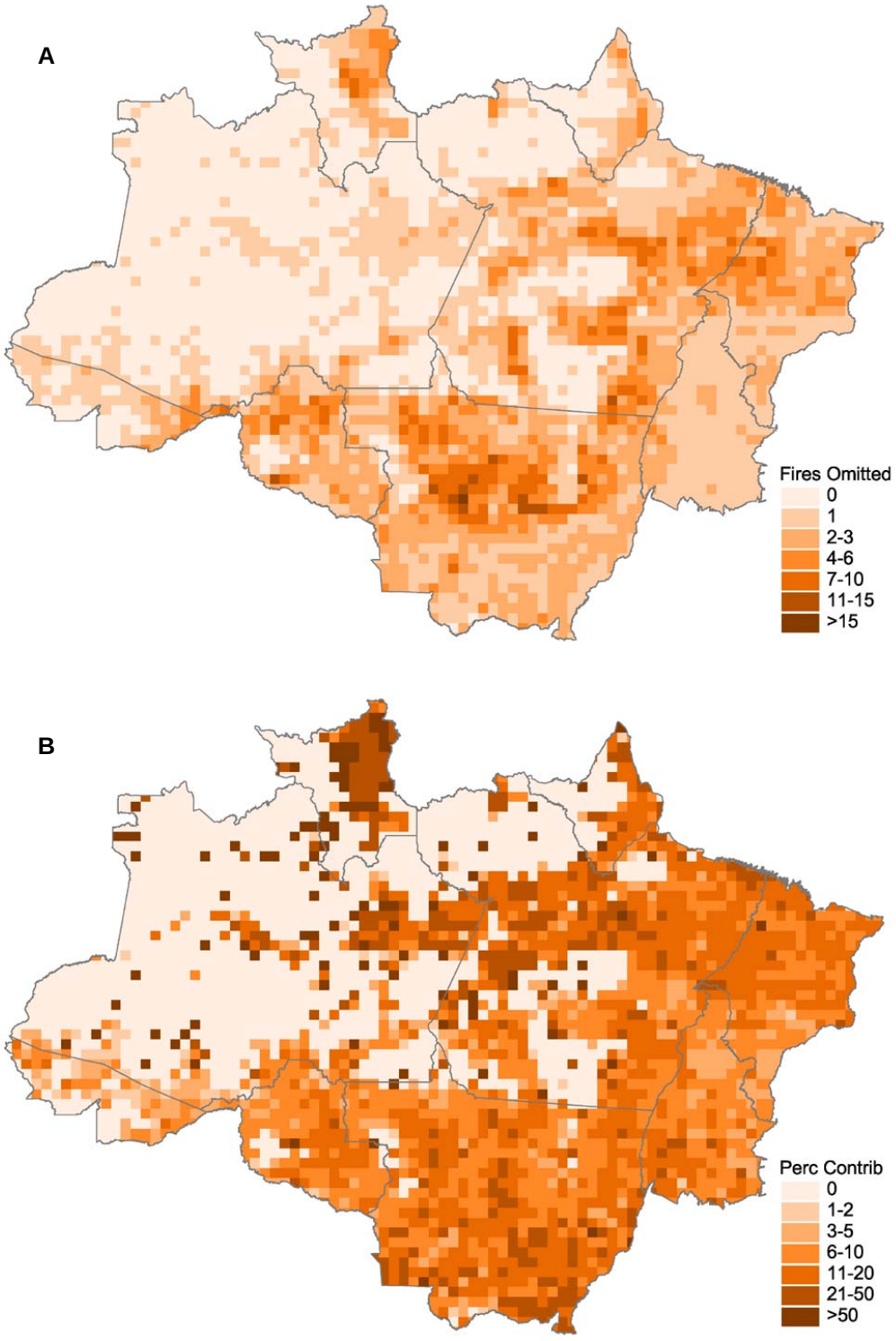

Figure 2.8. Fires omitted due to clouds (A) for year 2005 and the percentage contribution (B) of cloud adjusted fires in relation to the total number of GOESWF-ABBA fires detected in that same year for each 40×40 km grid cell covering Brazilian Amazonia.

The 2005 data set was also processed using the simple approach for compensating for clouds, which is based on the assumption that fires occur at the same frequency under clouds as they do in cloudless areas [Cardoso *et al*., 2003; Giglio *et al*., 2003b, 2006; Roberts *et al*., 2005]. In order to evaluate the impact of spatial sampling, the simple approach was implemented using two different grids of 40×40 km and 120×120 km resolution each. The average fire frequency was calculated for the cloud free fraction of each grid cell based on:

$$F_{F,i} = \frac{D_{z,i}}{S_{z,i}} \tag{10}$$

Where D_z is the number of actual fires detected within grid cell z during observation hour i, and S_z is the number of 4×4 km cloud free pixels in the same area. The number of cloud obscured pixels in each cell (i.e., 100—$S_{z,i}$ and 900—$S_{z,i}$ for the 40×40 km and 120×120 km grids, respectively) was then multiplied by Eq. (10) in order to derive the number of fires potentially missed. For both 40 km and 120 km grid resolutions used, the simple approach produced a larger number of potentially missed fires due to cloud obscuration (178,968 and 241,804 – 33% and 44% increment – respectively) as compared to the proposed methodology described above (Figure 2.9). The difference was particularly important in areas where fires were unequally distributed in space, causing fire free pixels (e.g., pixels located in forested areas and distant from human activities) to be erroneously classified as fire omission areas by the simple rule approach. The use of LUTs describing the fire activity in space helped reduce this effect with the methodology proposed by only selecting fire prone pixels during the cloud obscuration processing.

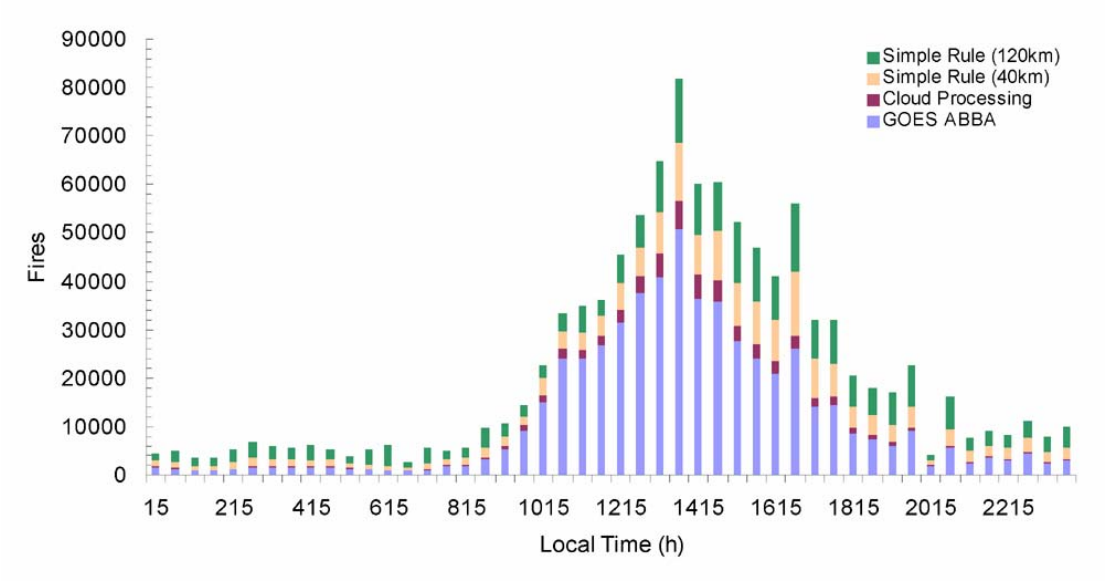

Figure 2.9. GOES WF-ABBA fire diurnal cycle distribution for Brazilian Amazonia and the corresponding adjustment produced using the cloud obscuration processing methodology and the simple rule approach using 40 km and 120 km sampling areas.

The majority of the fire omissions identified by the proposed methodology were associated with the conditions described by scenario 1, where all three observation hours $T-30$ min, T, and $T+30$ min are obscured by clouds. Average cloud coverage in the region varied between a minimum of 22% and a maximum of 78% depending on the observation hour, with the lowest values found in the areas surrounding the evergreen tropical forests in the southern and eastern parts of the basin (Figure 2.10). These areas are generally composed of Cerrado (savanna) vegetation and transition forests. The highest values occurred in the western part of the basin where the hydrological cycle is enhanced by the prevalence of closed canopy forests resulting in high evapotranspiration rates and by westerly winds that bring supplemental moisture from the eastern parts of the basin. From the remote sensing perspective, this spatial distribution of fires and cloud coverage is beneficial

as it minimizes the cloud obscuration problem in areas where fire activity is most pronounced (e.g., the states of Mato Grosso, Tocantins, Maranhão, and eastern Pará). Minimum cloud coverage was found to coincide with the early afternoon observation hours (Figure 2.10), which has major implications for fire detection as it approaches the hour of maximum fire activity in the region [Giglio, 2007; Kaufman *et al*., 1998a; Prins *et al*., 1998]. This latter finding corroborates the discussion presented in Schroeder *et al*. [2005] where inter-comparison analyses using multi-sensor fire data and visual confirmation of smoke plumes demonstrated the strong diurnal signature of fire activity in the region.

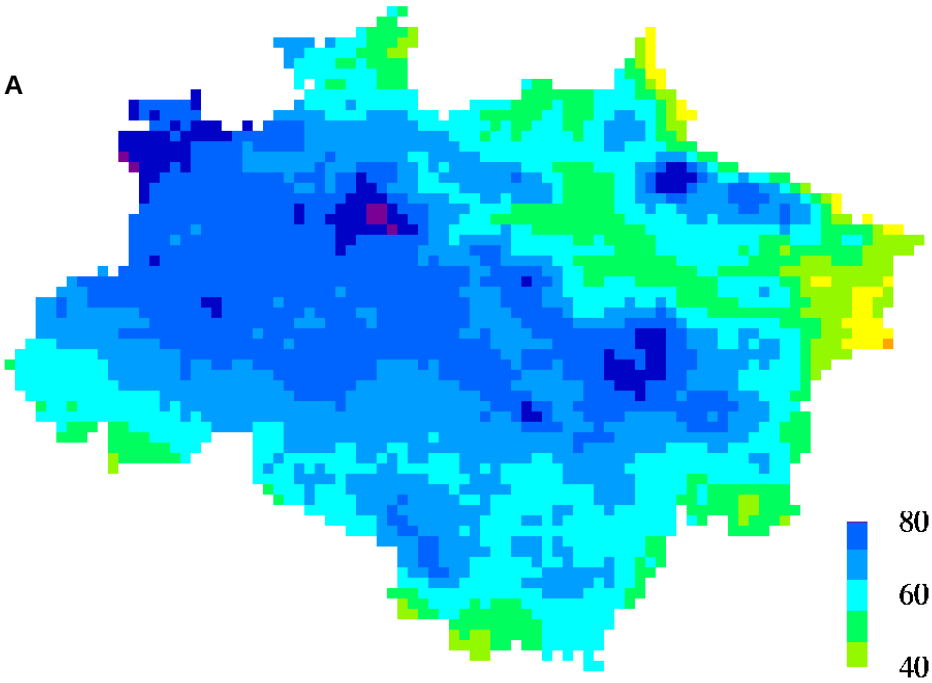

Figure 2.10. Average maximum and minimum percentage cloud coverage (A and B respectively) and hours of maximum and minimum occurrence arranged in 3 hour bins (C and d respectively).

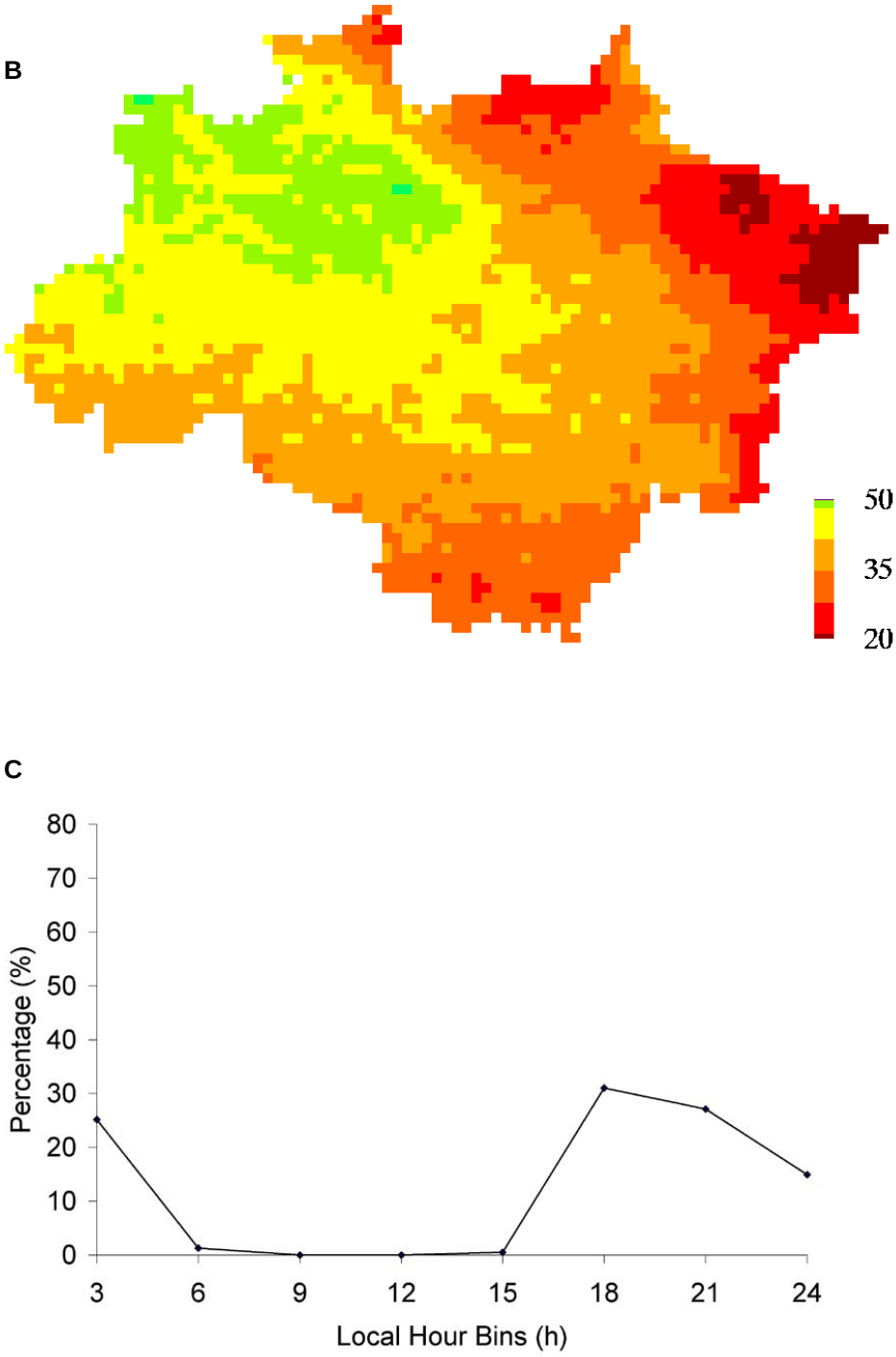

Figure 2.10. *continued*

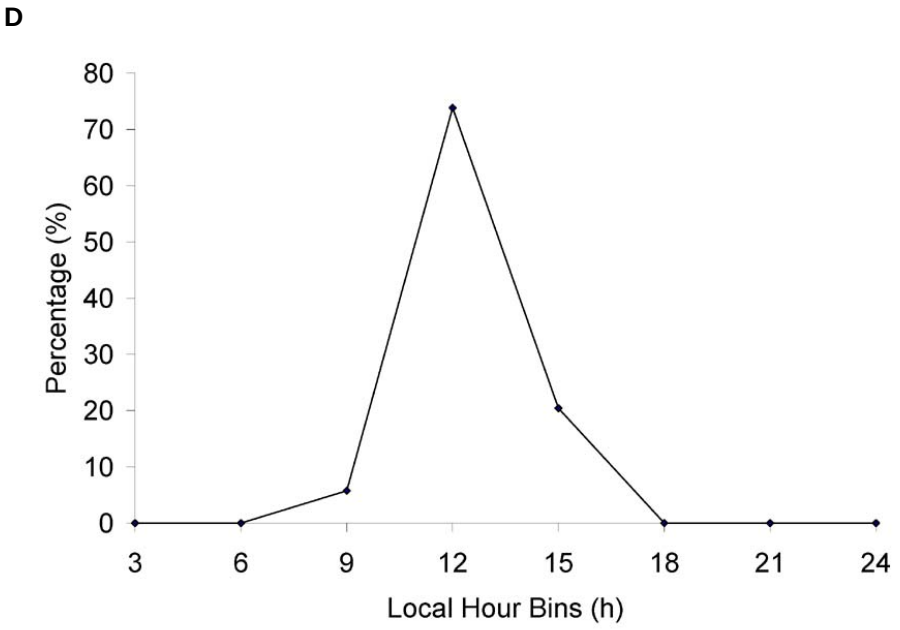

Figure 2.10. *continued*

In order to evaluate the implications of the method implemented above we used high resolution (20 m) China–Brazil Earth Resources Satellite (CBERS-2) burn scar maps to delineate areas of fire activity relating those areas to the fire omission pixels produced. The burn scar maps were generated for the state of Acre in the western Brazilian Amazonia covering the 2005 fire season in the region (July–September). Using supervised classification we produced a burnt area mosaic based on 9 CBERS images corresponding to two individual scene locations (i.e., path 180 rows 111 and 112) covering from early to late fire season in 2005 (i.e., July to October respectively). Detailed mapping of burn scars resulting from maintenance

(e.g., pasture and agricultural) and conversion (e.g., slash and burn) fires was produced for an area of roughly 22,000 km^2. The quality of the burnt area mosaic was assessed using GPS points and digital photos collected from 40 h of over-flights from which all burnt area sites inspected could be visually confirmed [Foster Brown — personal communication 2005]. Cloud obscuration in the region is known to significantly influence active fire products, usually limiting detection capacity irrespective of the sensor used [Brown *et al*., 2006]. The GOES WF-ABBA fire counts (excluding fire category 5) were spatially aggregated into nominal 4×4 km cells along with the burn scar areas and the fire increments produced independently by the method proposed above and the simple rule approach (using 40 km and 120 km grid resolutions) and error matrices were derived (Table 2.2a–d).

The original WF-ABBA active fires detected during the same period covered by the burn scar map showed an omission error of 58.3% and a commission error of 6.4%; multiple detections were frequently observed for individual 4×4 km cells across the area. Despite the reasonably high omission error, 4110 of a total of 4133 fire detections observed during the period analyzed had a spatially coincident burn scar (i.e., within ± 2 km of WF-ABBA's fire pixel coordinate); whereas 15 of 23 fire coordinates associated with false detection had large burn scars located in the immediate vicinity of the pixel. Nevertheless, the fire pixels detected accounted for 76% of the total area burned measured for the selected plot; with the remaining 24% associated with omission showing significantly different characteristics of mean burnt area size (4 times smaller than the confirmed detections) therefore potentially falling outside the detection envelope of the GOES imager.

Table 2.2: Error matrices for evaluating the performance of the original GOES WF-ABBA active fire data (a), the cloud processed data (b), and the simple rule approach using 40 km and 120 km area sampling (c, d respectively) based on 20 m resolution CBERS data (our "ground truth") covering part of Acre state in western Brazilian Amazonia.

	CBERS — fire	CBERS — non fire
(a)		
GOES — fire	519	8
GOES — non fire	727	117
Errors (omission/commission)	58.3%	6.4%
(b)		
Cloud processed — fire	702	11
Cloud processed — non fire	544	114
Errors (omission/commission)	43.7%	8.8%
(c)		
Simple rule (40 km) — fire	1116	79
Simple rule (40 km) — non fire	130	46
Errors (omission/commission)	10.4%	63.2%
(d)		
Simple rule (120 km) — fire	1246	125
Simple rule (120 km) — non fire	0	0
Errors (omission/commission)	0%	100%

The application of the cloud obscuration processing method showed a reduction in the omission error to 43.7% along with a minor increment of the commission error (8.8%). The pixels selected in this latter case accounted for 88% of the total area burned measured. The mean burned area size resembled the mean area size associated with the original WF-ABBA fire product to within 15%.

The application of the simple rule approach showed a major reduction of the omission errors for both 40 km and 120 km grids used (10% and 0%, respectively) at the cost of substantial commission errors being produced (63% and 100%,

respectively). The mean burned area size described by the simple rule approach was considerably smaller (45%) as compared to the value observed with the original WF-ABBA data, with the burned area frequency histogram having shifted towards smaller burn scars. Despite the improvements observed primarily in terms of the reduction of omission errors, the additional fires created during processing of the cloud obscuration did not have a significant impact on the relationship between the accumulated fire counts obtained for an individual pixel area and the associated size of the burn scar measured for that same plot. That relationship remained unresolved for all four data sets analyzed (i.e., the original GOES WF-ABBA active fire data, the cloud adjusted numbers derived with the above methodology, and with the simple approach at 40 and 120 km), with weak correlation being observed in all cases.

2.5 FINAL REMARKS

Fire detection omission due to cloud obscuration is a major problem affecting remote sensing of active fires. Here we described an approach designed to address the cloud obscuration problem using high frequency geostationary observations. The methodology takes advantage of three different input data, namely precipitation estimates, a cloud mask and active fire data that are derived from the same instrument. This consideration was especially important for facilitating data registration and also to reduce image navigation problems that can occasionally affect the GOES data. The use of active fire data from recent years along with precipitation data provided means to establish the general patterns of fire use in both space and

time across the entire study area, at the same time preserving specific regional and local characteristics with the implementation of pixel based processing.

The strong correlation between the predicted fires missed and the actual fires observed demonstrated the effectiveness of the approach. In terms of the overall trends caused by cloud obscuration across Brazilian Amazonia, we observed that the net effect of fire omission was partially minimized in areas of intense fire activity as these generally coincided with the areas of minimum cloud coverage. Nonetheless, in relation to the percentage contribution of fires missed due to clouds, we found areas where fire omission was significant (Figure 2.8) despite those being depicted as relatively low fire activity areas by the original WF-ABBA product (Figure 2.1). This could signal the need to more detailed analysis of fire dynamics in areas considered to be of low priority under current regional fire management programs (e.g., northeastern Roraima).

Another important aspect presented was the partial overlap between the hours of minimum cloud coverage and of maximum fire activity as a result of a strong basin-wide fire diurnal cycle signature. The cloud adjusted numbers maintained the same fire diurnal cycle signal confirming our field observations that indicated systematic use of fires in the mid-afternoon hours as part of regional land management techniques. As compared to a more simplistic approach, the methodology was proven successful in reducing the omission errors while maintaining the commission errors nearly unchanged, and preserving the general quality of the fires described by the original fire product from WF-ABBA.

By means of routine updating of the LUTs used during processing, this cloud obscuration modeling technique should be capable of consistently mapping fire omission in tropical areas such as Brazilian Amazonia. While the number of fire pixels missed due to clouds could be successfully defined, additional work is required to better describe the relationship between active fires and the total area burnt which modeling of biomass emissions so much depend on.

We consider this methodology to be applicable to other geostationary systems covering different regions of the globe provided that similar data layers are available for use. The proposed cloud correction scheme can be included in the current effort by the Global Observation of Forest and Land Cover Dynamics (GOFC-GOLD) Fire Mapping and Monitoring Theme (URL:http://gofc-fire.umd.edu) to establish a global fire monitoring network from geostationary satellites. This activity, also being coordinated using principles of the Committee on Earth Observation Satellites (CEOS; URL: http://www.ceos.org) constellation concept and incorporated into the Coordination Group for Meteorological Satellites (CGMS; URL: http://www.wmo.ch/web/sat/CGMShome.html) is also a contributor to Group on Earth Observations (GEO; URL: http://www.earthobservations.org/index.html) efforts. However, we must warn for the fact that sensor dependencies (e.g., detection omission and commission rates) need to be resolved before any global analysis of the effects of clouds on remote sensing fire products is attempted.

In principle, an improved scheme to correct for cloud obscuration effects is also needed for active fire detections from polar orbiting satellites. Consistent correction is needed to integrate all geostationary and polar orbiting data into a long-

term active fire data record as part of the Fire Disturbance Essential Climate Variable (ECV) as defined in the Global Climate Observing System Implementation plan (GCOS; URL: http://www.wmo.ch/web/gcos/gcoshome.html). However, due to their limited observation frequency, polar orbiting satellites would require a different approach from the one presented here for the estimation of fire omission due to clouds. For instance, scenario 2 described in Section 2.3.3 which uses the information from adjacent observations of GOES (30 min before and after observation time *t*) would not be applicable to a polar orbiting system. Other issues such as variable imaging geometry would also impact the cloud analysis using sensors such as MODIS and AVHRR.

Chapter 3: Validation of GOES and MODIS Active Fire Detection Products Using ASTER and ETM+ Data[1]

3.1 INTRODUCTION

Brazilian Amazonia currently represents one of the most active regions of deforestation and biomass burning in the world [Csiszar *et al*., 2005; Dwyer *et al*., 2000; Giglio *et al*., 2006]. Widespread use of fires for land clearing and management necessitates consistent methods for monitoring and mapping biomass burning on a routine basis [Korontzi *et al*., 2004; Schroeder *et al*., 2005].

The number of operational or near-operational fire products serving Amazonia has increased considerably in the past decade as a result of growing demand for fire information from the regional and global scientific communities, environmental enforcement agencies, and other end users. Information on fire activity for Amazonia is currently available from geostationary and polar orbiting satellites [CPTEC, 2008; Govaerts, *et al*., 2007; UW Madison CIMSS, 2008].

While some studies have assessed the performance of the polar orbiting and geostationary active fire products through validation exercises [Menzel and Prins, 1996; Prins *et al*., 1998; Morisette *et al*., 2005a; Morisette *et al*., 2005b; Csiszar *et al*., 2006], detailed characterization of these products on a regional to sub-continental

[1] The material presented in this Chapter is part of Schroeder *et al*. [2008b]

scale is still needed. The increased demand for these products requires that an effort be made to fully characterize the quality of their data.

In this study we investigate the performance of two major active fire detection products available for Brazilian Amazonia derived from the polar orbiting Moderate Resolution Imaging Spectroradiometer (MODIS), on board the EOS-AM (Terra) and EOS-PM (Aqua) satellites, and the imager on board the Geostationary Operational Environmental Satellite, positioned at 75°W longitude along the equator (GOES-East). We use a large selection of scenes from the Advanced Spaceborne Thermal Emission and Reflection Radiometer (ASTER) and the Landsat 7 Enhanced Thematic Mapper Plus (ETM+) at 30 m resolution to serve as our "ground truth" data to validate the coarser resolution products. The scene selection covers a wide range of vegetation fire conditions that are found across the study region.

We rigorously test the accuracy of the MODIS and GOES active fire products to quantify sources of commission and omission errors, and suggest a method to enhance the current contextual fire detection algorithms using brightness temperature temporal profiles to reduce the commission error rate over tropical forest regions. We apply a bottom-up approach by associating the fire statistics derived from the 30 m resolution data to the moderate and coarse resolution data of MODIS and GOES, respectively. Complementary *in-situ* measurements are also used in this study along with data from an airborne imaging instrument to independently analyze the properties of the fires mapped by the orbital systems.

3.2 DATA

The data used in this study cover nine states that form the Legal Brazilian Amazon, an area characterized by a large gradient of percentage tree cover (see Figure 3.1). In order to represent all of this variation in the validation process of GOES and MODIS, a large volume of data was processed. The details of each individual data set are given below:

3.2.1 GOES

The study region is centered within the regular scanning zone of the GOES East imager which produces 4×4 km resolution images at 30 min intervals. Centered in the fire sensitive mid-infrared region of 3.8–4.0 μm, channel 2 provides the primary radiometric measurement for GOES imager fire detection. In order to increase our sample size, we used a combination of versions 5.9 (2000–2002) and 6.0 (2002–2005) of the Wildfire Automated Biomass Burning Algorithm (WF-ABBA) generated by the Cooperative Institute for Meteorological Satellite Studies (CIMSS) at the University of Wisconsin, Madison. The two products are very similar; changes in version 6.0 were mainly associated with the implementation of more stringent tests to eliminate potential spurious fires from highly reflective clouds [Prins and Menzel, 1994; Prins *et al*., 2003].

We used the full resolution active fire masks provided by CIMSS as well as the regular ASCII data files commonly available to end users. GOES channel 2 Variable Format (GVAR) data were also obtained from NOAA's Comprehensive

Large Array data Stewardship System (NOAA-CLASS; URL: http://www.class.noaa.gov/saa/products/welcome). The GVAR data were used for the purpose of image registration as well as to derive brightness temperature estimates used in Section 3.4.4. A total of 119 individual images were used for the validation analysis covering the acquisition dates and hours of ASTER or ETM+ data. An additional 446 images were used in the analyses described in Sections 3.4.3–3.4.4.

3.2.2 MODIS

The two MODIS instruments on board the polar orbiting Terra and Aqua satellites provide daily images of Amazonia at nominal 1×1 km spatial resolution. We used the Collection 4 MODIS Level 2 (un-projected swath) fire product (MOD14) [Giglio *et al*., 2003a], available from NASA's Land Processes Distributed Active Archive Center (LP-DAAC) (URL:http://edcimswww.cr.usgs.gov/pub/imswelcome/), in conjunction with the MODIS geolocation product (MOD03), available from NASA's Level 1 and Atmosphere Archive and Distribution System (URL: http://ladsweb.nascom.nasa.gov/data/). A total of 135 data granules (5-minute orbit segments) from Terra MODIS were used for the validation analyses coinciding with the acquisition dates of our 2001–2005 ASTER scenes. An additional 164 MOD14 data granules were used along with the corresponding Level 1B Calibrated Radiance granules (MOD021km) to support the analyses described in Sections 3.4.3–3.4.4.

3.2.3 ASTER

ASTER is an on-demand radiometer flying on board the Terra satellite and therefore it collects data simultaneously with Terra MODIS [Yamaguchi *et al*., 1998]. Although the instrument does not possess a mid-infrared channel, active fire detection was proven successful in previous studies by combining the top of the atmosphere (TOA) reflectance estimates from channel 3 near infrared data resized from 15 to 30 m resolution and channel 8 short wave infrared data at 30 m resolution (Table 3.1) [Morisette *et al*., 2005b; Giglio *et al*., 2008].We used a total of 162 ASTER Level 1B Registered Radiance at the Sensor scenes obtained from the LP-DAAC (Figure 3.1).

3.2.4 ETM+

The ETM+ instrument flies on board Landsat-7, which has a similar orbital path as the Terra satellite, albeit with an earlier daytime equator crossing time of 1000 [Goward *et al*., 2001]. The spatial and spectral specifications of ETM+ channels 4 and 7 are similar to those of ASTER channels 3 and 8, respectively, making ETM+ equally suitable for active fire mapping (see Appendix A). In this study we used 123 scenes available through the National Institute for Space Research (INPE, Brazil) and the Global Land Cover Facility (GLCF; URL: http://glcf.umiacs.umd.edu/index.shtml). The scenes covered the period from 2000–2003.

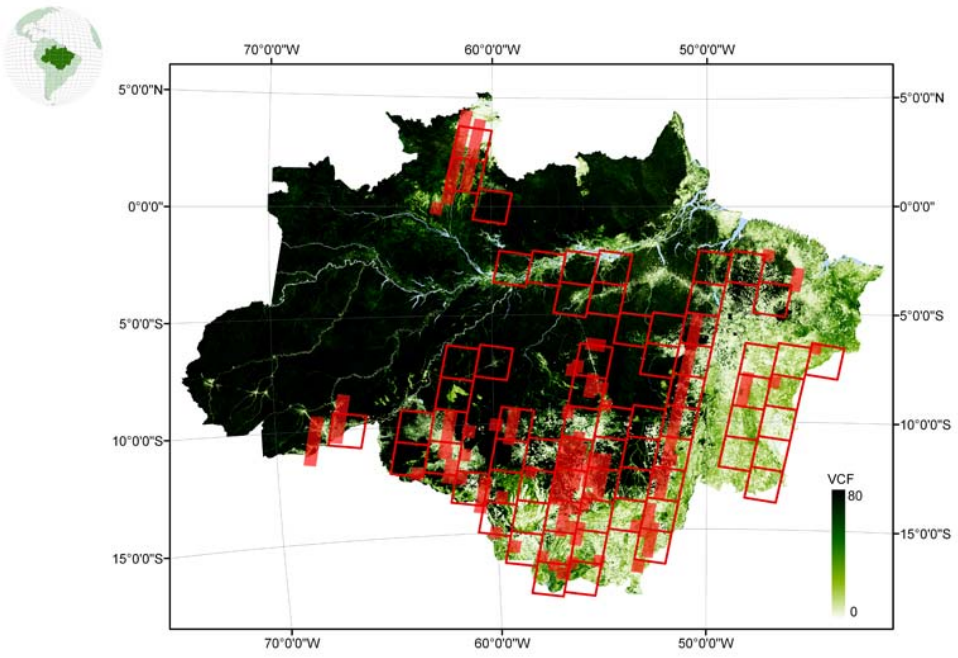

Figure 3.1: Location of ASTER (red shaded areas) and ETM+ (red open boxes) scenes used to validate the MOD14 and WF-ABBA fire detection products, over percentage tree cover data [Hansen *et al*., 2002].

3.2.5 Vegetation Data

The 500 m percentage tree cover data derived from the MODIS Vegetation Continuous Fields (VCF) [Hansen *et al*., 2002; Hansen *et al*., 2003] Collection 4 product was used in this study to stratify the study region into vegetation sub-groups. A total of 12 MODIS 10°×10° Sinusoidal Projection tiles were required to produce a mosaic covering the entire study region. The annual VCF product for 2000–2005 was available through GLCF.

3.2.6 Ground Data

In-situ fire temperature measurements were obtained for seven different burning locations. These measurements were derived as part of validation campaigns implemented during 2003–2004 when prescribed burns were arranged in different parts of the study region. We used a thermocouple linked to a data logger [Campbell Scientific Inc. CR21X] which recorded the development of the fire fronts at 0.2 Hz for the duration of the burning (i.e., from fire onset through the smoldering phase). These measurements were mainly intended to characterize the differences in fire intensity and duration among the main fire types typically observed in the study region.

3.2.7 Airborne Data

Airborne data were acquired for Roraima state in northern Brazilian Amazonia using the Airborne Hyperspectral Scanner [AHS AA5201, Argon ST] over two prescribed burns and over 90 randomly chosen fires during a 7-day field campaign in January 2003. The AHS sensor consists of a 50 channel scanner covering 0.445–12.08 μm. The instrument is owned and operated by the System for the Protection of Amazonia (SIPAM) and it was first flown over vegetation fires during the field campaign in January 2003. We applied supervised tests to the data in order to produce fire masks at ground resolutions of 1–1.65 m. The fire masks were used to delineate the contour of the active flaming areas in each image.

Table 3.1: Main characteristics of the satellite imagery used.

Instrument	*Primary Bands Used for Fire Detection*	*Spatial Resolution*	*Temporal Resolution*	*Number of images*
GOES Imager	Channel 2: 3.80-4.00µm	4km	30min	565
MODIS	Channels 21 & 22: 3.929-3.989µm	1km	1-2days	299
ASTER	Channel 8: 2.295-2.365 µm	30m	16days	162
ETM+	Channel 7: 2.09-2.35 µm	30m	16days	123

3.3 METHODS

Three previous studies relied on ASTER data to validate the Terra MODIS active fire detection product. First, Morisette *et al*. [2005b] used 18 ASTER scenes from August–October 2001 to validate the MOD14 collection 3 and 4 products over Southern Africa. Next, Morisette *et al*. [2005a] used 22 ASTER scenes to simultaneously validate two different active fire detection products based on Terra MODIS data for three sites in Brazilian Amazonia. Lastly, Csiszar *et al*. [2006] used 131 ASTER scenes to validate the MOD14 collection 4 product over Siberia. All three studies used active fire masks derived from ASTER imagery to validate the coincident Terra MODIS active fire product.

In order to validate and characterize the MOD14 fire product over Brazilian Amazonia, we used a similar approach as described in the studies listed above. We produced active fire masks for all 162 ASTER scenes using a contextual approach based on ASTER channels 3 (0.76–0.86 µm) and 8 (2.295–2.365 µm) [Giglio *et al*.,

2008]. The resulting 30-m mask indicates the presence ("1") or absence ("0") of active fires within each moderate-to-coarse resolution pixel, and 30-m pixel counts are used as surrogates for actively burning area. We recognize this is still an intermediate step towards deriving validation statistics based purely on "true" physical quantities defining fires.

We used information from the Terra MODIS geolocation product (MOD03) to overlay the MOD14 product on top of the ASTER fire masks. From the fire mask data we derived the sum of 30-m active fire pixels and the number of individual fire clusters within each MODIS pixel. These statistics were used to determine the detection performance of the MODIS instrument by means of a statistical logistic regression model defined as:

$$P(x_i) = \frac{e^{\alpha + \sum_{j=1}^{n} \beta_j x_{ij}}}{1 + e^{\alpha + \sum_{j=1}^{n} \beta_j x_{ij}}} \qquad (1)$$

Here $P(x_i)$ is the probability of detection (0-1) of MODIS pixel i based on the linear combination of ASTER fire pixel summary statistics ($j = 1, n$), and α and β_j are parameters derived from the data [Agresti, 1990; Morisette *et al*., 2005b]. Error matrix analysis was also applied using information on the number of 30-m active fire pixels to produce empirical curves defining the omission error estimates for the MODIS fire product.

In order to account for the effects of the MODIS triangular point spread function [Wolfe *et al*., 2002], the projected surface area for the MODIS pixel was considered equal to 2×1 km at the sub-satellite point. This procedure is applied for all MODIS pixels overlapping the ASTER image.

We tested the consistency of the fire masks using 1.5 m resolution data from the AHS instrument over two prescribed burns conducted in January 2003 which were coincident with ASTER imaging (Figure 3.2). Additionally, hundreds of image quick looks were produced to verify the consistency of the MOD14 detections when overlaid on top of the ASTER fire masks and false color composites.

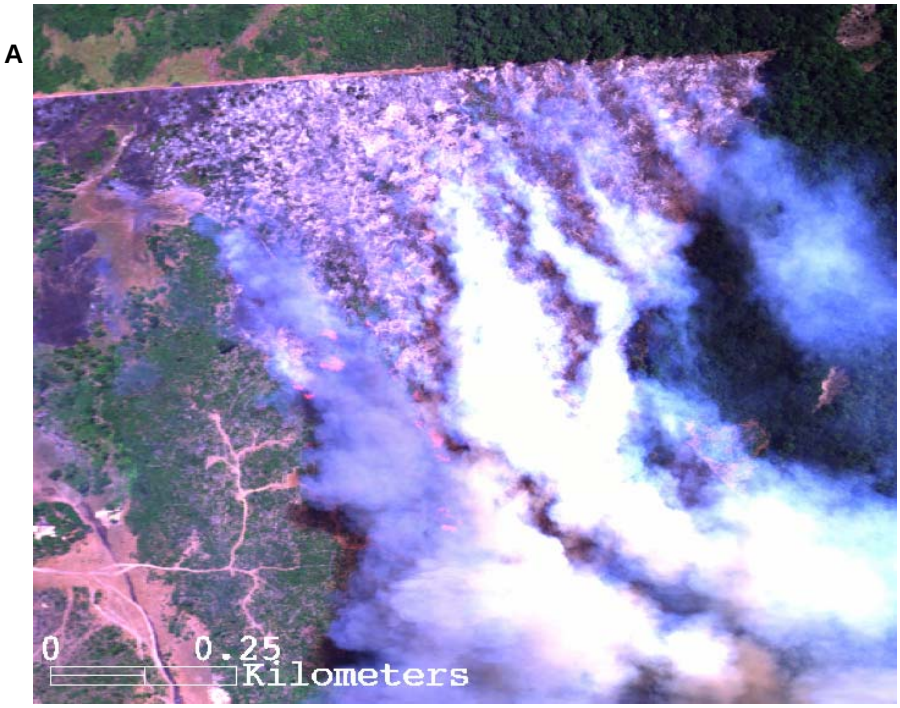

Figure 3.2: Prescribed burn of a deforestation plot located at 1º35'08" N 60º57'18"W on January 28, 2003. (A) 1.5m resolution data from AHS RGB combination of bands 9 (0.685 µm), 5 (0.565 µm) and 1(0.445 µm) acquired at 1438 UTC; (B) fire mask derived from AHS band 43 (4.95 µm); (C) ASTER image of the same fire (RGB bands 8-3-1) acquired at 1436 UTC. The fire perimeter (white contour) derived from the ASTER fire mask is also shown in (C).

B

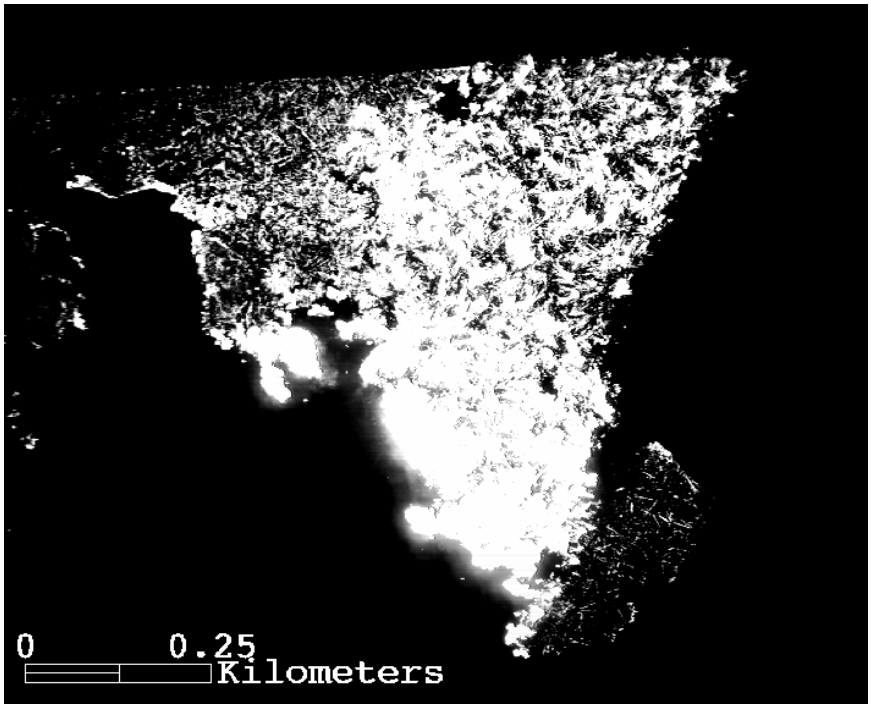

C

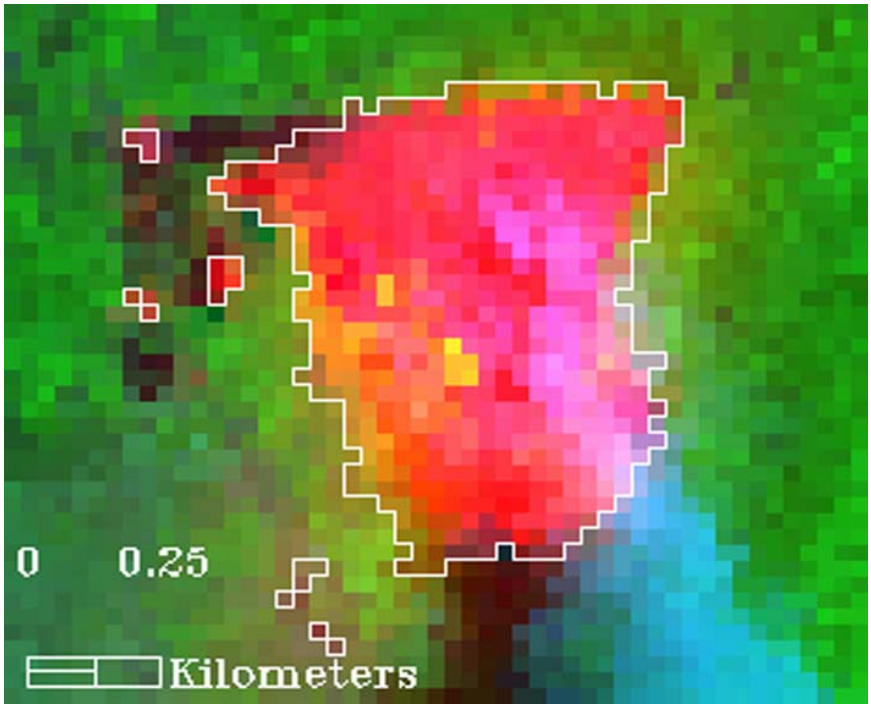

Figure 3.2 *continue*d

Our validation analyses of the GOES active fire detection product followed a similar approach to the one described above for the MODIS data. However, three major issues necessitated that a slightly different processing scheme be used for the GOES data:

(i) Temporal differences in image acquisition needed to be considered in order to avoid the effects of short-term changes in fire characteristics. As part of our field campaign in January 2003, multi-temporal data from the AHS instrument were acquired during a prescribed burn of a 75 ha deforestation plot in Roraima state. Approximately 1.5 hours of fire activity were monitored by the AHS instrument at 1.5 m resolution. Once the fire lines were well established and moving freely, four sequential AHS images were produced separated by 5 minute intervals from each other. We found the instantaneous fire-affected areas to be within 10% of the mean estimated area (35 ha) mapped during the 20 minute interval. In a separate study, Csiszar and Schroeder [2007] used ETM+ and ASTER images acquired 30 minutes apart to assess the impact of varying fire conditions on the performance of the MODIS active fire product. Their results suggested that short term changes in vegetation fire conditions have only a minor impact on moderate resolution active fire products. In this study we adopted a conservative approach limiting the use of the 119 GOES images

selected for the validation analysis to within 15 minutes of the acquisition of the available higher resolution data.

(ii) Navigation errors are known to affect the GOES images on a regular basis, and image geolocation problems can occur even between 30 minute acquisitions [Menzel and Purdom, 1994]. To eliminate the problem, all GOES images used were manually co-registered to within 1 pixel.

(iii) Due to the coarse resolution of the GOES imager, fewer pixels are sampled compared to MODIS for the same area covered by ASTER. Consequently, a larger number of ASTER scenes must be processed in order to create an equivalent sample size. Alternatively, one can use ETM+ data to increase the area covered by each scene processed (see Appendix A). Therefore our validation of the WF-ABBA product used ASTER and ETM+ fire mask data to produce 30 m active fire summary statistics for all co-located GOES pixels within a 15 min window between acquisition times.

For projecting the GOES pixel area on top of the higher resolution data we used a full nominal resolution pixel size in the along and across scan directions (i.e., 4×4 km in size near nadir). We considered this area estimate to be a good balance between the pixel size resulting from the over-sampled image matrix and the pixel dimensions if accounting for the GOES point spread function.

3.4 RESULTS AND DISCUSSION

Two major types of fires are normally observed across our study region, namely conversion and maintenance fires. Conversion fires will normally be associated with deforestation activities occurring along the new frontiers of land development dominated by high percentage tree cover (i.e., > 60%). As they burn large biomass volumes, these fires will normally be characterized by high flame temperatures followed by a relatively hot smoldering stage which can last from a few hours to a few days (Figure 3.3). Maintenance fires are normally used to rejuvenate pastures or to clear crop residue and are particularly important in areas dominated by low percentage tree cover (i.e., < 20%). As such, these fires are characterized by relatively low flame temperatures followed by a shorter smoldering stage ranging from a few minutes to a few hours. Compared to conversion fires, maintenance fires show a narrower flaming front as well as a shorter smoldering stage (Figure 3.3). Between these two major classes we can also find intermediate fire types (e.g., fires resulting from the clearing of secondary forests and woody *Cerrado* (savannas)) with reduced biomass load compared to old growth or pristine tropical forests. These fires can be more variable in terms of their flame temperature and burning duration. Data in Figure 3.3 suggest that the intensity and duration of conversion fires may facilitate their detection as compared to other types of tropical vegetation fires.

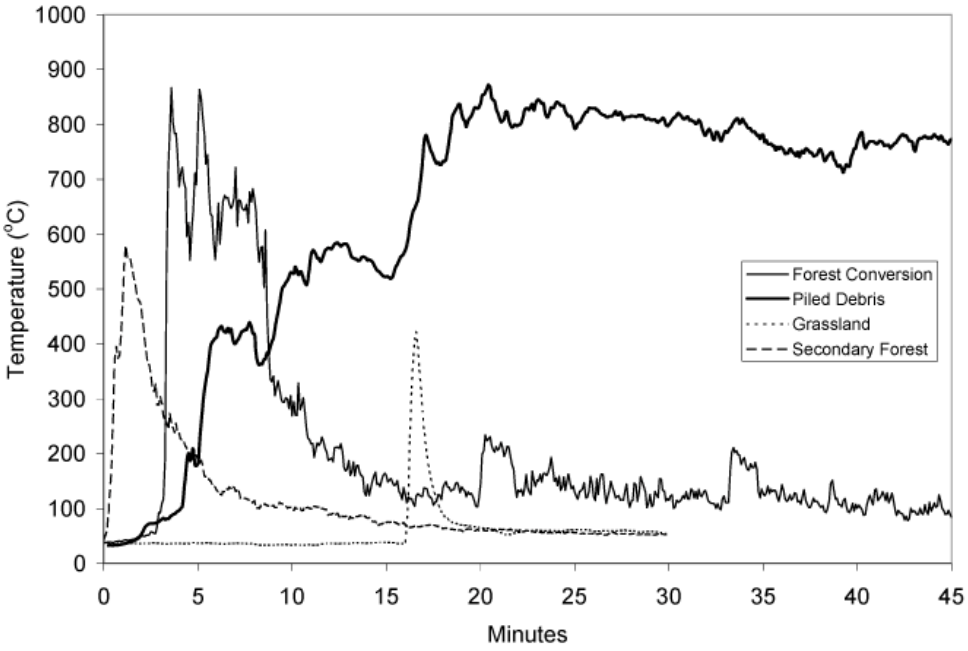

Figure 3.3: Typical temperature profiles associated with fires used for: forest conversion, burning of piled debris from deforestation, rejuvenating grassland, and clearing of secondary forest re-growth.

3.4.1 Overall Detection Performance

The processing of all pairs of MODIS-ASTER images resulted in approximately 7,300 MODIS pixels containing at least one ASTER 30 m active fire pixel. A total of 1,640 MOD14 pixels were flagged as "fire" for that data set. The pairs of GOES-ASTER images resulted in approximately 2,900 GOES pixels containing at least one ASTER active fire pixel; the pairs of GOES-ETM+ images covered another 14,500 GOES pixels with at least one ETM+ 30 m active fire pixel. This entire dataset included a total of 560 WF-ABBA fire detections.

Summary statistics were produced from the higher resolution fire masks for all MODIS and GOES pixels sampled. These statistics were used to fit the logistic

regression model in (1), from which the general detection probability curves for MOD14 and WF-ABBA were derived. The differences in detection performance between the MOD14 and WF-ABBA fire products are shown in Figures 3.4A and 3.4B, respectively. However, the distances that separate the curves and the associated performance of the two products are smaller than expected. For the MODIS-ASTER configuration used in this study, all MODIS pixels sampled were imaged close to nadir resulting in pixels with 1×1 km nominal spatial resolution. The pairs of GOES-ASTER and GOES-ETM+ images used were acquired under slightly variable conditions in terms of the pixel size sampled, ranging from near nadir geometry to cases where the additional pixel area enlargement was equivalent to about 20%. Consequently, the spatial resolution ratio of MODIS to GOES was always greater than or equal to 16×, which should result in an equivalent difference between their detection performances. However, an approximate ratio equal to or less than 4× separates the pairs of detection curves for each tree-cover interval described by the MOD14 and WF-ABBA products in Figures 3.4A and 3.4B.

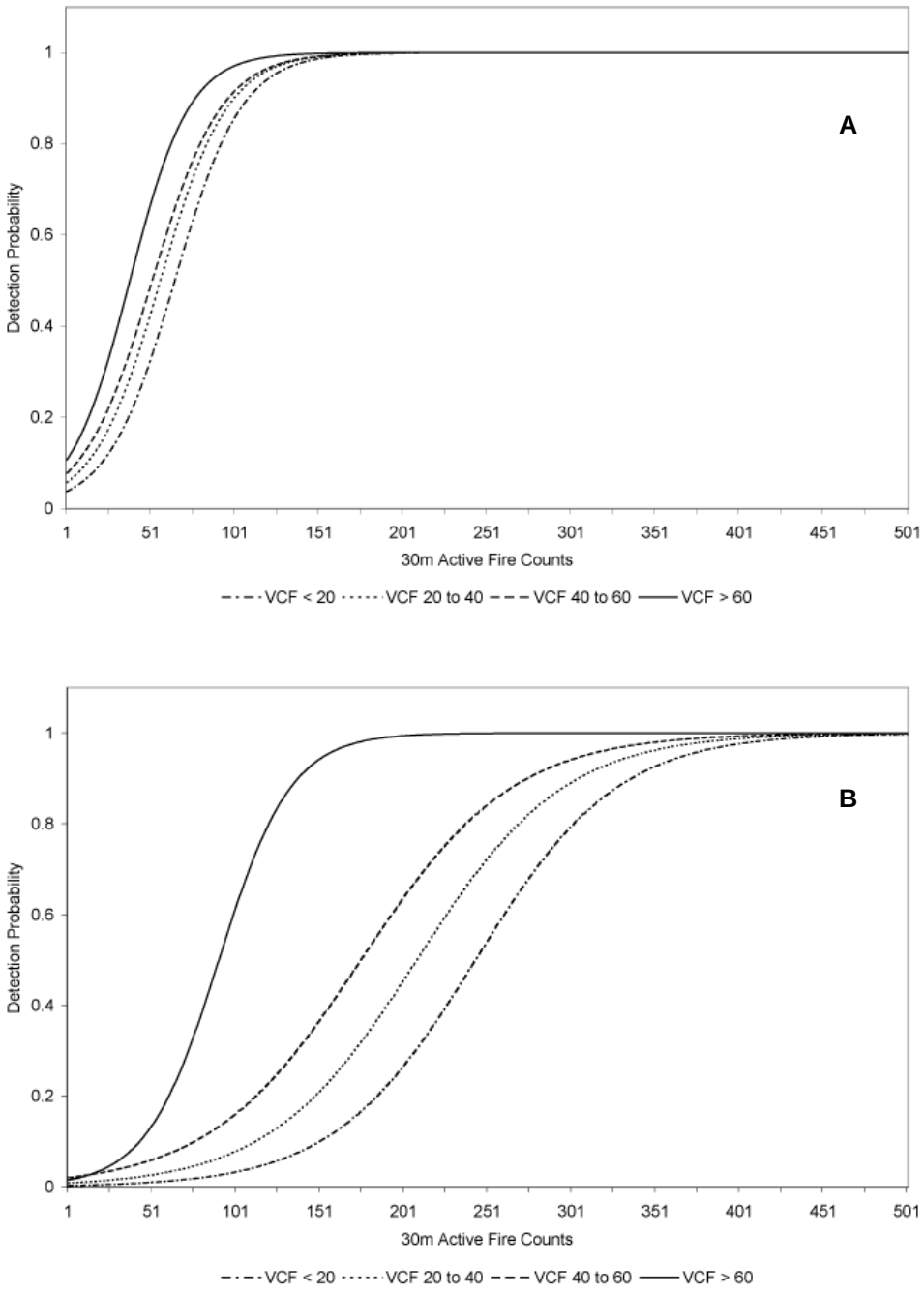

Figure 3.4: Fire detection probability curves for MOD14 (A) and WF-ABBA (B) fire detection products derived for four percentage tree cover intervals.

In the case of Figure 3.4, a one-to-one comparison of the two instruments is difficult even for a small case study analysis as differences between products will

likely be a result of: (i) varying sensor-target-sun relative positions; (ii) atmospheric attenuation, including fire obscuration by heavy smoke released during burning; (iii) relative position of the actual pixel area in relation to the location of the active fire zone and the effects of the point spread function, (iv) timing of acquisition, etc. Since the actual high-resolution validation data sets for MODIS and GOES are different, some difference in fire types may add uncertainty despite the rigorous sample used for this analysis.

Our field data indicated that conversion and maintenance fires can show temperature variations on the order of hundreds of Kelvins even over very small areas. Consequently, their peak in emittance is likely to spread over a broader spectral interval than most land surfaces (e.g., bare soils and vegetated areas). With the GOES imager having a broader mid-infrared channel compared to MODIS (Table 3.1), it is plausible that the former will sense the radiative signal from a wider range of fire temperatures. This increase in the fire signal compared to the background could produce a higher relative capacity of GOES to detect them.

3.4.2 Omission Errors

Omission estimates were empirically derived for WF-ABBA and MOD14 by assessing the number of 30 m active fire pixels corresponding to true fire detections using an error matrix analysis. We counted the number of WF-ABBA or MOD14 detections for each subset of GOES and MODIS pixels, respectively, showing a number of ASTER or ETM+ fire pixels greater or equal to *N*. By varying *N* between

1 and the maximum value in our data set (~1,200), we produced the omission error estimates for the two products (Figure 3.5).

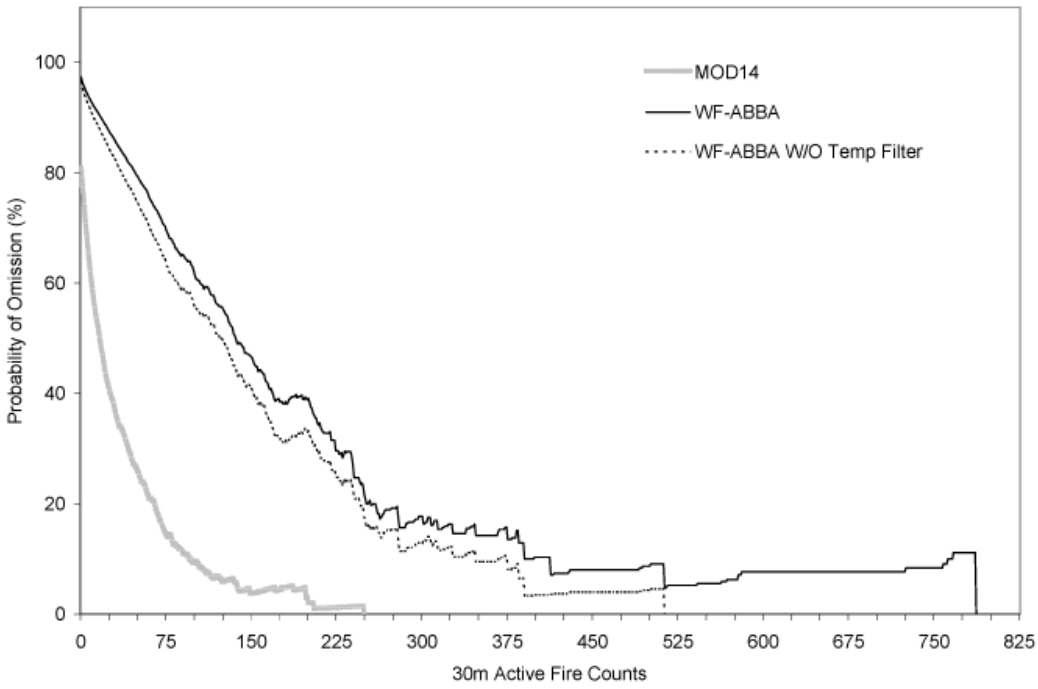

Figure 3.5: Omission error estimates produced for MODIS and GOES based on fires sampled at approximately 1030 local time.

Two areas of relatively high omission error are found for WF-ABBA at high counts of 30-m active fire pixels, one around 770 counts and a second one near 350 counts. Visual inspection of the areas affected by such large fires indicated that the vast majority of the events were indeed associated with long fire lines occurring over areas of savanna-like vegetation with associated percentage tree cover typically less than 20%. In this case, the fire characteristics are analogous to the maintenance fire

depicted in Figure 3.3. Consequently, the total radiant energy released is small compared to other types of fires rendering the detection of such events less likely. In addition, low thermal contrast with the warmer background was also found to contribute to the reduction in detection performance of WF-ABBA. In fact, we can distinguish two areas in the MOD14 curve where comparable high count omission errors are found, one near 170 counts and the second one near 245. As with WF-ABBA, the areas of high count omission in the MOD14 data were also found to be associated with fires occurring over low percentage tree cover areas.

Another factor potentially leading to high count omission errors in the GOES data is related to a nuance of the WF-ABBA detection algorithm. The detection code includes a persistence check analysis, which takes advantage of the high observation frequency of the GOES imager. The test checks each candidate fire pixel for the presence of any coincident detection in the previous 12 hours, allowing some tolerance in the spatial search criterion for small navigation drifts. In doing so, potential spurious detections can be filtered out of the product, therefore reducing commission errors. However, some new or short lived fires may also be removed from the final product. In order to quantify the effects of the temporal filtering, we also plotted in Figure 3.5 the corresponding omission error curve derived from the GOES data prior to the application of the persistency test. The result shows a significant increase in the total number of true detections produced (from 458 to 600) and a reduction of the omission errors especially towards the very high counts on the graph.

Although useful for eliminating spurious fires, the application of temporal filters could represent a problem if one considers the instantaneous impact on the omission of relatively large fires that were mistakenly discarded from the final product. However, if such fires persist and maintain or increase their size and intensity in the subsequent GOES observations hours, a second detection will likely occur over time, causing the pixel to pass the persistency test as the previous observations would serve to confirm it.

As suggested by previous studies [Giglio 2007; Menzel and Prins, 1996; Prins and Menzel, 1992, 1994; Prins *et al*., 1998], a strong fire diurnal cycle exists for regions such as Brazilian Amazonia. Under this circumstance, it is expected that fires observed during the mid to late-morning hours imaged by the ASTER and ETM+ instruments will likely grow in size and intensity towards the peak of fire activity located in the early to mid-afternoon hours. To assess the potential effects of changing fires conditions, we derived the overall omission error estimate for the WF-ABBA product data using all GOES acquisition hours following the time of observation of the fire event by the higher resolution imagery until about 20:00h local time. The resulting omission error of 38% indicates that a large fraction of the fires observed in the morning hours which have persisted over subsequent observation hours might have intensified or increased their areas therefore entering the detection envelope of the GOES imager WF-ABBA fire product.

3.4.3 Commission Errors

False detections were characterized in our analysis as those showing zero 30-m active fire pixels within their footprints. We identified a total of 245 false detections among the 1,640 detections produced by the MOD14 product, whereas 102 false detections were identified for WF-ABBA based on a total of 560 detections sampled by that product. Contrasting surface temperature between the target pixel and its background dominated the false detection occurrences of MOD14 and WF-ABBA representing 99% and 100% of the cases, respectively. Detection errors caused by the presence of clouds, sun glint zones or anthropogenic sources could not be identified in the data set.

The areas of high thermal contrast were particularly pronounced along the deforestation expansion regions throughout Brazilian Amazonia where relatively cool evergreen tropical forests are replaced by bare soil and senescent grasses -- surfaces with increased surface temperature. Despite the differences in instrument characteristics, spatial resolution and algorithm used, both products agree to a large extent in the commission errors produced for all four percentage tree cover intervals considered (Figure 3.6). Errors increase rapidly as a function of the percentage tree cover indicating a potentially larger thermal contrast between the target pixel - often characterized by little or no vegetation - and the gradually greener and cooler background.

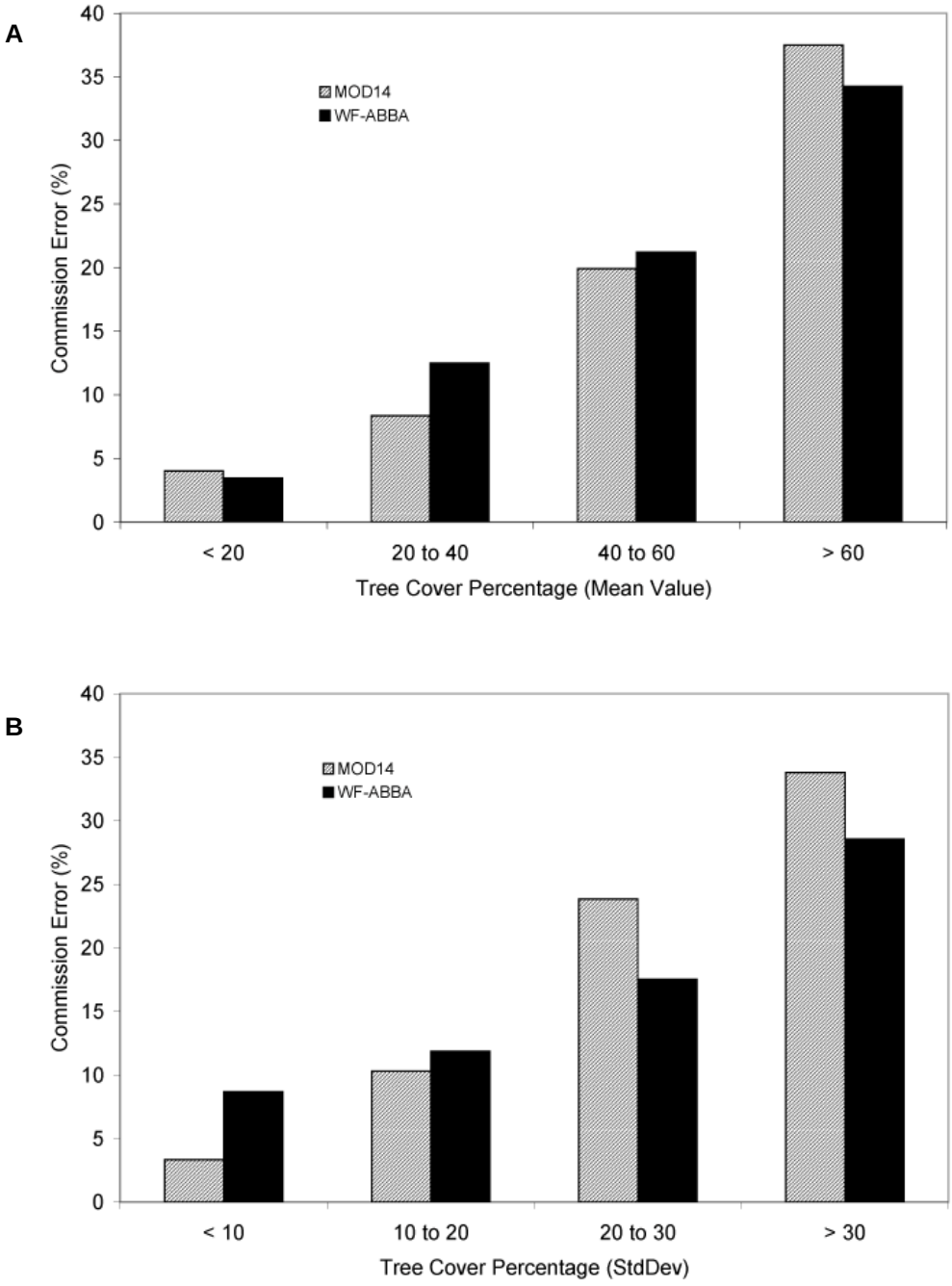

Figure 3.6: Commission error estimates for MOD14 and WF-ABBA. Mean tree cover values (A) estimated for an area of approximately 20×20 km centered on the commission error pixel; standard deviation values (B) determined by sampling a 9×9 pixels window centered on the commission error pixel.

Detailed inspection of each individual false detection occurrence using all available bands of ASTER and ETM+ at their highest spatial resolution enabled us to refine the classification of those areas and separate them into four different classes (Table 3.2). The data indicated that a large fraction of the false detections were indeed associated with recent burning activity as confirmed by the presence of fairly homogeneous areas of dark char covering part or all of the MODIS and GOES pixel footprints. Areas of smoldering were also confirmed over a smaller number of cases via the identification of smoke traces or the indication of warm pixels in the short wave infrared channels 8 and 7 of ASTER and ETM+, respectively. When summed, these false detections over areas of fire-related activity corresponded to approximately 87% and 81% of the commission errors of MOD14 and WF-ABBA, respectively. The remaining false detections were unrelated to fire and mainly the result of warm and reflective bare soils surrounded by contrasting green vegetation. These false detections corresponded to approximately 3% of all detections made by the MOD14 and the WF-ABBA products. This later result agrees with the findings of Csiszar *et al*. [2006] for the MOD14 product over Northern Eurasia.

Table 3.2: Classification of MOD14 and WF-ABBA commission errors based on visual inspection of 30 m RGB composites of ASTER and ETM+ data.

Product	*Recent Burning (scars visible)*	*Bare Soil*	*Smoldering*	*Spurious detection*
MOD14	79%	12%	8%	1%
WF-ABBA	75%	19%	6%	-

As most of the false detections were associated with areas of recent burning, it is possible that these locations show a strong contrast with their backgrounds for as long as the dark char and ashes remain evenly spread across the burning site. This could lead to repeated false detections affecting those locations over multiple days or even weeks or until the signs of burning are removed from the surface. To investigate this possibility, we checked every false detection location sampled by our data set for the presence of equivalent detections in the previous days. We restricted our analysis to the 30 day period occurring before the observation of the false detection based on the 30 m resolution imagery. The use of a 30 day sampling period was based on the assumption that char and ashes can be removed by wind and rain or by land use (e.g., plowing, seeding, and irrigation). Using spatially coincident 30 m resolution data acquired 16, 32 and 48 days apart we could confirm that scars remained visible for as long as 32 days. For periods greater than that, the burning imprint on the landscape becomes less evident.

We searched for all fire detections from Terra (MOD14) and Aqua (MYD14) data co-located to within 1 km of the original false detection. Aqua data was used to improve observation frequency to identify the very first detection made in the 30 day period along with all subsequent ones. Lacking other forms of confirmation, we assigned the actual fire occurrence date to the first detection found for each location and labeled all subsequent detections as potential false detections (Figure 3.7). Approximately 60% of the false detections in our data set had co-located detections from MOD14 or MYD14 occurring in the previous 30 days. Of those, about 50% had

the first detection occurring in the previous 14 days. The average number of subsequent false detections was 4.

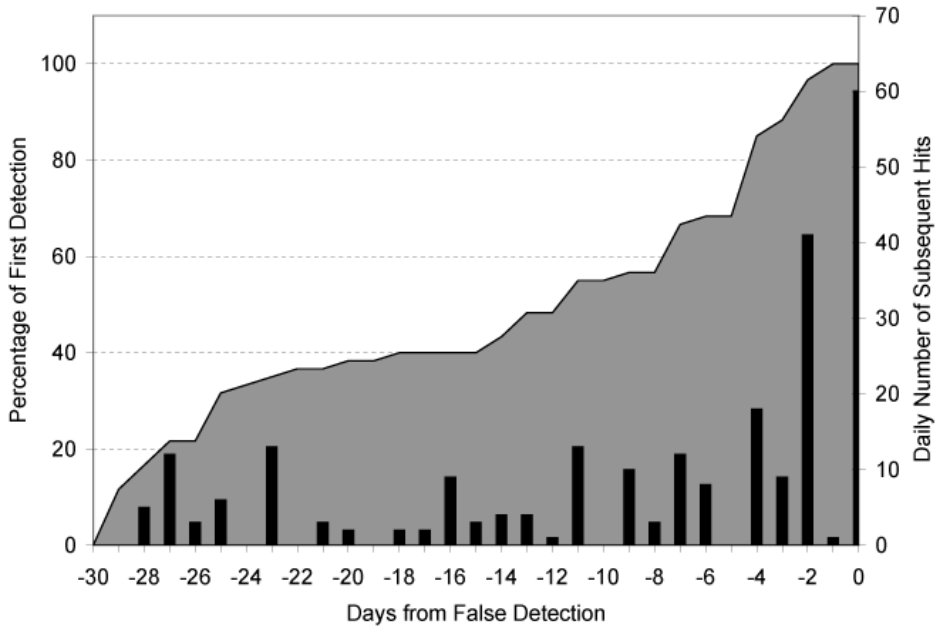

Figure 3.7: Daily number of hot spot detections from Terra MODIS (MOD14) and Aqua MODIS (MYD14) data coincident with 60 different locations where MOD14 false detections were identified via 30 m ASTER imagery. The shaded area describes the accumulated percentage of all 60 locations for which a first detection was assigned during the 30-day period before the confirmed false detection.

The locations mapped with the analysis above showed that the Terra (MOD14) product produced almost twice as many false detections as Aqua (MYD14) (117 vs. 67). The two products are processed using identical routines, reducing or even eliminating the chance of algorithm artifacts affecting our results. To compare these MODIS results to the GOES data, we analyzed all WF-ABBA false detections

found in our validation data set by monitoring their progress throughout the day. We searched for co-located WF-ABBA detections occurring during the GOES observation hours made after the false detection was observed. In this case, we applied a search radius of 0.1º (or the equivalent to about 10 km) to allow some flexibility due to potential navigation drift affecting some of the unregistered data used. The number of persisting detections was mapped along with the occurrence of clouds, sun glint areas and gaps in image coverage due to rapid scan operations which could prevent proper observation of the target pixel. The number of false detections persisting in the data gradually decreased with the hours of the day (Figure 3.8). At about the same overpass time as Aqua (i.e., 1715-1845 UTC) the number of false detections was reduced by approximately 50%. Our results for the commission errors of GOES (WF-ABBA) were similar to the results produced for MODIS (MOD14 and MYD14) suggesting a good agreement between the two fire products. Although the WF-ABBA detection algorithm includes an adjustment to one of the primary tests used (i.e., the brightness temperature (BT) test on channel 2) based on the solar zenith angle measured for every pixel and observation hour ($BT_2 >$ *cosine* (solar zenith angle) × 15 K + 285 K), the resulting correction factors for the approximate overpass times of Terra and Aqua were found to be similar for the study region therefore reducing their influence on the result above.

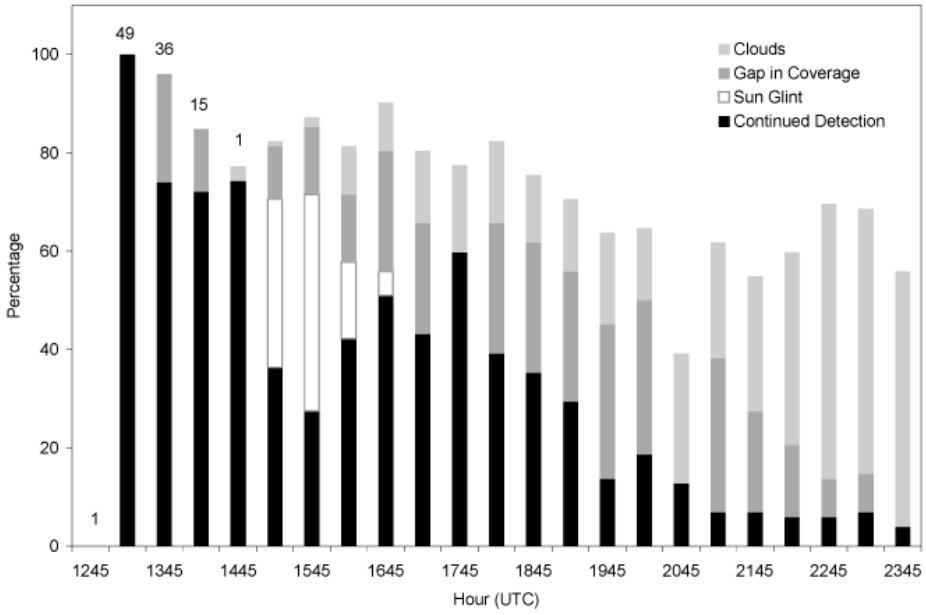

Figure 3.8: Half hourly distribution of WF-ABBA false detections identified in the validation data set. The absolute number of confirmed false detections identified via ASTER or ETM+ is shown on top of the vertical bars.

Two major factors can contribute to the reduction in commission errors towards the afternoon hours. First, cloud coverage in tropical areas such as Amazonia may have a pronounced effect limiting the imaging of the land surface by passive remote sensing instruments. The impact of cloud obscuration on the detection of active fires in Amazonia has already been documented and it is suggested to account for an omission rate of approximately 11% of all fires imaged by coarse resolution sensors [Schroeder *et al*., 2008a]. In the case of the commission errors reported above however, areas of cloud shadow and semitransparent clouds which may not interfere on the detection of active fires will affect the thermal properties of the surface thereby potentially enhancing their impact beyond the 11% estimate produced for the active fire data.

Changes in the thermal contrast between adjacent areas with different vegetation cover conditions could also influence the commission errors. To test this assumption, we randomly selected 20 areas of low vegetation cover surrounded by forests to evaluate the changes in thermal contrast measured between the two surfaces throughout the day. We used two sets of GOES imagery acquired on 19 September 2001 and 4 August 2002 covering the entire day at 30 min observation frequency. The two sets of images were characterized by low cloud coverage over the areas of major deforestation activity in Brazilian Amazonia favoring the extraction of cloud free brightness temperature profiles for the selected areas.

Overall, the results showed a decrease in the thermal contrast between forested and non-forested areas measured for the approximate overpass time of Aqua compared to Terra, with the thermal contrast for the latter being 1 K to 10 K greater than the former. Figure 3.9 shows the profiles obtained for two adjacent areas of forest and non-forest surfaces where false detections were produced by the WF-ABBA product. The difference between the two curves is included along with the approximate overpass times for Terra and Aqua. For the particular location used in Figure 3.9, clear sky conditions prevailed during the majority of the time. We can see in Figure 3.9 that the increased thermal inertia of the forest causes the peak in contrast with the deforested area to move closer to the observation hour of the Terra satellite. The false detections are found equally distributed around the area of greater thermal contrast and therefore tend to become more evident near the observation hours close to the Terra overpass and less so near the observation hour of Aqua. In this case, the reduction in thermal contrast for the two surfaces between the Terra and Aqua

overpasses was small (~ 2 K) and false detections could also be observed until about 15 minutes after the Aqua overpass time. In other situations where the change in surface conditions between Terra and Aqua overpasses is greater, the peak in thermal contrast approaches the Terra overpass time leading to fewer false detects during the observation hours near and after the Aqua overpass time.

In many cases the effects of clouds and changes in thermal contrast were seen to manifest concomitantly making it difficult to separate and properly quantify the exact contribution of each term to the reduction of the commission errors observed.

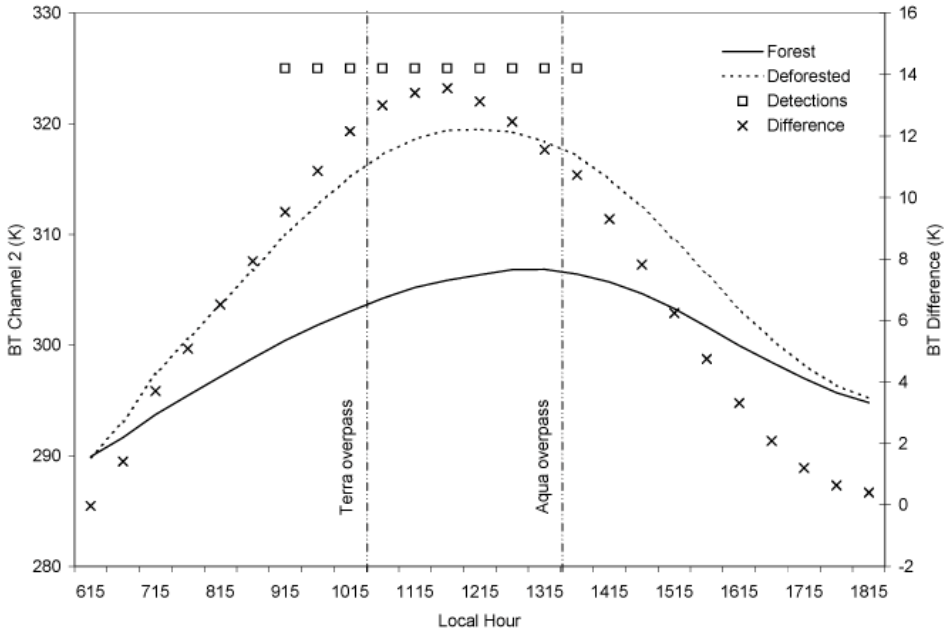

Figure 3.9: Diurnal cycle of brightness temperature derived from channel 2 of the GOES imager for two adjacent areas characterized by contrasting vegetation cover conditions. The images were acquired on 04 August 2002 and the forested and deforested areas were located at 11º59'29" S 52º49'52" W and 12º06'20 S 52º49'09" W, respectively. The two curves describe the mean values based on 3 and 4 pixels representing the deforested and forest areas, respectively. The occurrence of WF-ABBA false detections are presented along with the difference between the two curves.

3.4.4 Reducing Commission Errors

From the results presented above it becomes clear that one of the major complications involved with the application of contextual fire detection methods over tropical forest regions is the effect of contrasting warm and bright surfaces generating false detections. The parameters available with the MOD14 product Scientific Data show significant overlap between true and false detections (Figure 3.10), which eliminates the potential for successful post-processing of false detections using any of the available fire pixel information.

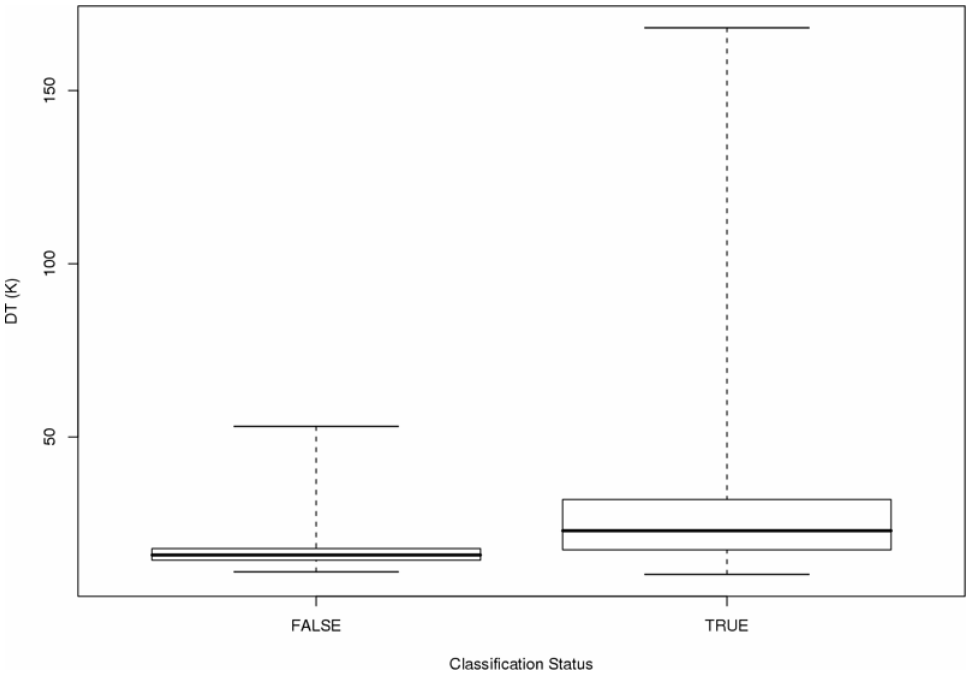

Figure 3.10: Boxplots for channel 21 brightness temperature differences between the target pixel and its background for true and false MOD14 detections. Parameters depicted in the plot include: minimum, 25th percentile (lower quartile), mean, 75th percentile (upper quartile) and maximum value.

Another approach to resolve the commission errors affecting the two data sets is the use of temporal metrics to complement the spatial analysis provided by the contextual method. Change detection methods based on the application of temporal metrics to assess sudden variations in the pixel signature of moderate and coarse resolution sensors are growing in importance as satellite data sets with improved navigation quality become available [Calle *et al*., 2006; Koltunov and Ustin, 2007; Schaaf *et al*., 2002].

We selected over 100 detections from each of our MODIS and GOES validation data sets including true and false detections. Brightness temperatures (BT) were derived from the mid-infrared channels 21 and 22 of MODIS and channel 2 of GOES using MOD02 and GVAR Man computer Interactive Data Access System (McIDAS) AREA file data, respectively. The BT data were used to construct 30-day profiles from which the mean and standard deviation were extracted for each pixel. Figures 3.11A and 3.11B show a plot of the BT temporal profiles for two pixels fixed in space representing different cases of true and false detections in the MODIS and GOES data, respectively. The plots describe two important aspects of the data. First, MODIS shows a greater variability of the BT values compared to GOES, likely a function of variable imaging geometry. Despite its lower navigation quality, the GOES brightness temperatures show less variation over time. Second, since MODIS pixels are smaller compared to GOES, fires naturally occupy larger fractions of them, resulting in a greater departure from the mean value observed for the 30-day period analyzed. As a result, the potential limitations caused by a variable pixel size could be balanced by a high sensitivity to the presence of active fires within the pixel footprint,

rendering this kind of application useful to separate false detections from true detections. On average, true detections departed by more than 4 standard deviations from the 30 day mean BT values, whereas for false detections the departure was limited to about 2 standard deviations. These results were equally valid for MODIS and GOES.

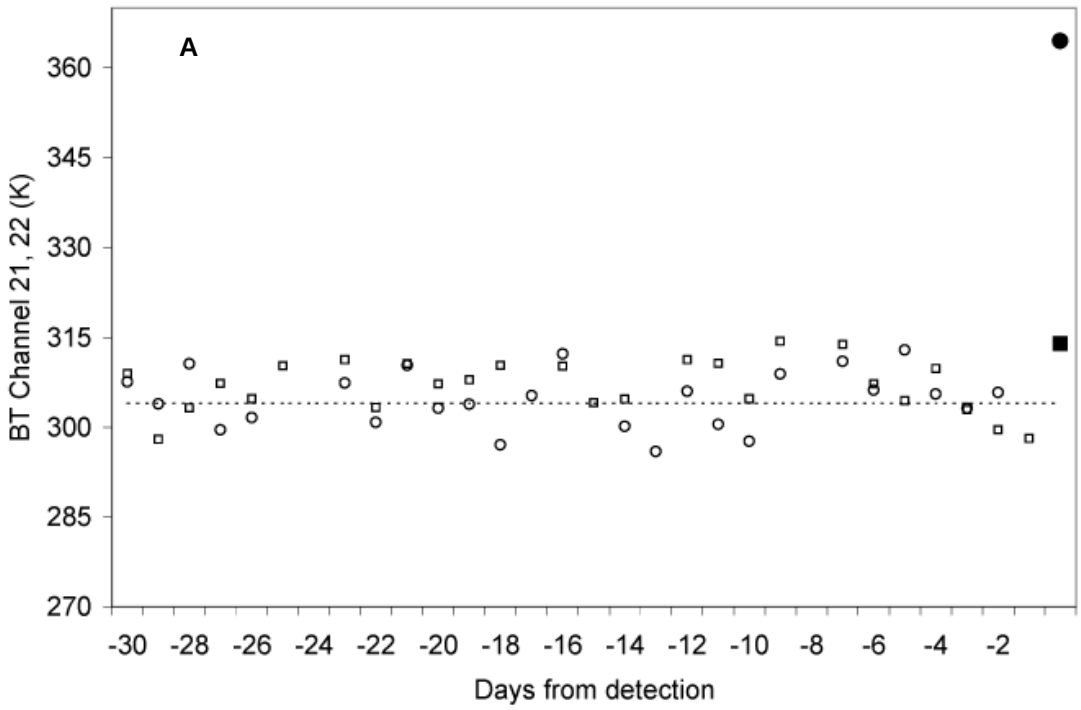

Figure 3.11: Brightness temperature (BT) profiles for true (filled circle) and false (filled square) detections using MODIS (A) and GOES (B) data. Open circles and squares represent the BT values during detection-free days. Detection information for the pixels marked in (C-F): false MOD14 detection (C): 55.1237^{o} W 12.129^{o} S, 23 May 2002 at 1403 UTC; true MOD14 detection (D): 56.4828^{o} W 13.225^{o} S, 05 October 2002 at 1409 UTC; false WF-ABBA detection (E): 50.879^{o} W 8.4169^{o} S, 29 August 2002 at 1315 UTC; true WF-ABBA detection (F): 50.711^{o} W 10.0335^{o} S, 29 August 2002 at 1315 UTC. False color composites used: 30 m ASTER image (C-D); 30 m ETM+ image (E-F).

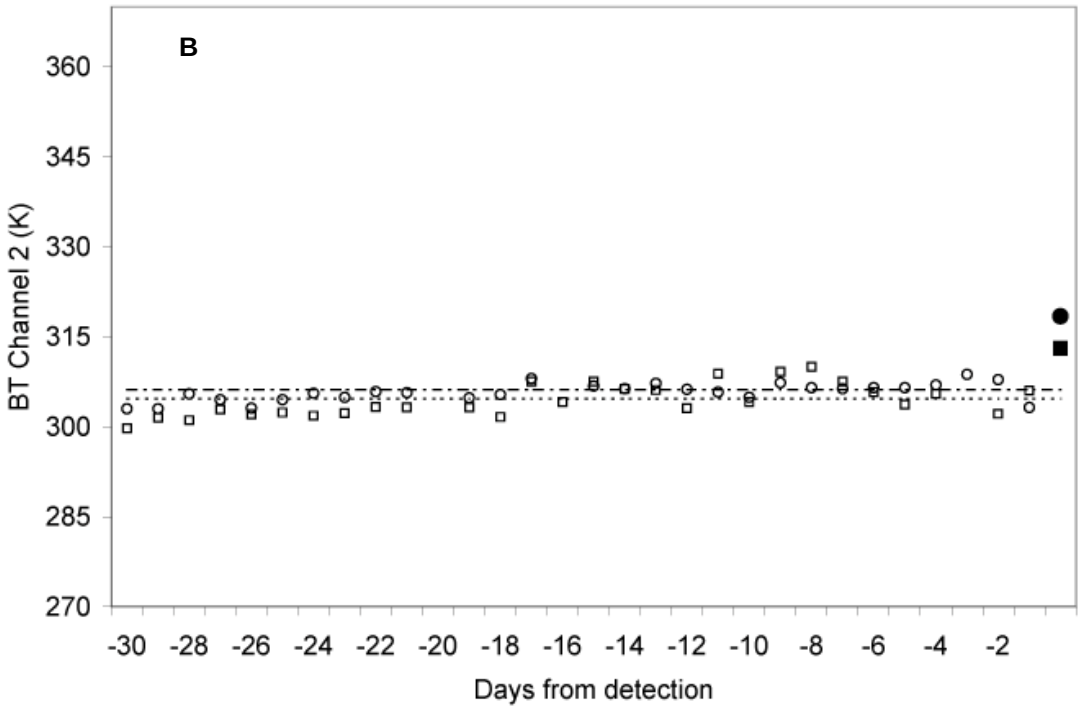

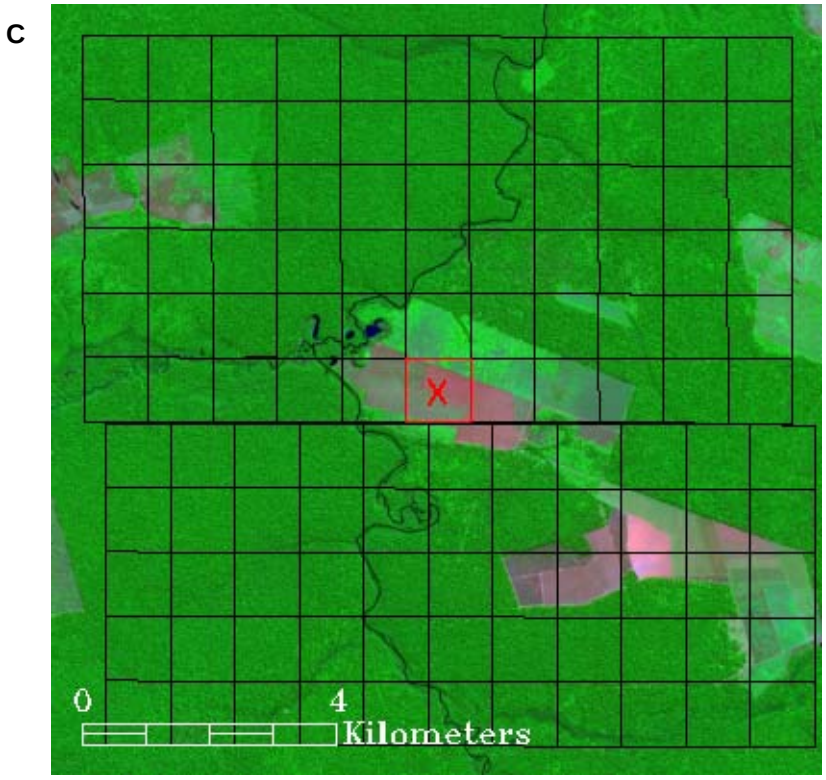

Figure 3.11. *continued*

D

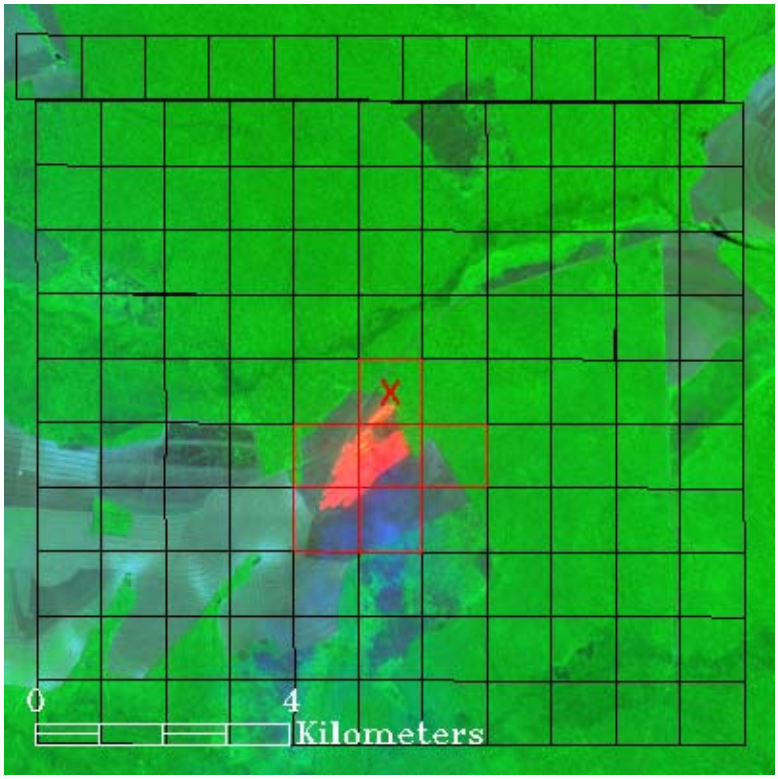

E

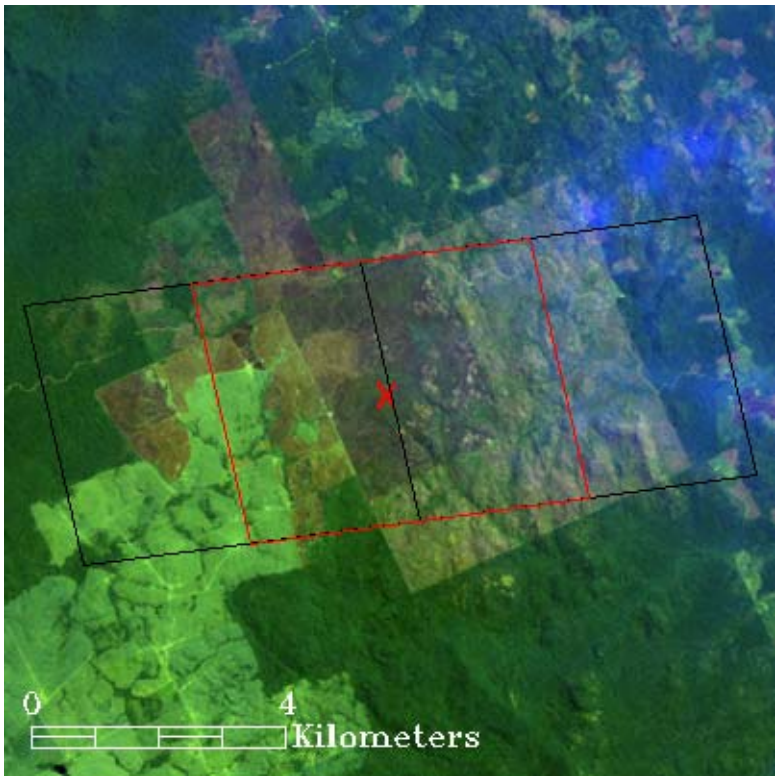

Figure 3.11. *continued*

F

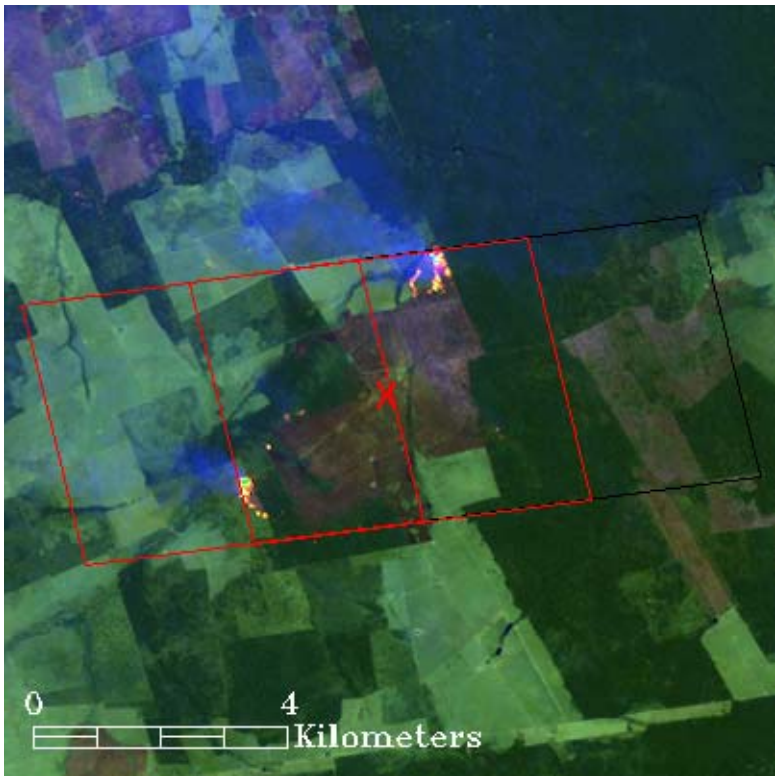

Figure 3.11. *continued*

The graphs in Figure 3.11 did not receive any rigorous treatment to reduce spurious oscillations in the derived BT values. Appropriate techniques could, however, be used for instance to model the daily variation of the MODIS BT data. In addition, the BT profiles in Figure 3.11 benefit from the favorable conditions observed in Amazonia where stable surface temperature conditions prevail throughout most of the year [da Rocha *et al*., 2004]. Nevertheless, the commission errors described above appear to be mainly associated with land use regimes marked

by large deforestation rates typical of the tropical forest regions. In these regions, similar surface conditions should be expected.

3.5 CONCLUSIONS

The MODIS and GOES fire products assessed in the validation analysis described above utilize conceptually similar algorithms based on the use of contextual tests to detect pixels with active fires. However, these algorithms are applied to images of markedly different spatial and spectral resolutions. The resulting detection performance estimates obtained through the validation analysis indicated that an approximate factor of 4 separates the detection curves of MOD14 and WF-ABBA products, a relatively small difference compared to the 16× factor between their nominal spatial resolutions.

Although MODIS and GOES showed relatively high overall omission errors, their interpretation should be oriented by the type of application pursued. In this case, fire data users interested in larger biomass burning events may find both MODIS and GOES to have reasonably high rates of successful detection as is evidenced by the sharp decrease in omission errors especially near the low end of fire clusters described in Figure 3.5.

The background conditions associated with active deforestation regions in Amazonia had a major effect on the false detections produced with both products. False detections can span multiple days provided that the burning scars remain evident and similar thermal conditions are preserved between adjacent areas. The

reduction in commission error rates observed towards the afternoon hours has important consequences for the derivation of the fire diurnal cycle using contextual algorithms. In this case, an enhanced contrast between morning and afternoon hours should be noticed if all potential false detections are removed from the data.

Removal of false detections based on the metrics which are routinely produced by the contextual algorithms proved difficult. Alternatively, we successfully tested the application of temporal metrics of brightness temperature to isolate false detections in our data set. The use of a hybrid fire detection algorithm which implements change detection methods in addition to the contextual tests appears promising especially over tropical regions. In these areas, stable surface thermal conditions might facilitate the extraction of temporal metrics which could be used to separate false detections or increase our confidence about the true ones. However, we recognize that this is a topic for further investigation necessitating careful consideration of all aspects involved.

The results described above are valid for open sky fires typical of forest conversion and agricultural maintenance in Amazonia, but do not apply to cases of understory burning. Although a few sub-canopy fires could be visually confirmed in our validation data, proper identification of those events via automated detection was difficult even at the 30 m resolution level. Consequently, detection of active understory fires using MODIS or GOES data appears to be significantly difficult using standard mid-infrared detection algorithms.

Another limitation of our analyses involves the conversion of 30 m active fire pixels statistics derived from ASTER and ETM+ into fire area and temperature

estimates. Although theoretical assessment of ASTER channel 8 saturation was attempted relating minimum fire area and temperature [Giglio *et al*., 2008], a more complete characterization of fire properties is still under investigation. Advancement in this area is limited primarily by inadequate specifications of existing orbital sensors.

This study extends a series of validation analyses applied to the MODIS *Thermal Anomalies* product and is the first one of its kind applied to the GOES WF-ABBA product. Our results corroborate previous findings and include new aspects involving the performance of the MODIS and GOES fire detection algorithms which can help the fire data user community optimize their use of these products.

Lessons learned from the validation of MODIS and GOES imager will be used to develop validation procedures for the fire products from new generation of US polar orbiter (NPOESS Visible Infrared Imager Radiometer Suite -- VIIRS) and geostationary (GOES-R Advance Baseline Imager -- ABI) platforms. Of particular importance is the development of a multi-platform validation system and the quantification of validation errors stemming from the use of non-simultaneous space-based or airborne reference data. In addition, the better understanding of the detection envelopes of MODIS and GOES imager derived from this study can be used to assess the expected performance of the higher resolution VIIRS and ABI fire products.

Chapter 4: Integrating Geostationary and Polar Orbiting Data for Monitoring Vegetation Fires in Brazilian Amazonia

4.1 INTRODUCTION

Biomass burning is a major problem affecting in particular the tropical regions [Crutzen *et al*., 1979; Andreae, 1991; Hao and Liu, 1994]. Vegetation fires contribute to large amounts of trace gases and aerosols emitted during combustion [Crutzen and Andreae, 1990; Crutzen *et al*., 1979; Seiler and Crutzen, 1980]. The large rate of emissions from tropical fires was found to have important consequences to atmospheric composition and to the global radiation budget [Penner *et al*., 1992, Andreae *et al*., 2004]. Chemically reactive constituents produced during combustion such as CO and nitrogen oxides (NOx) may combine to form tropospheric O_3 [Crutzen, 1979; Delany *et al*., 1985; Rummel *et al*., 2007; Watson *et al*., 1990], which under high concentrations near the surface can have adverse effects on live vegetation and human health [Crutzen and Andreae, 1990; Hansen *et al*., 2000; Vitousek *et al*., 1997]. The role of biomass burning aerosols as cloud condensation nuclei was also proven to alter the nature and distribution of clouds in tropical regions especially when smoke concentrations are high [Andreae *et al*., 2004; Koren *et al*., 2004].

Quantification of vegetation fire activity and the associated emissions from biomass burning in Amazonia has been approached via remote sensing and modeling techniques [Andreae *et al*., 2004; Freitas *et al*., 2005; Kaufman *et al*., 1990, 1992;

Setzer and Pereira, 1991]. In both cases, satellite active fire detection data represent one of the most important parameter for calculating source emissions. Fire alert systems alike depend heavily on satellite data to monitor fire activity in Amazonia as this is the only form of systematic observation available for the region [CONAE, 2008; CPTEC, 2008; DIMARENA, 2008].

Fire monitoring and emissions modeling applications usually require the best spatial and temporal resolution data available [GCOS, 2006]. Early detection is most important for fire alert systems demanding information at high observation frequency and fine spatial resolution to increase the probability of detecting a fire immediately after its initiation or when its active area is still small. Similar data needs are valid for emissions modeling applications which depend on high temporal and spatial resolution data to determine the lifetime of individual fires and to calculate the resulting emissions [Freitas *et al*., 2005]. Emissions modeling applications also require characterization of fire properties (e.g., total radiative energy, area, temperature) for calculating emissions, demanding quality pixel data which can only be achieved by non-saturating satellite sensors [Justice *et al*., 2002; Kaufman *et al*., 1998b].

The lack of orbital systems capable of delivering fire detection data at both the spatial and temporal resolutions required by users is a major limitation affecting current fire products [Schroeder *et al*., 2005]. Variations in product performance as a result of sensor characteristics and the diurnal cycle of fires introduce additional complications for fire data users influencing the use of the data [Giglio, 2007; Schroeder *et al*., 2005, 2008b]. To cope with these limitations, fire data users must

incorporate assumptions in their analyses (e.g., emissions modelers need to estimate the lifetime of a fire using hypothetical curves) or prioritize one data set over others thereby avoiding conflicts among different products. However, the tendency of most emissions models and fire alert systems to deliver increasingly detailed data on fire activity creates a great demand for an integrated satellite product which takes advantage of the complementarities among current fire detection data [GOFC, 2006].

In this study, we assess the potential for integrating the fire product information derived from the Moderate Resolution Imaging Spectroradiometer (MODIS) on board Terra and Aqua satellites and the Geostationary Operational Environmental Satellite (GOES) imager. We use in our analyses the *Thermal Anomalies* MOD14 and MYD14 Collection 4 active fire detection products for MODIS Terra and Aqua, respectively, and the Wildfire Automated Biomass Burning Algorithm (WF-ABBA) version 6.0 for GOES [Giglio *et al*., 2003a; UW Madison CIMSS, 2008]. The high temporal resolution of the GOES imager and the moderate spatial resolution of MODIS provide a unique opportunity to test how fire detection products from instruments with very different configurations complement each other. Our main objective is to investigate how the fire detections from MODIS and GOES can be used in concert to improve fire monitoring capability and to assess the feasibility of developing a hybrid product based on the two products. We focus our analyses on Brazilian Amazonia, a region routinely covered by MODIS Terra and Aqua and the GOES imager. In this region, significantly high annual fire activity spreading over rather remote areas requires that optimized monitoring systems be used.

We tested the hypothesis of data complementarity using two different approaches. First, we analyzed the MODIS and GOES imager fire detection information by assessing the Fire Radiative Power (FRP) estimates produced from each data set. The reasons for using FRP estimates to relate MODIS and GOES fire information are threefold: (i) it provides a physical parameter which facilitates interpretation of the results, (ii) it provides quantitative characterization of fire activity which is more informative compared the to categorical data represented by simple fire detection and (iii) it has been demonstrated that FRP can be used to estimate biomass combustion rates, an important parameter in emissions modeling [Kaufman *et al*., 1998b; Wooster, 2002; Wooster *et al*., 2003]. Therefore FRP becomes a potentially valuable parameter for fire data users and emissions modelling applications. Secondly, we assess the relationship between spatially and temporally coincident MODIS and GOES active fire detections using the binary classification (i.e., 1 = fire detection; 0 = no fire detection). Although less informative, binary fire detections are by far the most commonly used information among satellite fire data users. The comparison of the binary data examines the factors that influence the rates of the spatially and temporally coincident detections produced by MODIS *Thermal Anomalies* and WF-ABBA products. We substantiate our analyses of the MODIS and GOES fire products using sub-pixel fire characterization derived from higher resolution imagery from the Advanced Spaceborne Thermal Emission and Reflection Radiometer (ASTER) and the Enhanced Thematic Mapper Plus (ETM+) instruments.

4.2 VEGETATION FIRES IN BRAZILIAN AMAZONIA

Fires are used in Amazonia primarily for land clearing and maintenance applications [Andreae, 1991; Cochrane, 2003]. Burning occurs in a somewhat controlled fashion and is used to eliminate forest debris, or crop residues, or to replace or rejuvenate grasslands. Under these circumstances, fires tend to be constrained to the perimeter of the land being used although escaped fires are also commonly reported [Alencar *et al*., 2006].

The humid climate of Amazonia limits fire use to a small window of opportunity centered in the peak months of the dry season [Schroeder *et al*., 2005, 2008a]. The decision to burn is highly influenced by the development of the dry season and the "signs" of the subsequent wet season. Correct identification of those "signs", especially by small farmers, can represent the difference between a prosperous year or perhaps starvation. The strong bonds among individuals occupying adjacent areas limit the apparent window of opportunity for burning even further. In this case, initiation of a fire in one property can influence others to follow. Consequently, vegetation fires can become significantly concentrated in time. For instance, Schroeder *et al*. (2005) reported that approximately 2,000 MODIS Aqua (MYD14) fire detections were produced for the state of Acre in western Brazilian Amazonia during 1-3 September 2003, representing nearly 30% of all fire detections in that year.

We used 285 ASTER and ETM+ scenes to quantify active fire size in Brazilian Amazonia and the minimum distance between adjacent fire clusters. The scenes were distributed in the main areas of fire activity in the region and were

acquired during 2001-2005. Active fire masks at 30 m resolution were produced for ASTER and ETM+ data following the approach described in Giglio *et al*. (2008) and Schroeder *et al*. (2008b), respectively. Contiguous 30 m active fire pixels were clustered together to produce individual fire size estimates. Figure 4.1A shows the distribution of fire cluster size for the region. Fire size statistics derived from the data above are valid for fires imaged at around 10:00-10:30 local time; it is plausible that larger fires might prevail during the early afternoon hours as a result of the diurnal cycle of fires [Giglio, 2007; Prins *et al*., 1998]. Also, fire cluster sizes depicted in Figure 4.1A are expressed in terms of 30 m active fire pixels derived from the fire masks and will likely differ from the actual area occupied by flaming fronts. Regardless of the approximations involved, the typical spatial scale of Amazonian fires is seen to represent only a small fraction of a nominal 1×1 km MODIS or 4×4 km GOES pixel areas.

The minimum distance between adjacent fire clusters was determined using the same data set above (Figure 4.1B). Approximately 50% of the fire locations derived from the 30 m fire masks showed an adjacent fire cluster within 2 km or less from their outer limits. This proximity between clusters reinforces the concept that fires are used simultaneously at several properties in one particular region, making them concentrated in time as well as in space.

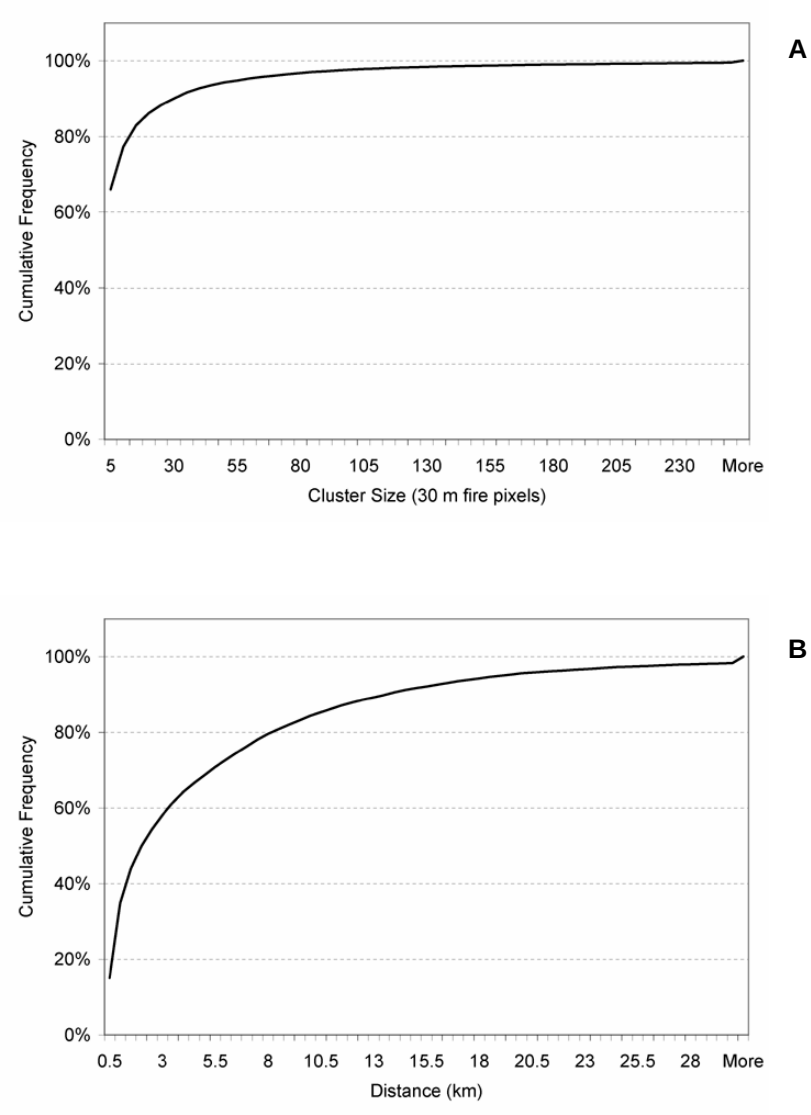

Figure 4.1: Cumulative frequency graphs of fire cluster size (A) and minimum distance to nearest fire (B).

Complementing the characterization of vegetation fire conditions in Amazonia, 2,785 burnt area polygons were digitized using a representative subset of the 30 m resolution data above composed of 33 ETM+ scenes. While active fires represented only a small fraction of a moderate-to-coarse resolution pixel footprint, the resulting burnt area polygons were large enough to approach or even exceed the

size of a MODIS or GOES pixel (Figure 4.2). The occurrence of pixel-size burn scars in Amazonia has important implications for active fire detection in particular in areas of high percentage tree cover where there is a high contrast between forest and non-forested pixels in the mid-infrared spectral region [Tucker *et al*., 1984]. The occurrence of burn scars occupying large fractions of non-forested pixels may further reinforce the contrast with surrounding forest areas causing contextual algorithms such as used by the MOD14, MYD14 and WF-ABBA products to generate false detections, therefore resulting in high commission error rates [Schroeder *et al*., 2008b].

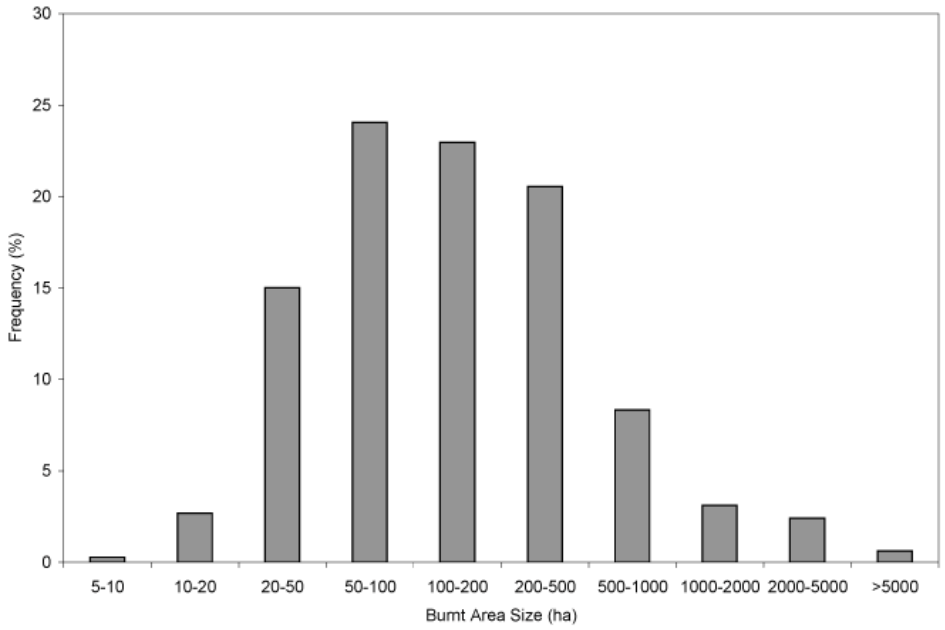

Figure 4.2: Burnt area size histogram derived using ETM+ data for Brazilian Amazonia. Data are representative of 2,785 individual burn sites extracted from 33 ETM+ scenes. A nominal MODIS pixel is equivalent to 100 ha, whereas the nominal GOES pixel covers an area of approximately 1600 ha.

4.3 METHODS

The use of pixel level analyses methods applied to the active fire detection data from MODIS and GOES was not implemented in this study primarily due to limitations involving the distinct image geometry of the two instruments. Geometric distortion of off-nadir pixels introduced important across-image mapping and resampling errors [Wolfe *et al*., 2002]. Also, orbit oscillations affecting in particular the GOES data resulted in different navigation offsets across sectors of the images often leading to poor overall navigation quality. Persistent cloud coverage across Amazonia created major limitations for the use of automated methods to register data sets and to reduce navigation differences. Lastly, the spatial characteristics of Amazonian fires described in Figure 4.1 suggest that moderate or coarse resolution fire products may likely contain multiple fires distributed over adjacent detections. To cope with the limitations involving instruments' characteristics and the spatial characteristics of fires in the region, we opted to aggregate the fire detection information into clusters by analyzing groups of contiguous detections. When analyzing fire detections from MODIS and GOES, we also used area averaged estimates of fire activity in order to minimize the effects of localized fire detection differences.

4.3.1 MODIS FRP

In our analyses we used the FRP estimates available as part of the MODIS *Thermal Anomalies* Collection 4 product Scientific Data Set [Giglio *et al*., 2003a]. The MODIS FRP derivation is based on the relationship between the emitted fire energy

and the mid-infrared brightness temperature, and is expressed as [Kaufman *et al*., 1998b]:

$$FRP = 4.34 \times 10^{-19} \left(T_4^8 - T_{4b}^8 \right) \quad (1)$$

Where T_4 and T_{4b} are the brightness temperature estimates in the 4 μm region of band 22 (or alternatively band 21 when band 22 becomes saturated) for the target and the background pixels, respectively. The constant in equation (1) is adjusted for the spectral interval of MODIS channel 21-22.

4.3.2 GOES FRP

Currently there is no FRP estimate available with the operational WF-ABBA version 6.0 product. Alternatively, fire size and temperature estimates derived using Dozier's (1981) approach are available with the product. However, problems inherent to Dozier's technique are known to affect the estimates produced [Giglio and Kendall, 2001], limiting their application for FRP retrievals. Nonetheless, Wooster *et al*. (2003) have demonstrated that it is possible to derive physically sound FRP by approximating Planck's Radiation law using a fourth order power law applied to mid-infrared remote sensing data (e.g., channel 2 on the GOES imager) over the interval of typical vegetation fire temperatures (i.e., 600 – 1500 K). After relatively simple considerations are made following the approximation above, FRP estimates can be calculated through the application of the following equation [Wooster *et al*., 2005]:

$$FRP = \frac{\sigma}{a}\left(L_{2,f} - L_{2,b}\right)S \quad (2)$$

Where $L_{2,f}$ and $L_{2,b}$ are here represented by the GOES channel 2 radiances (W m^{-2} sr^{-1} μm^{-1}) estimated for the target pixel containing the fire and for the background pixels, respectively, σ is the Stefan-Boltzmann constant (5.67×10^{-8} W m^{-2} K^{-4}), *a* is a constant derived for the particular spectral response function of channel 2 (value for GOES-12 imager: 3.08×10^{-9} Wm^{-2} sr^{-1} μm^{-1} K^{-4}), and *S* is the ground equivalent pixel area (m^2).

Derivation of the GOES FRP must take into consideration the significant along scan pixel overlap which occurs during normal imager operation [Menzel and Purdom, 1994]. Under such conditions, every point on the surface is effectively imaged by two adjacent pixels. Consequently, two WF-ABBA detections will likely be produced representing an individual surface fire. This condition could lead to an overestimation of GOES FRP based on (2), as term *S* would be biased by a factor of two. To deal with the uncertainties in sub-pixel fire location and the effects of along scan pixel overlap, we calculated GOES FRP for fire clusters containing two or more adjacent pixels in the along scan direction by assigning variable weights to those pixels. The criterion for determining the weight of different cluster elements was based on the brightness temperature of each pixel; brighter pixels were assigned greater weight in the FRP calculations. For a fire detection cluster composed of three adjacent pixels in the along scan direction we calculated the GOES FRP using the following two steps:

(i) Rank pixels according to their brightness temperatures (e.g., $T_2>T_1>T_3$)

(ii) Assign greater weight to brighter pixels in the calculations by adjusting the pixel area in (2) using:

$$FRP_1 = \frac{\sigma}{a}\left(L_{1,f} - L_{1,b}\right)\times\left(S_1 - S_{2\cap 1}\right)$$
$$FRP_2 = \frac{\sigma}{a}\left(L_{2,f} - L_{2,b}\right)\times\left(S_2\right)$$
$$FRP_3 = \frac{\sigma}{a}\left(L_{3,f} - L_{3,b}\right)\times\left(S_3 - S_{2\cap 3}\right)$$
$$FRP_{cluster} = FRP_1 + FRP_2 + FRP_3$$

Where the symbols are similar to equation (2) except for $S_{i\cap j}$, which indicates the area of overlap between adjacent pixels *i* and *j*.

4.3.3 Simulation Data

As shown in Figure 4.1A, Amazonian fires are relatively small and therefore occupy only a reduced fraction of a moderate-to-coarse resolution pixel. Because of the Point Spread Function (PSF) characteristics of sensors such as MODIS and GOES, the radiance corresponding to each pixel will be influenced by the spatial arrangement of the sub-pixel features and might as well be affected by radiance coming from surface elements located just outside the pixel's nominal area [Cahoon *et al*., 2000; Zhang *et al*., 2006]. Using simulation data, we investigated how the relative position of a fire line contained in a moderate-to-coarse resolution pixel affects the FRP estimates derived from MODIS and GOES. Target pixels of nominal spatial resolution (1×1 km for MODIS and 4×4 km for GOES) were reproduced containing two distinct thermal components, namely: (i) the fire background at 311 K, and (ii) a high temperature

source at 800 K with a fixed area of approximately 5.5 ha (155×365 m). The background pixels necessary for the calculation of FRP were simulated as single thermal component pixels with their temperatures set at the same fire background temperature of 311 K. Those conditions were considered representative of typical Amazonian fires detected by MODIS and GOES. The location of the fire line relative to the pixel center varied in our simulations to the extent permitted by each instrument, i.e., 0.5 km along scan and 0.5 km along track for MODIS; 1.25 km along scan and 2 km across scan for GOES. The reduced along scan spatial tolerance in GOES was designed to reproduce the over-sampling characteristic of its imager. The formats of the PSF used for MODIS and GOES are shown in Figure 4.3A and 4.3B, respectively.

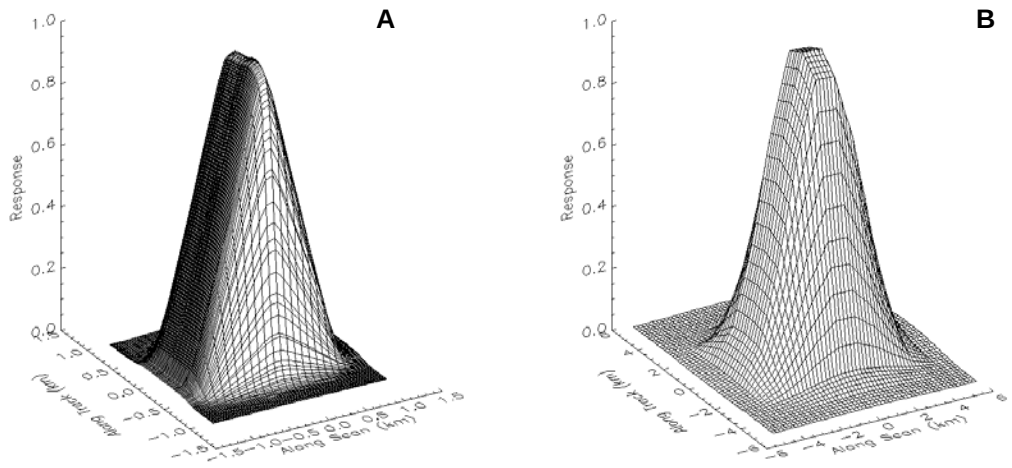

Figure 4.3: 3D scheme of the Point Spread Function of MODIS (A) and GOES (B) 4 μm channels.

4.3.4 Comparing MODIS and GOES Fire Detections

The relationship between MODIS (MOD14 and MYD14) and GOES (WF-ABBA) fire detections was derived using three years (2003-2005) of daytime data for Amazonia. The main objective of this analysis was to determine the rates of spatially and temporally coincident detections produced by the two products above. The instantaneous rate of coincident detections was derived from pairs of MODIS and GOES acquisitions separated by less than 15 minutes. Contiguous fire detections were aggregated into clusters and a search radius of 8 km was used to locate WF-ABBA detections corresponding to a MOD14 (or MYD14) cluster, and vice-versa. This larger search radius was intended to accommodate navigations errors in the GOES data.

We also derived the rates of coincident detections between MOD14 (and MYD14) and WF-ABBA using all daytime observations from GOES. In this case, the objective was to determine how the increased observation frequency of GOES would influence the rates of coincident detections. Using the spatial criterion above, we searched for same day WF-ABBA detections produced during the period of approximately 7:00 to 19:00 local time.

To facilitate the interpretation of the results, the rates of spatially and temporally coincident fire detections produced by MODIS and GOES were separated into four discrete intervals of percentage tree cover based on the 500 m Vegetation Continuous Fields (VCF) product [Hansen *et al*., 2002; Hansen *et al*., 2003].

Complementing the analysis above, we derived the relationship between MOD14 (and MYD14) and WF-ABBA detections for a rectangular area of 200×300

km^2 centered in Mato Grosso state, southern Brazilian Amazonia. The area was oriented following the orbit inclination of Terra and Aqua in order to sample portions of the daily MODIS images showing similar pixel geometry. We derived the sum of MOD14 (and MYD14) and WF-ABBA fire detections occurring within 15 minutes from each other for the spatial subset above. The results were summarized according to discrete MODIS scan angle intervals in order to evaluate the effects of variable imaging conditions on the MODIS product.

4.4 RESULTS AND DISCUSSION

4.4.1 MODIS and GOES FRP

FRP estimates were produced for 12 pairs of near coincident MODIS Terra and GOES imagery and for 11 pairs of near coincident MODIS Aqua and GOES imagery, each containing several fire detection clusters. The GOES images were registered to MODIS in order to minimize navigation errors, and FRP values were derived for each detection cluster. Clusters with one or more saturated pixels (more commonly seen in the GOES data) were not used. To ensure that individual pairs of MODIS and GOES detection clusters were representative of the same surface fire, we discarded all cases having more than one detection cluster from each instrument within a 10 km radius.

The spatially and temporally coincident FRP estimates for MODIS Terra and GOES and MODIS Aqua and GOES are shown in Figures 4.4A and 4.4B, respectively. The correlation between MODIS and GOES remained low despite all measures adopted to reduce artifact contamination of the pairs of FRP values

produced. Visual inspection of a subset of 77 pairs of MODIS Terra and GOES fire detection clusters using coincident ASTER data helped us identify the major factors influencing our results.

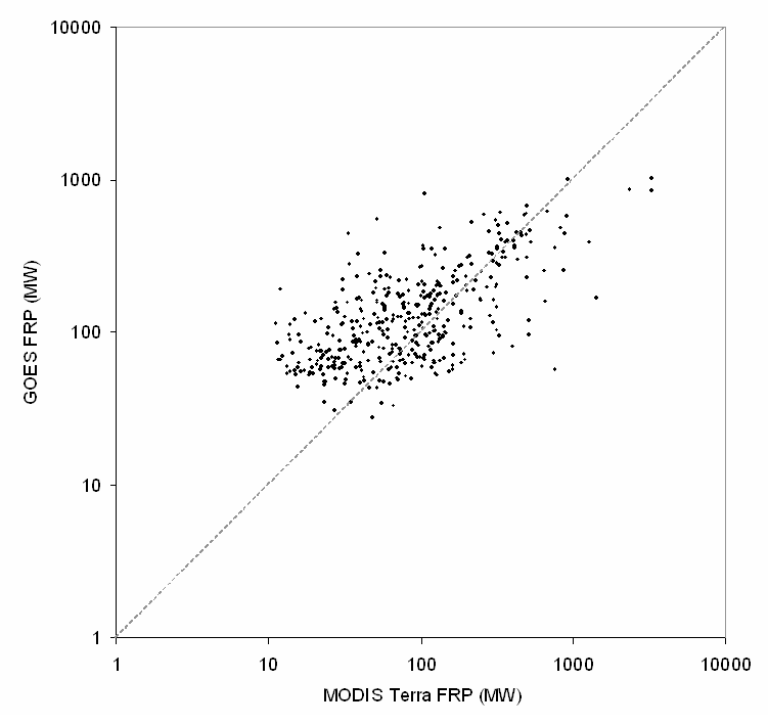

Figure 4.4: Scatter plots of FRP estimates produced for spatially and temporally coincident MOD14-WF-ABBA (A) and MYD14-WF-ABBA (B) fire detections clusters. The one-to-one line is plotted for reference.

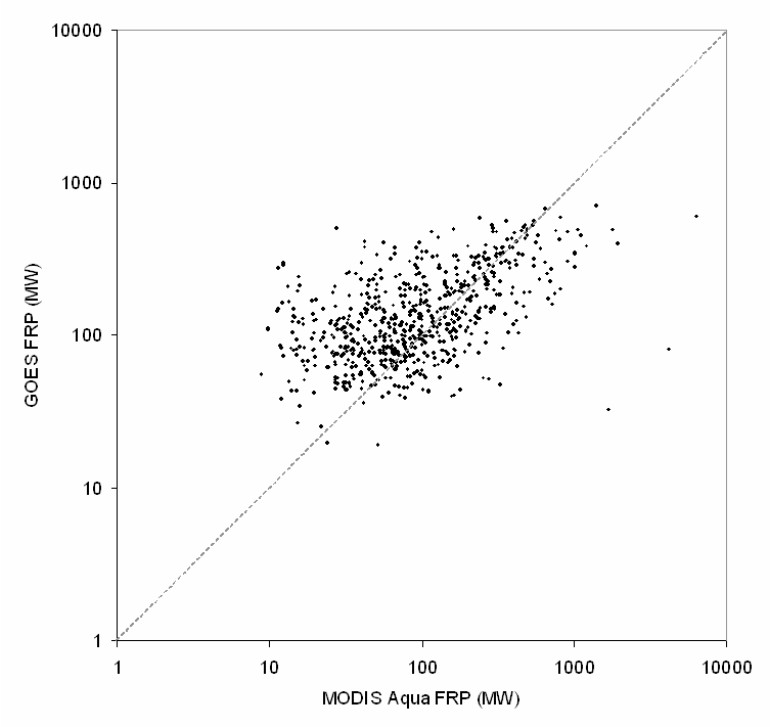

Figure 4.4 *continued*

First, differences in FRP were found to prevail over areas of high landscape heterogeneity. Fire detections located in areas of marked variation in vegetation cover occurring at the same spatial scale of the MODIS or GOES pixel (e.g., deforestation sites in high percentage tree cover regions) showed systematically larger differences in FRP compared to areas of homogeneous background (e.g., grasslands in low percentage tree cover regions) (Figure 4.5). Differences between the vegetation cover of the target pixels and their surrounding areas are expected to influence the background characterization affecting the derivation of FRP through (1) and (2) [Wooster *et al*., 2003]. Detection clusters covering areas of deforestation where the surrounding pixels were partially or entirely covered by evergreen tropical forests were particularly prone to produce large differences between MODIS and GOES FRP

values. In these cases, the brightness temperature of the forested pixels can be 15 K cooler than the fire pixel background, resulting in a potential overestimation of FRP > 20% according to (1) (assuming an intermediate fire detection condition).

Differences between FRP estimates from MODIS Terra and GOES were also associated with omission of secondary fire lines contained in adjacent pixels. The landscape heterogeneity was equally important in this case as it influenced the propagation of fire lines, resulting in fragmented fires composed of several small flaming areas. Omission pixels constitute a relatively small percentage of the total energy of a fire cluster; however, their occurrence can also influence the characterization of the background pixels therefore amplifying their net effect on the FRP calculation.

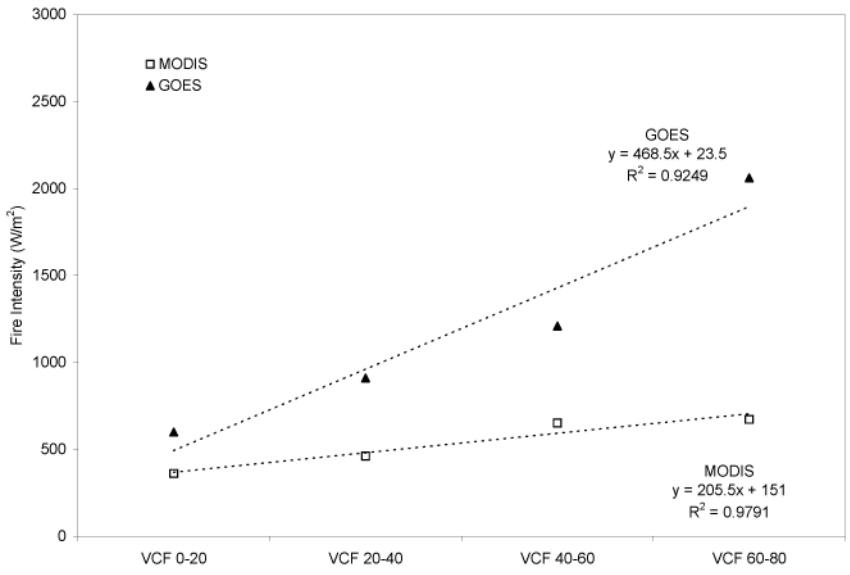

Figure 4.5: Fire intensity (Wm^{-2}) estimates for four percentage tree cover intervals [VCF, Hansen et al., 2002] calculated by dividing per pixel FRP estimates for GOES and MODIS by the approximate active fire area determined using coincident 30 m resolution ASTER and ETM+ imagery [Schroeder *et al*., 2008b]. Values plotted represent the median of the fire intensity data available for each VCF interval.

Finally, large differences between MODIS and GOES FRP values were found to result from the effects of the PSF of each instrument. The same fires occupying the center of a pixel from one sensor and the edge of a pixel from the other sensor resulted in significantly different FRP estimates. Using the simulation data described in Section 4.3.3, we evaluated the contribution of the PSF of MODIS and GOES to the FRP values calculated (Figure 4.6). The reduction in FRP observed when a fire cluster is located away from the more responsive area near the pixel's center represented the single most important factor contributing to the differences in FRP estimates produced by MODIS and GOES. Due to the predominantly small size of Amazonian fires, the effects of PSF become particularly pronounced in the GOES and MODIS data.

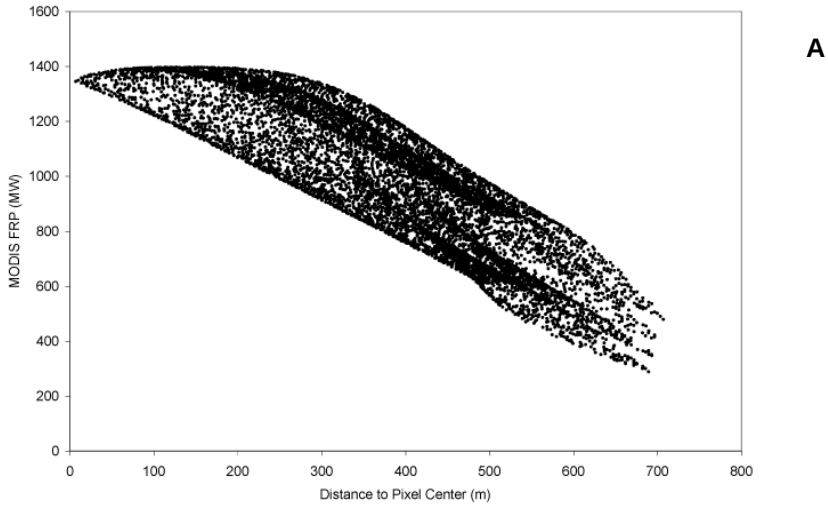

Figure 4.6: Simulated FRP for MODIS (A) and GOES (B) as a function of distance to the pixel's center. FRP estimates are calculated for a single thermal component fire at 800 K covering an area of approximately 5.5 ha, with background temperature of 311 K.

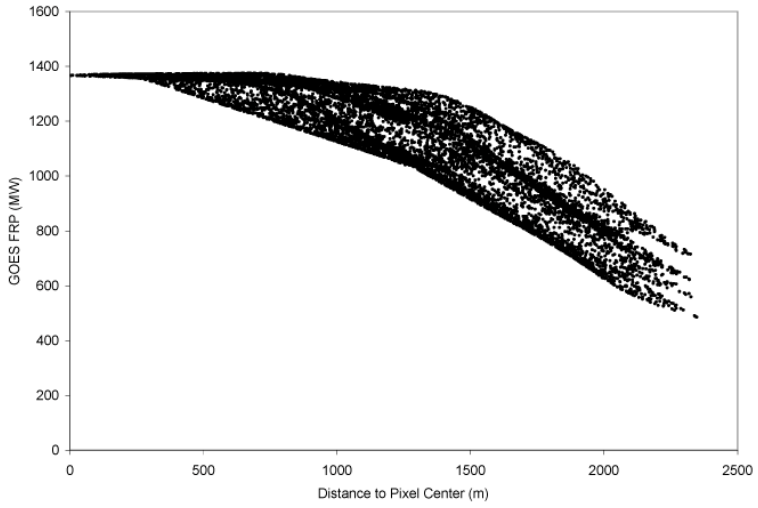

Figure 4.6 *continued*

4.4.2 MODIS and GOES Fire Detections

Our analysis of correspondence between the MODIS *Thermal Anomalies* and GOES WF-ABBA products used approximately 115,000 MOD14 detections, 225,000 MYD14 detections, and 25,000 and 93,000 WF-ABBA detections produced within 15 minutes from the MODIS Terra and Aqua overpasses, respectively.

Figures 4.7A and 4.7B show the rates of coincident detection between MOD14 and WF-ABBA and between MYD14 and WF-ABBA, respectively, using the instantaneous observation of GOES at near the same overpass time of Terra and Aqua. Commission error estimates derived in Chapter 3 are also shown in Figures 4.7A and 4.7B for reference. The low overall rate of MOD14 and MYD14 detections having a coincident WF-ABBA match occurs primarily due to the greater detection performance of the MODIS product [Schroeder *et al*., 2008b]. The rate of coincident detections increases towards intermediate-to-high percentage tree cover intervals as a

result of longer lasting and higher intensity fires which are typically found in those regions. These fires have a greater probability of detection by WF-ABBA [Schroeder *et al*., 2008b], thereby contributing to the increase of coincident detection rates with MOD14 and MYD14. Figures 4.7A and 4.7B also show the effects of the fire diurnal cycle on the results. The systematically lower (higher) rates of coincident detections between MOD14 (MYD14) and WF-ABBA show the contribution of smaller (larger) fires which predominate in the morning (afternoon) hours in response to the local atmospheric and fuel conditions. Due to its coarser spatial resolution, the WF-ABBA product will likely omit a greater percentage of the small morning fires compared to MOD14 creating the differences seen between Figures 4.7A and 4.7B.

The results describing the rates of coincident detection between MOD14 and WF-ABBA and between MYD14 and WF-ABBA using all daytime observations from GOES are shown in Figures 4.7C and 4.7D, respectively. Similar to Figures 4.7A and 4.7B, commission error rates for MOD14 and MYD14 derived from Chapter 3 are displayed in Figures 4.7C and 4.7D for reference. The increased rates of coincident detection produced demonstrate how effective the high observation frequency of GOES is in reducing the overall differences in detection performance seen in Figures 4.7A and 4.7B. The higher rates of coincident detection of MOD14 and WF-ABBA in Figure 4.7C show once again the effects of the diurnal cycle of fires. Compared to MYD14, morning MOD14 fires have a greater potential to benefit from the diurnal variation in atmospheric and fuel conditions as they enjoy an extended number of hours of increasing temperature and decreasing humidity of both fuel (i.e., vegetation) and the surface air layer. Therefore, small fires detected only by

MOD14 in the morning hours can develop into larger and more intense burning events until they become active enough to trigger a WF-ABBA detection during the subsequent observation hours [Schroeder *et al*., 2008b].

The fraction of MOD14 and MYD14 detections in Figures 4.7C and 4.7D occurring over intermediate-to-high percentage tree cover areas (VCF >40%) without a coincident WF-ABBA detection was similar to the commission error rates estimated for the MODIS products. Visual interpretation of 30 m ASTER scenes covering 46 MOD14 false detections coincidently imaged by GOES data showed that the majority of the cases (n = 44) did not produce a coincident WF-ABBA detection; whereas all coincident MOD14 and WF-ABBA detections examined (n = 73) showed visual confirmation of fire activity. This result suggests that: (i) coincident detections produced by different products can be classified as true positives; and (ii) isolated MOD14 detections occurring in densely vegetated areas could be associated with false detections (more so than MYD14 based on Figures 4.7C and 4.7D). Consideration of commission errors could not help explain a large fraction of MOD14 and MYD14 detections without spatially coincident WF-ABBA detections over low percentage tree cover areas. Short duration and low intensity fires which typically occur in Cerrado (savanna) regions may be the primary cause for the lower rates of coincident detections found as MOD14, MYD14 and WF-ABBA will show only small probability of detecting these highly dynamic fires.

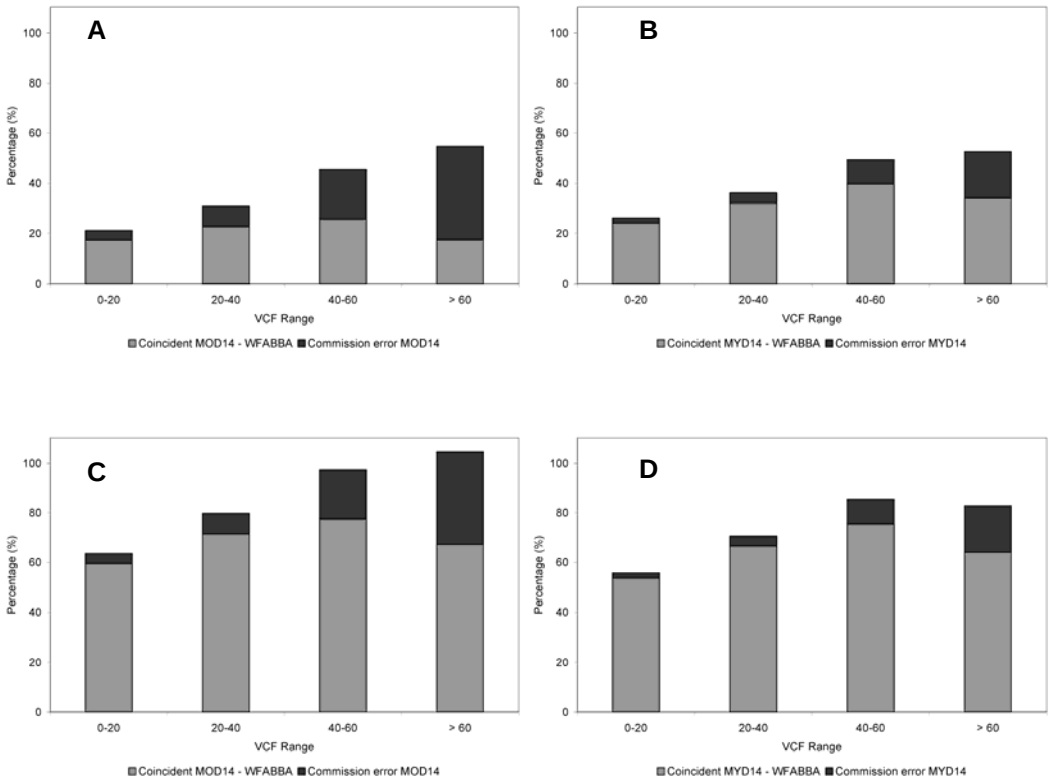

Figure 4.7: Rates of coincident detection (gray bars) for MOD14-WF_ABBA instantaneous (A), MYD14-WF_ABBA instantaneous (B), MOD14-WF_ABBA day-time (C), and MYD14-WF_ABBA day-time (D) observations. Commission error rates for MOD14 and MYD14 are also shown (black bars).

The results in Figures 4.7A-D describe the rates of MODIS (MOD14 or MYD14) fire detections having a spatially coincident WF-ABBA detection. We also assessed the opposite condition, i.e., we derived the rates of WF-ABBA fire detections having spatially coincident MODIS detections. The results were considerably less intuitive in this case. On average, only 50% of the WF-ABBA detections produced at the time of MODIS Terra overpass showed spatially coincident MOD14 detections (Figure 4.8A). An even lower percentage (40%) of WF-ABBA detections produced at the time of MODIS Aqua overpass had spatially

coincident MYD14 detections (Figure 4.8B). The low rates of coincident detections were consistent across all four percentage tree cover intervals. Visual inspection of 30 WF-ABBA morning fire detections without a coincident MOD14 detection using ASTER 30 m scenes revealed that the majority of the cases (75%) were associated with a false detection. The remaining 25% of the WF-ABBA detections inspected had significantly small active fires within the GOES pixel footprint, and could indicate potential false alarms induced by relatively cooler background conditions.

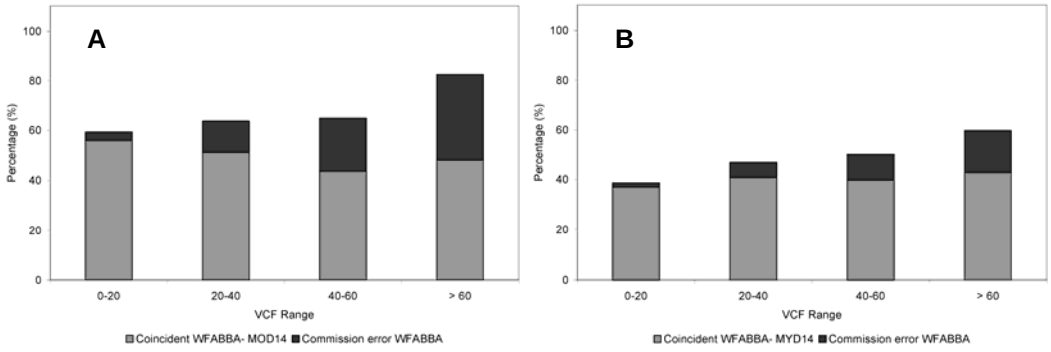

Figure 4.8: Rates of coincident detection (gray bars) for WF-ABBA-MOD14 (A), WF-ABBA-MYD14 using instantaneous GOES data. Commission error rates for WF-ABBA are also shown (black bars).

The daily sums of paired MOD14-WF-ABBA and MYD14-WF-ABBA detections derived for a 200×300 km^2 area centered in Mato Grosso state, southern Brazilian Amazonia are shown in Figure 4.9. We used three years of data (2003-2005) totaling 15,000 MODIS and 8,000 GOES fire detections overlapping with the area above. The fixed location of the spatial subset used resulted in constant GOES viewing conditions, while the observation geometry of MODIS varied on a daily

basis. Consequently, the performance of the MODIS fire product changed as a function of scan angle due to the pixel distortion towards the edges of the swath.

The diurnal cycle signature was also found to be pronounced in Figure 4.9. Morning fire detections were predominantly originated from MODIS Terra data, with the contribution of GOES detections increasing towards the afternoon. Both MODIS Terra and Aqua data showed the effects of pixel distortion. Assuming the detection performance of WF-ABBA to be invariant across the subset area and period analyzed, we estimated the detection performance of MODIS near the edge of the swath to be on average approximately 40% lower compared to nadir viewing conditions. Greater variability in detection performance is seen to affect both MOD14 and MYD14 products at higher scan angles as indicated by the boxes and lines in Figure 4.9. The longer atmospheric path described at extreme MODIS scan angles could help explain such variability as it will likely affect the detection probability of underlying active fires for heavily contaminated atmospheres. The *bow tie* effect which produces significant pixel overlap at large MODIS scan angles could also contribute to the detection variability observed. In this case, the pixel overlap can produce duplicate detections composed of single or multi-pixel clusters with consequences to the daily sum statistics of fire detections of MODIS Terra and Aqua.

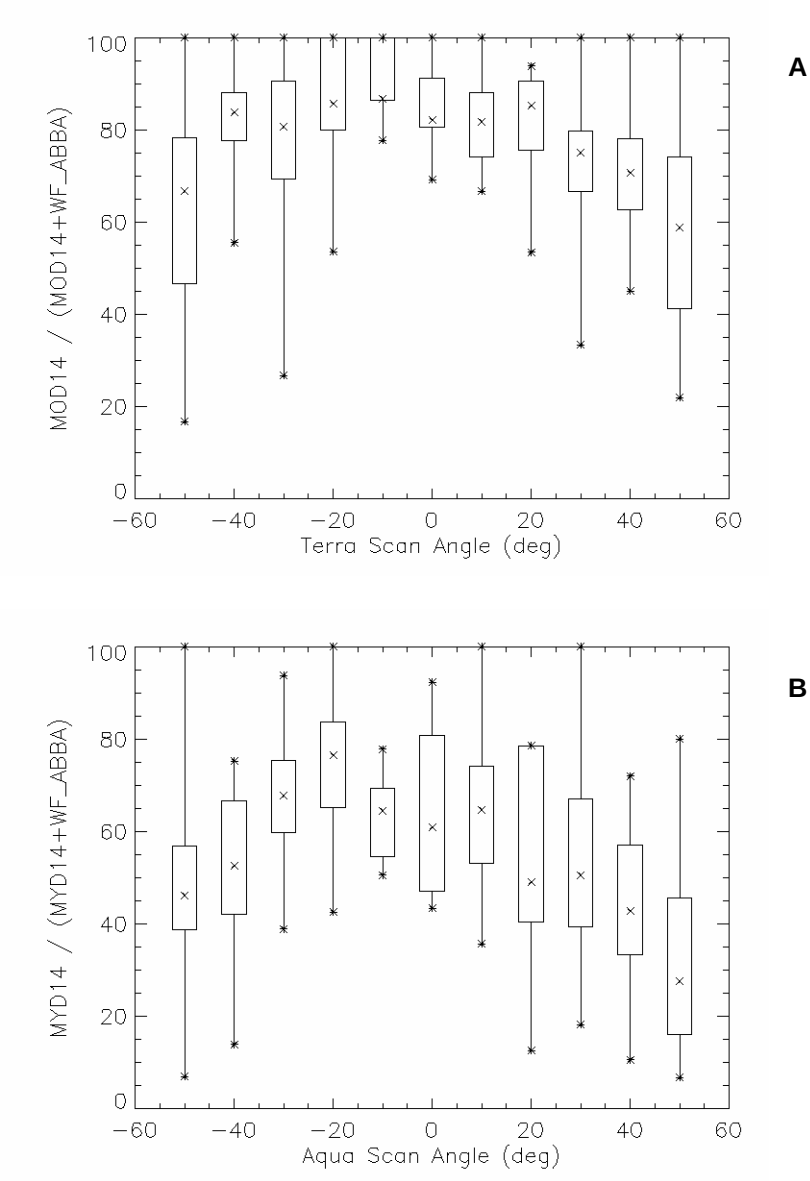

Figure 4.9: Box plots for the relative contribution of MOD14 (A) and MYD14 (B) products to the sum of MODIS and GOES fire detections produced using an area of 200×300 km^2 centered in Mato Grosso state, southern Brazilian Amazonia. Parameters depicted in the plot include: minimum, 25th percentile, median, 75th percentile, and maximum values. Results were separated into 10^{o} scan angle intervals of MODIS. Positive and negative scan angles describe the east and west parts of the MODIS swath, respectively.

4.5 CONCLUSIONS

Each year earth remote sensing satellites detect hundreds of thousands of vegetation fires across Brazilian Amazonia and thereby represent the primary source of information for a large number of fire data users. In this study, we assessed how different satellite active fire detection data might be used synergistically to provide improved detection rates with higher confidence than can be obtained from individual products.

Our study showed that fires of relatively small active area predominate in Brazilian Amazonia. Approximately 90% of all fires sampled had an area of less than 3 hectares (assuming the ASTER and ETM+ 30 m pixels used to create the statistics were completely covered by active fires), therefore representing a significantly small fraction of a moderate-to-coarse resolution pixel. Amazonian fires were also found to be both spatially and temporally concentrated, with multiple fires occurring simultaneously within a few kilometers from each other. Consequently, single or multi-pixel fire detection clusters coincidently produced by MOD14 (MYD14) and WF-ABBA were prone to contain different amounts of fire activity within each pixel.

The challenges for active fire detection products based on moderate-to-coarse resolution data are many in this case, regardless of the algorithm used. For instance, fire characterization via FRP may result in biased estimates depending in particular on the number of individual active fires contained within the fire detection pixel and on how the energy released by the fire is represented by the instrument's PSF. Additionally, Amazonian fires tend to concentrate in areas of deforestation where the landscape heterogeneity is high making the derivation of FRP values even more

difficult. As a result, the potential for creating a hybrid fire product combining MODIS and GOES FRP estimates is significantly limited.

The analyses of fire detections revealed that if one is interested in representing the total fire occurrence for high percentage tree cover areas (>40%), the better temporal resolution of the GOES data detecting the diurnal cycle of fires improves upon the twice daily detection of MODIS at a higher spatial resolution. Therefore, differences in daily fire detection in particular between MOD14 and WF-ABBA may be reduced or even eliminated. False detections produced by MOD14 were predominantly isolated from WF-ABBA detections, while 100% of the areas showing coincident detections from those two products had visual confirmation of fire activity. Consequently, MOD14 (and similarly MYD14) could be used to reinforce our confidence of coincident WF-ABBA detections, while the remaining non-coincident MOD14 detections (more so than MYD14 ones) may indicate areas of potential commission errors particularly in high percentage tree cover areas (>40%).

For low percentage tree cover areas, omission errors are high and fires are very dynamic thereby reducing the number of coincident detection between MOD14 (MYD14) and WF-ABBA. In this case, the low overall commission error rates suggest that combining MOD14, MYD14 and WF-ABBA fire detections could be the best approach to improve biomass burning monitoring in those regions.

Visual inspection of 30 m resolution ASTER imagery suggested that commission errors in WF-ABBA could be largely responsible for the low rates of coincident detections between WF-ABBA and MOD14. Large burnt areas occurring at the same spatial scale of the GOES pixels were seen to produce WF-ABBA fire

detection clusters without a MOD14 match. The percentage of WF-ABBA fire pixels without a coincident MOD14 or MYD14 detection exceeded the commission errors estimated for the WF-ABBA by Schroeder *et al*. [2008], and further investigation is required.

The detection performance of the MOD14 and MYD14 at extreme scan angles (55º) was found to be approximately 40% lower compared to nadir viewing conditions. The use of area averaged statistics of daily MOD14 (MYD14) and WF-ABBA fire detections as a means to compare the two products resulted in poor correlation between those datasets across a range of MODIS observation conditions. The ratio between MOD14 (MYD14) and WF-ABBA detections were especially variable at high MODIS scan angles, where the *bow tie* effects and the occurrence of thick smoke plumes could influence the number of detections produced.

The results above summarize some of the major limitations of current satellite active fire detection products. The nature of fire activity in Brazilian Amazonia and the image characteristics of MODIS and GOES were found to affect fire detection probability and the retrieval of physical parameters of a large percentage of vegetation fires in the region.

Regardless of the limitations above, increasingly sophisticated fire alert systems and biomass burning emissions models create a large demand for higher temporal and spatial resolution fire data [Freitas *et al*., 2005; GCOS, 2006; GOFC, 2006; Wooster *et al*., 2003]. The next generation suite of sensors to become operational on board the National Polar-orbiting Operational Environmental Satellite System (NPOESS) and the GOES-R will show improvements in terms of spatial (and

temporal in the case of GOES-R) resolution which could result in greater fire detection and characterization capabilities compared to existing products. However, the primary channel for active fire detection located in the mid-infrared region in both systems might be affected by inadequate pixel saturation specifications and pixel resampling methods which could penalize the performance of future fire detection products derived from those data sets. Unless the quality and the integrity of the new data are preserved, the user community may continue to experience a shortage of detailed information about fire activity with important consequences to the understanding of regional and global climate system processes and their implications to society.

Chapter 5: Integrated Fire Product

5.1 INTRODUCTION

The results derived from Chapters 2-4 were used to guide the production of a new integrated fire product for Brazilian Amazonia based on MOD14, MYD14 and WF-ABBA input data. The new product was aimed to generate the best possible fire detection data with reduced commission and omission errors. A 4 km grid was used to process daily MODIS and GOES data including all daytime and nighttime detections. A set of criteria was developed utilizing the complementarity of the above products to generate an integrated product of fire detection data, namely:

i. Cloud obscuration omission errors were calculated for each 4×4 km cell using the methodology described in Chapter 2;
ii. Commission errors were calculated for each 4×4 km cell as a function of percentage tree cover based on the results from Chapter 3;
iii. False detections in MOD14 (MYD14) and WF-ABBA were considered non-coincident. Based on the results from Chapter 4, spatially coincident detections (i.e., detections within the same 4×4 km cell) produced by more than one product were classified as true positives;

iv. Daytime MOD14 fire detections without a spatially coincident MYD14 or WF-ABBA detection were discarded for high percentage tree cover areas (>40%) based on the results from Chapter 4.

In addition, nighttime detections were all considered true positives based on the analysis of 20 ASTER scenes used to validate the MOD14 product derived from nighttime MODIS Terra overpasses using the same methodology described in Chapter 3. All nighttime detections validated (n = 62) were classified as true positives, suggesting that false detections are primarily a result of daytime land surface temperature dynamics.

5.2 METHODS

The integrated product differs from the simple sum of MODIS and GOES fire detection products as it is based on the use of multiple criteria to determine the consistency of fire detections produced for an individual 4×4 km area. Starting at 00:30 h local time each day, individual 4×4 km cells contained within Brazilian Amazonia were monitored for the occurrence of fire detections produced by MOD14, MYD14 and WF-ABBA until 24:00 h local time (Figure 5.1); all hours reported hereafter are considered local time.

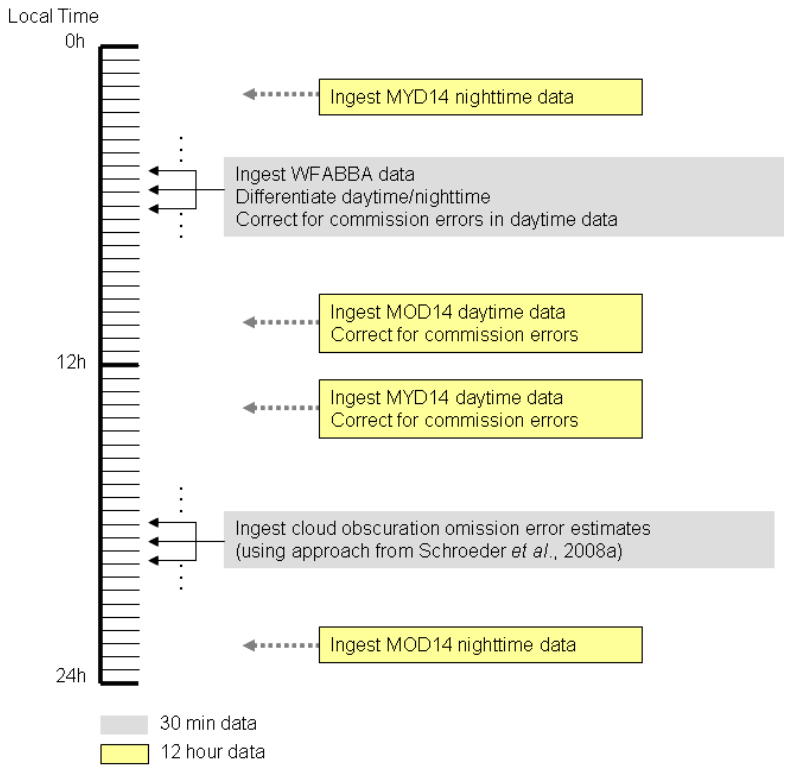

Figure 5.1: Flow diagram describing the processing scheme used to integrate MOD14, MYD14 and WF-ABBA fire detections. Ingestion of WF-ABBA and cloud obscuration omission error estimates occurs at 30 min intervals during day and nighttime periods of every 24 h cycle.

Daytime fire detections were adjusted for commission errors based on the percentage tree cover values of the affected 4×4 km cell following the error matrix analysis presented in Chapter 3. Percentage tree cover estimates were derived using the 2005 500 m Vegetation Continuous Fields (VCF) product [Hansen *et al*., 2002; Hansen *et al*., 2003]. Commission error rates at the time of Aqua overpass were assumed 50% lower compared to the time of Terra overpass based on the results from Section 3.4.3. Commission error rates for the WF-ABBA product at observation

hours different from the Terra and Aqua overpass times analyzed in Chapter 3 were estimated using information describing the approximate diurnal cycle of brightness temperature of forest and non-forested pixels in the mid-infrared spectral region (Section 3.4.3, Figure 3.9). Large differences in brightness temperature values between forest and non-forested pixels were found to be an important factor leading to false detections in the MODIS and GOES active fire detection products validated in Chapter 3. Using the false detection and brightness temperature data shown in Figure 3.9, a second order polynomial was fitted to the curve representing the brightness temperature contrast between forest and non-forested GOES pixels and normalized. This was done in order to have the commission error rate at 13:30 h being 50% lower than at 10:30 h, with a peak (value equal to 1) centered at approximately 11:45 h. The resulting curve intercepts the zero commission error mark at approximately 8:30 h and 14:30 h; i.e., commission errors are considered null for GOES images acquired earlier than 8:30 h or later than 14:30 h. This approximation may be revised in the future provided that improved commission error estimates become available.

For deriving the integrated product, when multiple daytime WF-ABBA fire detections occur for an individual 4×4 km cell, we used the lowest commission error estimated from all the observation hours producing detections. Based on the assumption that false detections from different products do not overlap, grid cells showing multiple daytime fire detections originated from more than one fire detection product are confirmed to have vegetation fire activity for the calendar date in question.

Omission errors due to cloud obscuration estimated at 30 min intervals for individual 4×4 km cells are accumulated for each 24 hour cycle, resulting in a 0-100% chance of fire omission at the end of each calendar date.

Lastly, the occurrence of any nighttime fire detection overrules any of the previous assumptions, leading to confirmed fire activity for a 4×4 km cell irrespective of the product which originated the entry.

5.3 RESULTS

The integration analysis used data from 2005 for which the cloud obscuration omission error estimates derived in Chapter 2 were available. The 2005 MOD14, MYD14, WF-ABBA, and integrated fire detection density maps re-sampled to a 40 km grid are shown in Figure 5.2A-D, respectively. Although the spatial extent of most features depicted by the original MOD14, MYD14 and WF-ABBA fire detection maps are similar, the integrated product helped highlight areas of increased fire activity across the region. Active deforestation areas including southeastern Pará, central Mato Grosso, and northern Rondônia resulted in the largest fire detection densities in Brazilian Amazonia. Areas typically associated with low percentage tree cover (east and south regions on the map) also showed large fire detection densities in the integrated product suggesting that fire activity in those areas could be underestimated by the original fire products. The relatively small fire detection densities depicted by the MOD14 product in Figure 5.2A show that a strong fire diurnal cycle could significantly limit the detection rates of sensors flying on morning orbits.

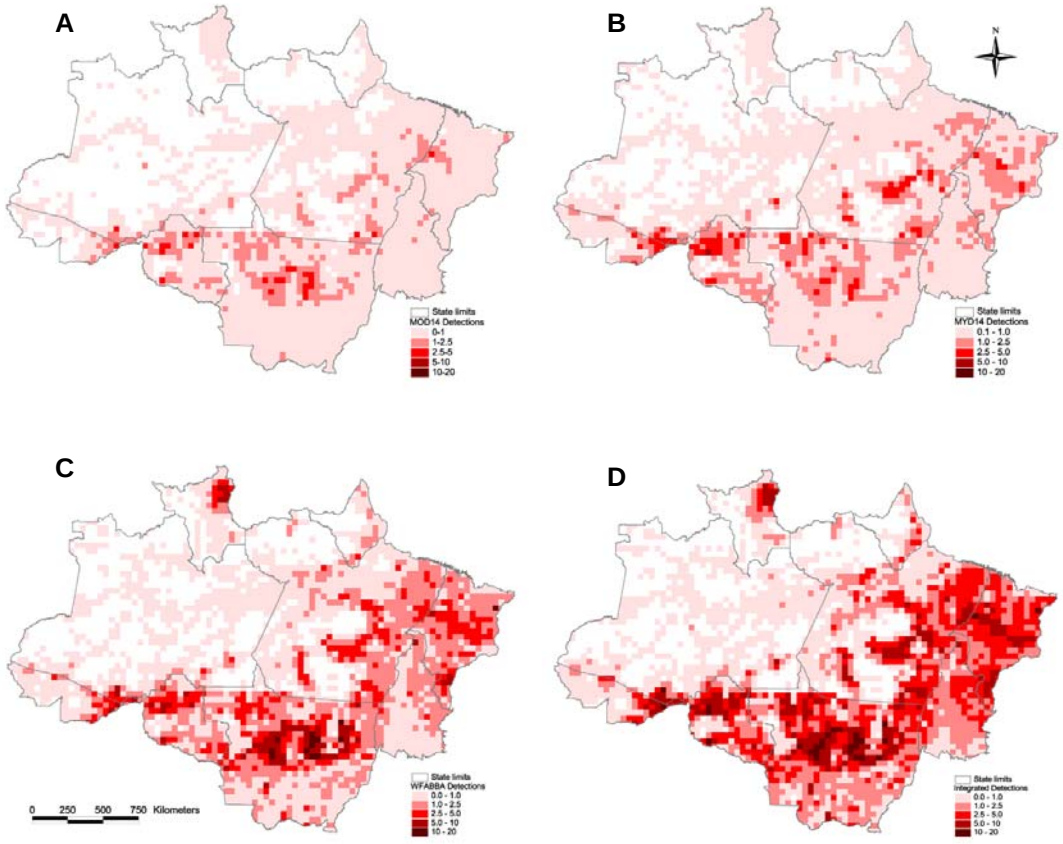

Figure 5.2: Annual (2005) fire detection density maps for the original MOD14 (A), MYD14 (B), and WF-ABBA (C) products, and the integrated product (D) for Brazilian Amazonia. The scales represent the average number of days with detections calculated for individual 40 km cells.

The differences in detections between the integrated product and the simple sum of fire products are shown in Figure 5.3. Negative and positive values result primarily from corrections applied to the integrated product to reduce commission errors and omission errors due to cloud obscuration, respectively. The result suggests that large areas of Brazilian Amazonia showing small differences between the

integrated product and the simple sum of fire products could have those errors balanced. However, small regions including central Mato Grosso state could be under the influence of a systematic bias resulting in an overestimation of fire activity. In fact, high fire detection rates were observed in the integrated product over certain locations described by individual 4×4 km sub-cells. In those areas, potentially unrealistic annual detection rates exceeding 30 days of co-located burning activity suggested that the bias due to commission errors could be even larger than is depicted in Figure 5.3. While the number of individual locations with high fire detection rates was relatively small (approximately 1,000 sites compared to 340,000 cells contained in region), the persistent burning signal which results from those areas could have important implications for both fire alert systems and biomass burning emissions modeling.

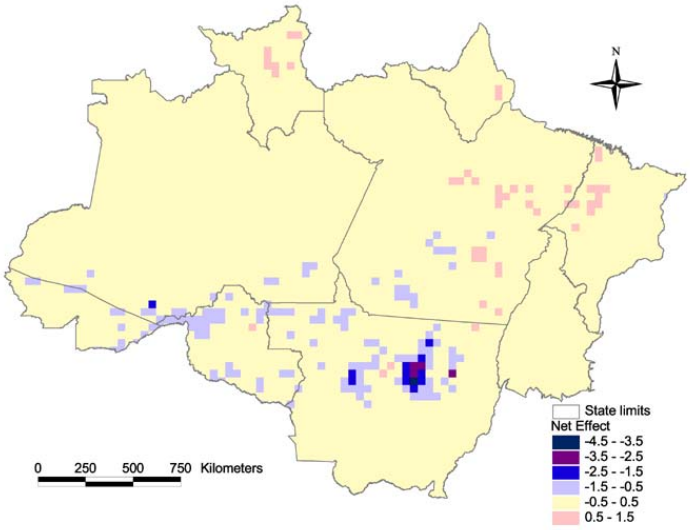

Figure 5.3: Net correction applied to the combined detections of MOD14, MYD14 and WF-ABBA based primarily on commission error rates and omission errors due to cloud obscuration. The scale represent the average number of days with detection that were added (positive values) or subtracted (negative values) from the integrated data for individual 40 km cells compared to the simple sum of the products above.

5.4 QUALITY ASSESSMENT

A quality assessment of the results produced by the integrated product in central Mato Grosso was performed using two sets of Landsat 5 Thematic Mapper (TM) scenes at 30 m resolution acquired 16 days apart (row/path: 227/68; first set acquired on July 01 and July 17 2005; second set acquired on August 02 and August 18 2005). The Landsat 5 TM data were complemented by two collocated 20 m resolution China-Brazil Earth Resources Satellite (CBERS) images acquired on July 13 2005 and August 08 2005. The selection of the central Mato Grosso region to assess the quality of the integrated product was motivated by two primary reasons: (i) results from Chapter 3 and from Section 5.3 above suggest that this area could have high commission errors; and (ii) the availability of Landsat 5 TM and CBERS images acquired within only a few days from each other provided a unique opportunity to generate detailed fire information for the area.

To derive the reference burn area maps, the image data covering the 0.77-0.90 μm region in each sensor were inter-calibrated in order to provide comparable top of the atmosphere reflectance measurements. In this spectral region, burned areas can be easily distinguished from the surface background as a result of a sharp reduction in the reflectance values measured over ash and char covered pixels. After resizing the CBERS images to 30 m resolution and registering them to the Landsat 5 TM data, image differences were computed and an empirical threshold was applied to classify new burn scars occurring between two consecutive acquisition dates.

The reference burn scar data produced using the approach described above, supported the assessment of the integrated fire product generated for the same time

periods separating two consecutive Landsat 5 TM and CBERS images. The 4×4 km cells showing burn scars of any size were identified and compared to the integrated fire detections produced using the same grid cell resolution and time interval.

Despite the large number of fire detections appearing in the integrated product during the periods analyzed, the number of new burn scars was relatively small suggesting that potentially large commission errors could remain in the integrated fire product. However, inspection of active fire pixels identified using an empirical threshold applied to the 2.09-2.35 μm channel of Landsat 5 TM showed that the large majority of the fires (> 90%) occurring in that region and time period did not produce a detectable burn scar. Visual interpretation of the active fires mapped indicated the prevalence of small areas of burning often associated with closely aligned fire lines typical of piled debris. Therefore, the use of higher resolution imagery acquired only a few days apart did not provide appropriate means to assess the quality of the integrated product at the critical area of central Mato Grosso.

Alternatively, evaluation of the integrated product was attempted using the 30 m active fire pixels mapped with the Landsat 5 TM data. The integrated product was processed for four individual calendar dates corresponding to the same acquisition dates of the Landsat 5 TM images selected. The main purpose of this analysis was to compare the fire detections produced by the original input fire products to the fire information resulting from the integrated product using the 30 m active fire data to validate the results. Only fire detections initiated at the approximate overpass time of Landsat 5 TM were considered (± 30 min tolerance); detections produced for those same locations during subsequent hours were also used for processing the integrated

product. The time difference constraint limited the analysis to the WF-ABBA data only, since the Landsat 5 TM images in Amazonia overlap with areas without daytime MOD14 coverage for the same acquisition date. This lack of coverage results from the MODIS ground sampling characteristics near the equator which creates large spatial gaps [Wolfe *et al*., 2002]. The use of MYD14 was equally compromised due to the large differences in overpass time separating the orbits of the Landsat 5 and Aqua satellites.

The WF-ABBA detections were classified as true positives and false positives depending on the presence or absence of coincident 30 m active fires, respectively. Similarly, the locations classified as fire in the integrated product were validated using the 30 m active fire data. Table 5.1 shows the classification of all fire locations indicated by WF-ABBA and the integrated product. Fractional numbers appearing in the columns representing the integrated product in Table 5.1 resulted primarily from the application of corrections to account for commission error rates in the WF-ABBA data ingested into the integrated product processing routine. Compared to the original WF-ABBA fire detection data, the integrated product resulted in a small decrease in false positives while preserving true positive detections nearly unchanged. This first evaluation suggests that the integrated product could improve the fire detection information of WF-ABBA although we recognize that due to the small sample used, a more comprehensive quality assessment of the integrated product should be in the subject for future study.

Table 5.1: Evaluation of WF-ABBA detections and the integrated fire product data using 30 m active fire data derived from Landsat 5 TM imagery.

	True Positives (number of detections)	*False Positives (number of detections)*
WF-ABBA	28	16
Integrated Product	27.8	14.1

5.5 CONCLUSIONS

A new integrated fire detection product based on the MOD14, MYD14 and WF-ABBA products was presented in this Chapter. A set of judicious criteria was used to exploit the complementarity among those products and to increase the consistency of the detections represented in the integrated product. Areas of high detection frequency were highlighted in the integrated product. Those areas coincided with active deforestation regions reinforcing the concept that conversion fires are responsible for the largest detection frequencies in Brazilian Amazonia [Eva and Fritz, 2003; Morton *et al*., 2008]. The large differences among the detection rates derived using MODIS Terra and Aqua and GOES data reflected the importance of the fire diurnal cycle in the region and the need for more systematic high temporal resolution imaging of fire activity in Brazilian Amazonia.

A complete quality assessment of the integrated fire product over areas including central Mato Grosso state could not be accomplished primarily due to the scarce availability of validation data and the absence of burn scars from these fires.

Those two aspects limited the evaluation of the integrated fire product to the times near the acquisition hours of Landsat-equivalent data when fire activity is reduced.

The occurrence of fires without a distinguishable burn scar in areas such as central Mato Grosso state raise some of the potential limitations involving burn scar mapping products using classification schemes based on visible and near-infrared bands (e.g., the MODIS burned area product [Roy *et al*., 2005]). It also highlights the importance of complementing those burn scar products with active fire data in order to achieve a more complete representation of biomass burning in the region.

Although some problems undoubtedly remain in the integrated fire product described above, it improves upon single source and multisource products based on the simple accumulation of individual fire detections. The quantification of some of the primary sources of errors influencing the MOD14, MYD14 and WF-ABBA products and the relationships between them could provide invaluable information to assess the main implications for biomass burning emissions modeling in South America as well as to guide future improvements of the fire detection products.

Consideration of the full diurnal cycle during processing of multiple fire detections required that improved validation data sets be used to fully assess the qualities and limitations of the new integrated product. The use of airborne systems providing higher frequency image acquisition may be necessary to comprehensively assess the diurnal cycle of commission errors and the performance of the integrated product.

Chapter 6: Conclusions

6.1 SYNTHESIS OF RESEARCH

The demand for information on fire activity in Amazonia has significantly increased in the past two decades with the concern about the fate of the tropical rainforest [Nepstad *et al*., 1999b; Nepstad *et al*., 2001; Morton *et al*., 2006; Shukla *et al*., 1990]. Satellite active fire detection products represent the primary data source for Amazonian fire alert systems. These data are also of interest to the scientific community. However, little information is available about the performance of the current products and differences among data sets create additional problems for the user community. This dissertation was designed to quantify the errors and to assess the complementarity amongst different products. The main objective of the research was to improve the quantification of vegetation fire activity in Brazilian Amazonia through the use of multiple satellite remote sensing fire data.

6.1.1 Omission Errors due to Cloud Obscuration

Fire detection omission errors due to cloud obscuration in the WF-ABBA product derived from GOES-East imager data were quantified in Chapter 2. A pixel based probabilistic approach was proposed, using information on previous fire occurrence and precipitation. The methodology was implemented using data covering

the entire diurnal cycle of fire activity and cloud occurrence. The results suggested that by ignoring land use patterns and rainfall regimes and by adopting generalized grid based analyses, previous studies using more simplistic approaches have overestimated the effects of cloud obscuration on fire detections.

Fire occurrence was found to be influenced by regional precipitation regimes which limit fire use to a short period of time in the dry season, and was largely related to areas of rapid land cover change found in particular along the Arc of Deforestation. The assessment of the omission errors due to cloud obscuration used satellite precipitation data and WF-ABBA fire detection records from previous years to delineate the spatial and temporal characteristics of fire activity in the region. A cloud mask was generated for the GOES data and omission errors were estimated using a 4 km grid to reproduce the nominal spatial resolution of the GOES imager. The methodology was proven successful, resulting in consistent cloud obscuration omission error estimates for the WF-ABBA fire product.

6.1.2 Clear Sky Omission and Commission Errors

Following the analyses of fire omission errors due to clouds, a comprehensive validation study was implemented to quantify clear sky omission and commission errors for the WF-ABBA and the MOD14 products over Amazonia. The analyses discussed in Chapter 3 represent the first in depth assessment of the fire detection performance of the WF-ABBA product using real time validation data. The validation approach built on the work of Morisette *et al*. (2005a) who first tested the application of 30 m resolution ASTER imagery to assess the detection performance of the

MODIS Fire product (MOD14) for Southern Africa. That methodology was expanded to incorporate the GOES data into the analyses and a new active fire detection product was generated using Landsat ETM+ imagery. As with the ASTER data, the 30 m resolution Landsat ETM+ fire product was used as "ground truth" data to validate the WF-ABBA fire detections. This validation approach fulfills the requirements for independent data usage to assess the quality of remote sensing satellite products defined by Morisette *et al*. [2002]. Compared to ground validation, higher resolution imagery provide more appropriate means to tackle related scaling issues of fine-scale processes in moderate resolution data, and in this respect the use of 30 m Landsat ETM+ and ASTER data to validate MODIS and GOES products is recognized as a viable alternative [Morisette *et al*., 2002]. To assure the quality of fire masks derived from the Landsat ETM+ and ASTER, an extensive quality control was performed including detailed visual inspection of all images used. Errors in the Landsat ETM+ and ASTER fire mask data were therefore considered negligible. Also, comparison of near coincident Landsat ETM+ and ASTER fire masks showed that the two data sets produced similar results and therefore could be used interchangeably. Sum statistics of 30 m active fire pixels derived from ASTER and ETM+ were produced for the footprint of individual GOES pixels and used to fit a logistic regression model describing the detection probability curve for the WF-ABBA product.

The differences in detection performance for MOD14 and the instantaneous WF-ABBA product were systematically validated for different surface conditions. On average, WF-ABBA required four times more active fire area than MOD14 to

achieve equivalent detection probability rates for similar fire conditions. The distance separating the detection probability curves of MOD14 and WF-ABBA derived from the logistic regression analysis was proportionally less than the difference in spatial resolution of the two instruments. In this case, other sensor characteristics including the spectral location and bandwidth of the mid-infrared GOES channel could have contributed to enhance the response of the WF-ABBA product to sub-pixel fires, thereby reducing the difference in detection performance relative to the MOD14 product.

Omission error rates estimated for the approximate time of the ASTER and ETM+ overpasses (i.e., 10:00-10:30 local time) were high for both WF-ABBA and MOD14 products when fires of all sizes detected with the 30 m resolution fire masks were considered. In particular, high omission errors were seen to affect the MOD14 and the WF-ABBA products in areas of low percentage tree cover. Major differences in fire conditions across different land uses and land cover types were found through the analysis of data collected from multiple prescribed burns during three different field campaigns in Brazilian Amazonia. Maintenance fires (e.g., pasture and crop residue burning) predominating in areas of low percentage tree cover were characterized by lower temperature (~ 700 K) and narrow flaming fronts, followed by a relatively cool smoldering phase. These highly dynamic conditions result in a significantly small window of time during which fire detection is possible. The surrounding background conditions associated with those fires was also found to be an important factor influencing detection probability of contextual algorithms based on moderate or coarse resolution sensor data. The occurrence of warm and bright

background pixels in low percentage tree cover regions resulted in reduced contrast with the fire affected pixel, therefore causing the latter to fail the contextual tests. Consequently, detection performance of moderate (500 -1 km) and coarse resolution (> 1 km) fire products over low percentage tree cover conditions could be considered limited, being subjected to potentially large omission errors.

Vegetation fires used for clearing forest debris along biomass-rich deforestation areas showed different characteristics compared to the fires occurring in low percentage tree cover regions and omission error rates were consequently smaller. Forest conversion fires burned at very high temperatures (~ 1100 K) and for a prolonged time (hours as opposed to minutes), significantly increasing the chances of detection by one or more instruments.

The high temporal resolution of the GOES imager proved very useful to reduce the instantaneous omission error rates derived for the WF-ABBA product using coincident ASTER and ETM+ data. In fact, when all daytime GOES imager data were considered the estimated WF-ABBA omission error was half of that found for the instantaneous MOD14 product based on a similar fire sample. This finding reinforces the importance of fire diurnal cycle in the region, suggesting that fire activity tends to intensify towards the afternoon hours enabling the detection of an increased number of fire pixels by the WF-ABBA product.

Similarities among the commission error rates estimated for WF-ABBA and MOD14 showed a tendency of contextual algorithms to fail over areas characterized by large gradient in percentage tree cover. False detections were particularly prone to occur along areas of active deforestation in Brazilian Amazonia, resulting from the

strong brightness temperature contrast in the mid-infrared region established between recently burned deforestation sites and the surrounding forests. Multiple false detections persisting over the same location suggested that the radiometric signature of some burn scars could remain unaltered for as many as 32 days, the maximum separation found for spatially coincident false detections in the MOD14 data.

Smaller differences in thermal inertia between forested and deforested areas were largely responsible for a 50% reduction in commission errors during the early afternoon hours when fire activity approaches its maximum. This decrease in commission error rates should enhance the character of the diurnal cycle of fire detections even further provided that false alarms occurring during mid-to-late morning hours are accounted for. Fire-unrelated commission errors (i.e., pixels with no indication of active burning or burn scars) accounted for only 3% of all fire detections produced by WF-ABBA and MOD14. Therefore, active fire detection products could provide useful information for burned area mapping algorithms by identifying areas of fire occurrence with low commission error rates.

Commission errors in MOD14 could not be reduced using the additional scientific data available for the detection pixel and its surroundings provided in the product. The data include the brightness temperature in the mid-infrared and thermal infrared channels for the target pixel and its background, detection confidence estimate, and fire radiative power derived for the fire pixel. Due primarily to the ambiguity between the conditions describing true and false detections based on the parameters above, post-processing of commission errors was not possible. However, refinement of both MODIS *Thermal Anomalies* and WF-ABBA products could be

accomplished through the adoption of additional tests to help differentiate true and false detections. For instance, a method to reduce commission error rates was tested using temporal metrics based on the brightness temperature calculated for the mid-infrared channels of GOES and MODIS. The application of such method to a subset of the validation data proved successful in separating true and false detections and thereby represents a potential area for future development of active fire detection products. Regions of tropical deforestation where high commission error rates (> 30%) predominate are particularly suited to the application of a fire detection algorithm which incorporates the use of temporal metrics in the mid-infrared region. In those areas, surface temperature conditions remain mostly invariant for prolonged times favoring the use of change detection schemes to capture anomalous variations in pixel brightness temperature values between images that can be caused by vegetation fires.

The clear sky omission and commission errors reported in Chapter 3 were largely a function of the fire use and land cover types found in Brazilian Amazonia. High commission error rates associated with recently burned forest clearings of approximately the same size of a MODIS or GOES pixel footprint could be specific to the Arc of Deforestation and less common elsewhere. Despite the commission problem identified in this study, MODIS and GOES fire detection data provide invaluable information for the Amazon fire data user communities. Basin wide commission errors were approximately 15% for both MODIS and GOES fire products, with commission problem almost exclusively (> 80%) associated with recent fire activity. The estimated fire-unrelated commission error rates of 3% agreed

with the results of Csiszar *et al*. [2006] and Schroeder *et al*. [2008c] who derived clear sky commission and omission errors for the MODIS Terra *Thermal Anomalies* product over Northern Eurasia and the conterminous United States, respectively. This result suggests that a global commission error rate for the MODIS fire product may be ~3%.

Additional fire product error assessment remains an important topic for regional studies. Priority regions for validation analyses include parts of Africa and southeast Asia where high fire detection frequency and intensive land use and land cover change similar to Amazonia may result in comparable commission issues.

6.1.3 Towards Integrating MODIS and GOES Fire Detection Data

With the characterization of omission and commission errors completed, Chapter 4 discussed the potential for integrating MODIS and GOES active fire data. The use of high temporal resolution GOES data combined with the moderate spatial resolution of MODIS created an optimum environment to test how fire products generated from sensors with different characteristics complement each other.

The spatial and temporal characteristics of Amazonian fires were first considered in order to determine the most appropriate approach to use for the integration analyses. Fire size statistics derived from 30 m resolution ASTER and ETM+ data suggested that nearly 90% of the fires actively burning at 10:00 local time were composed of fire clusters with less than 30 pixels, or the equivalent to approximately 3 ha of a variable mix of flaming and smoldering fire components and unburned background vegetation. Fire size statistics demonstrated how vegetation

fires in Amazonia are small in size. In most cases fires are used in a controlled fashion therefore being constrained to small subsets of individual properties where the land is being managed. Consequently, Amazonian fires usually occupy only a reduced fraction of a MODIS (<3%) or GOES (<0.2%) pixel.

The communal use of fires involving simultaneous burning in neighboring properties which predominates in various parts of Amazonia was clearly depicted by the statistics describing the distance separating adjacent active fires. Approximately 80% of the fires showed a second area of burning within less than 8 km. This small separation is equivalent to just about two adjacent GOES pixels, and is similar to the navigation error of the GOES data.

The small size of vegetation fires in Amazonia and the proximity between areas of simultaneous burning created major limitations for the use of any kind of pixel level analysis to integrate the MODIS and GOES fire detection products since overlapping pixels would likely contain different amounts of fire activity. To overcome this constraint, the effects associated with a high fire spatial frequency were minimized by aggregating adjacent MODIS or GOES fire detections into clusters.

The integration analysis tested the use of Fire Radiative Power (FRP) to integrate the MODIS and GOES fire data. FRP is a physical parameter describing the energy released primarily by the flaming components of vegetation fires; therefore it facilitates the comparison between different products while also being useful to estimate biomass burning combustion rates [Kaufman *et al*., 1998b; Wooster, 2002; Wooster *et al*., 2003]. The analysis involving MODIS and GOES FRP estimates was

implemented using a conservative approach to reduce artifact contamination of the results, including the adoption of strict spatial criteria and removal of data points containing saturated pixels. Spatially and temporally coincident MODIS and GOES detection clusters produced significantly different FRP estimates for a large fraction of the cases analyzed. The results suggested that due to the conditions describing Amazonian fires, FRP estimates derived from moderate and coarse resolution data could be systematically subjected to large and variable errors, making it difficult to relate MODIS *Thermal Anomalies* and GOES WF-ABBA data via this parameter. The divergence between MODIS and GOES FRP estimates was particularly large in areas of high percentage tree cover, providing indications that landscape heterogeneity is an important factor limiting accurate FRP retrievals in Amazonia.

Previous studies have almost entirely neglected the effects of Point Spread Function (PSF) on the calculation of FRP of MODIS and GOES. However, the simulation analysis implemented in Chapter 4 suggested that PSF could represent the largest single source of error on FRP estimates derived from those sensors. The results revealed that fires situated away from the more responsive area of the PSF located near the pixel center can have their energy underestimated by the FRP estimates produced. The simulations of MODIS and GOES pixels containing a typically small Amazonian fire were prone to significantly underestimate true FRP values due to the effects of PSF of those instruments. This result suggests that the potential for using FRP for biomass emissions modelling applications in Amazonia using MODIS or GOES data might be limited, since emission rates calculated from underestimated FRP values could be negatively biased.

The results produced by the analyses using MOD14 (MYD14) and WF-ABBA fire detection clusters suggested a strong influence of the diurnal cycle of fires on the rates of spatially and temporally coincident detections. Relative to MOD14, a larger number of MYD14 fire detections showed coincident WF-ABBA detections indicating that greater fire activity predominates during the afternoon hours. Inclusion of the daytime GOES data in the analysis significantly increased the rate of MOD14 (MYD14) and WF-ABBA coincident detections. This result suggests that an important fraction of the smaller fires only detected by MOD14 and MYD14 could show variations in size and intensity during their life cycle, which evidently based on the temperature profiles shown in Chapter 3 (Figure 3.3) extends beyond the acquisition times of MODIS Terra and Aqua.

The fraction of MOD14 and MYD14 detections without a corresponding WF-ABBA detection occurring over high percentage tree cover areas was similar to the commission error rates derived for those MODIS products. This result suggests that MOD14 and MYD14 detections without a WF-ABBA match occurring in those areas could be primarily associated with false detections. Therefore, use of WF-ABBA detections to describe fire activity in high percentage tree cover areas (i.e., > 40%) could provide similar detection rates for most (> 90%) fires observed by MOD14 and MYD14 without the limitations of spatial coverage which create gaps in the MODIS data along the equator. Nonetheless, false detections in the WF-ABBA data need to be corrected for in order to reduce the commission errors observed over those high tree cover areas.

In areas characterized by low percentage tree cover (i.e., < 40%), small rates of coincident detections for MOD14 (MYD14) and WF-ABBA resulted as a consequence of lower temperature and short duration fires influencing the detection probability of those products. Nonetheless, commission error rates were significantly reduced in low percentage tree cover areas therefore the combined use of MOD14, MYD14 and WF-ABBA should provide the highest detection rates for those areas.

Large daily variations in detection performance of MOD14 (MYD14) and WF-ABBA could be verified using daily fire detection sum statistics from those products for a fixed area centered in southern Brazilian Amazonia. The variable pixel geometry of MODIS as a function of scan angle resulted on average in a 40% reduction of fire detection rates at the edge of the swath (i.e., ±55º) compared to nadir conditions. Differences between area averaged MOD14 (MYD14) and WF-ABBA fire detection statistics were particularly large over extreme MODIS scan angles where the *bow tie* effect in the MODIS imagery and the longer atmospheric path which cause greater attenuation of the fire emitted radiation could introduce additional variations in detection rates. Consequently, the use of area averaged statistics to integrate WF-ABBA, MOD14 and MYD14 detections was considered inadequate due to the large uncertainties involved.

6.1.4 Integrated Fire Product

In Chapter 5 a new integrated fire detection product was derived based on MOD14, MYD14 and WFABBA 2005 data. The results from Chapters 2-4 were used to generate a set of judicious criteria which takes advantage of multiple detections

produced from daytime and nighttime MODIS and GOES imagery. These criteria were applied to the data to generate improved daily fire information for Brazilian Amazonia. The integrated data product was generated using a 4×4 km grid at 30 min temporal resolution.

Areas of high detection frequency were highlighted in the integrated product reinforcing the strong association between forest conversion and areas of high fire activity in Brazilian Amazonia. The low overall fire detection densities generated from MODIS Terra data indicated that a strong fire diurnal cycle prevails in most of the region, whereas the high fire detection frequencies produced with the GOES data suggested that higher temporal resolution instruments may offer great advantage for Amazonian fire monitoring.

A validation exercise designed to assess the quality of the integrated product near central Mato Grosso state, an area under the influence of potentially large commission errors, revealed that numerous active fires in that region could result from the burning of crop residue or piled forest debris which leave no distinguishable burn scars on the surface. Consequently, future validation of the integrated detections must rely on coincident ground reference data to permit proper characterization of the product's quality.

6.2 Implications for Satellite-Based Fire Monitoring in Brazilian Amazonia

Amazonian fire alert systems and biomass burning emissions models demand high quality remote sensing data at the highest temporal and spatial resolution available,

requiring that active fire detection products from different sensors be combined. In order to integrate different satellite active fire detection data sets, the performance of individual products must be fully characterized and omission and commission errors quantified.

The main objective of this dissertation was to assess the potential for integrating the MOD14, MYD14 and WF-ABBA fire detections products in order to improve fire monitoring in Amazonia. Those products are routinely generated for the region providing important fire information for a large number of users. The WF-ABBA product derived from the GOES data has been running operationally since 1995, representing one of the longest time series of fire detection data available for Amazonia. The WF-ABBA product generates the highest temporal resolution fire detection data available for the region, serving rapid response fire alert systems as well as biomass burning emissions models [CPTEC, 2008; Freitas *et al*., 2005]. Despite their shorter time series, the MOD14 and MYD14 products quickly gained a large number of users in Amazonia as they provide moderate resolution fire detection data with lower saturation levels and improved navigation quality compared to other polar orbiting sensors such as the Advanced Very High Resolution Radiometer (AVHRR) series.

For the first time ever cloud obscuration omission errors and clear sky omission and commission errors were quantified in detail for the MOD14, MYD14 and WF-ABBA products over Amazonia. The results suggested that additional data layers such as vegetation, precipitation and cloud mask products must be used in conjunction with the active fire data in order to reduce errors in those products.

One of the big advantages of the method developed to quantify the cloud obscuration omission errors consisted in using GOES imager data to derive all input layers required to calculate the omission errors, including: a cloud mask, precipitation estimates and the land use data. In doing so, pixel level processing could be implemented and data registration errors and differences in data acquisition could be minimized. The use of pixel based processing is also advantageous as it facilitates aggregation of the omission error estimates for any particular grid cell resolution of current biomass burning emissions models. In fact, the methodology described in Chapter 2 will be used to generate fire detection omission error estimates due to cloud obscuration for the Coupled Aerosol and Tracer model to the Brazilian developments on the Regional Atmospheric Modelling System (CATT-BRAMS) dedicated to model biomass burning emissions in South America.

The large number of false detections found in areas of high percentage tree cover demonstrated the importance of using land cover information to estimate commission error rates. The use of the 500 m Vegetation Continuous Fields data [Hansen *et al*., 2002; Hansen *et al*., 2003] in combination with the fire detection data proved particularly successful in this study as it allowed easy determination of the dependency of commission error rates on percentage tree cover. Based on the commission error rates derived in Chapter 3, the approximate number of MOD14 (MYD14) and WF-ABBA false detections can be determined by weighting the distribution of fire detections as a function of percentage tree cover for any given area. The use of alternative land cover maps is contingent on users' preferences and

on the potential of those maps to reproduce a continuum of vegetation classes that can be easily related to commission error rates.

The potential for improving current contextual fire detection algorithms with the use of additional tests based on mid-infrared brightness temperature data to reduce commission errors was also demonstrated in Chapter 3. The results suggested that the stable surface thermodynamic conditions of Amazonia could facilitate the use of pixel based temporal metrics of brightness temperature estimates derived from the mid-infrared channels of MODIS and GOES to identify false detections or increase our confidence about the true ones. In Section 3.4.4, 30-day averaged brightness temperature estimates derived for the pixel were used to detect changes in instantaneous brightness temperature measurements that were typically associated with true or false detections.

The high clear sky omission error rates found for MOD14 and WF-ABBA have important implications for early warning fire alert systems, as the low detection probabilities of small fires will likely increase the latency of those systems. For other applications such as biomass burning emissions modeling which prioritize the detection information for larger and potentially more important fires with respect to their emissions, the relatively rapid decrease in omission errors with the increase in active fire area results in improved detection performance.

Errors in the FRP estimates from MODIS and GOES suggest that the use of such parameter for modeling of biomass burning emissions in Amazonia could be significantly compromised. The increased uncertainty found over higher percentage tree cover areas is a major limitation to the use of FRP. Because FRP is being

considered as a means to estimate biomass combustion rates [Kaufman *et al*., 1998b; Wooster, 2002; Wooster *et al*., 2003], even small errors in the total FRP value estimated for a fire detection cluster in high percentage tree cover areas will likely introduce large errors in the emission rates produced due to the high rates of biomass combustion involved.

Consideration of land cover conditions was proven essential for the integration of fire detection data from MOD14 (MYD14) and WF-ABBA. Regions characterized by high percentage tree cover including the core of Amazonian forests and the surrounding areas of active deforestation must be treated separately from other regions where low percentage tree cover vegetation types such as the Cerrado (savanna) predominate. By doing so, the complementarities among MOD (MYD14) and WF-ABBA fire detections can be better assessed and commission errors properly accounted for.

Finally, the close proximity between simultaneous active fires and consequently between burnt areas suggest that any validation analysis of active fire detection in Amazonia must use coincident ground truth information such as provided by ASTER and ETM+ data. This consideration significantly reduces the potential for validation of fire detection products derived from sensors flying on afternoon orbits. In this case, higher resolution data from sensors such as ASTER or ETM+ are not available and the potential for airborne and field data collection is limited as costs tend to be prohibitive. Greater coordination of the scientific community will be required to enable proper assessment of fire detection data sets without coincident

higher resolution spaceborne imaging in order to leverage costs and optimize the results of future validation campaigns.

This study targeted two main Amazonian fire data user communities: 1) regional fire monitoring and management, and 2) regional biomass burning emissions and smoke transport modeling. Both groups require accurate and timely fire detection information. Different tolerance for omission and commission errors between communities suggests that the results of this study apply differently to the policy, management, and science objectives users. Key limitations involving primarily the spatial resolution of GOES and MODIS and the geolocation accuracy of the GOES imager can significantly reduce the capacity of the related fire detection products to resolve individual fire clusters and to quantify their properties. Nonetheless, other fire data user groups including decision makers and climate modelers usually show less stringent data requirements. In Table 6.1 user requirements derived from the implementation plan for the Global Climate Observing System [GCOS, 2006], from the report on the Committee on Earth Observation Satellites (CEOS) Land Product Validation (LPV) working group workshop on global geostationary fire monitoring applications [GOFC 2004], from current regional and global emissions models [Freitas *et al*., 2005; van der Werf *et al*., 2006], and from personal communication with Amazonian fire managers are presented. While most users may benefit from the integrated fire product presented in Chapter 5, fire alert systems in Amazonia usually have low tolerance to commission errors as resources designated to law enforcement and field inspection tend to be limited. Consequently, fire alert systems might gain additional benefits from using regionally adjusted fire detection algorithms that lower

false detection rates to complement the information provided by the hemispheric- to global-scale GOES and MODIS algorithms used in this study.

Table 6.1: Fire data requirements applicable for five major fire data user groups.

User Group & Source	*Spatial Resolution*	*Temporal Resolution*	*Geolocation Accuracy*	*Tolerance to omission & commission errors*
Fire Alert Systems GOFC [2004]	500 m	5 min	Not specified; assumed equal or better than spatial resolution (500 m)	Low
Resource Managers Personal communication	County level	Daily	~ 500 m	Low
Regional emissions modeling Freitas *et al*. [2005]	Limited to a few tens of kilometers	Daily	Dependent on spatial resolution of land cover classification used (500 m - 1 km)	Moderate
Global scale emissions modeling van der Werf *et al*.[2006]	Gridded data of 0.25º×0.25º to 1º×1º resolution	Weekly to monthly	Dependent on spatial resolution of land cover classification used (500 m < grid size)	High
Global Climate change community GCOS [2006]	250 m	Daily	Not specified; assumed equal or better than spatial resolution (250 m)	Moderate

6.3 FUTURE DEVELOPMENTS

The analyses discussed in this dissertation represent the first detailed assessment of two of the major active fire detection products currently available for Brazilian Amazonia. Consideration of commission and omission errors and product inter-comparison discussed in Chapters 2-4 should provide the basis for future development of fire detection algorithms and integration of different products in tropical areas.

The quantification of omission errors due to cloud obscuration will be used to create a 10+ years time series of WF-ABBA fire detections for Brazilian Amazonia as part of the Large Scale Biosphere-Atmosphere Experiment in Amazonia (LBA). Improvements in WF-ABBA fire data information are already being implemented for the new version 6.5 product, including an opaque cloud mask layer which could allow direct derivation of cloud obscuration omission errors using the methodology described in Chapter 2.

The next generation of sensors which will replace the existing GOES imager series and the MODIS sensors should provide enhanced capabilities for active fire monitoring. For instance, the improved geolocation accuracy and higher spatial resolution of the Advanced Baseline Imager (ABI) which will fly on board the GOES-R series and the reduced along scan pixel size variation of the Visible Infrared Imaging Radiometer Suite (VIIRS) which will fly on the upcoming National Polar-orbiting Operational Environmental Satellite System (NPOESS) could facilitate the application of tests based on temporal change detection in addition to the spatial contextual tests to identify potential false detections in the fire products derived from

those data. Consequently, problem areas such as high percentage tree cover regions where high commission errors are currently observed could benefit from the use of more comprehensive set of detection tests. Similarly, derivation of FRP should benefit from higher spatial resolution imagery as average Amazonian fires will tend to occupy a considerably larger fraction of the higher spatial resolution pixel footprints reducing the PSF effects on those estimates. The creation of temporal metrics aimed for active fire detection may also be advantageous to estimate the fire background conditions necessary to derive FRP values, since average brightness temperature conditions may be estimated for the fire affected pixel reducing the need to use information from radiometric distinct adjacent pixels.

The need for continued validation of current and future remote sensing active fire detection products requires that higher resolution data be available for the scientific community. In this respect, changes in data sharing policy to be implemented by the United States Geological Survey (USGS) should facilitate significantly the access to higher resolution imagery from the Landsat mission and the upcoming Landsat Data Continuity Mission (LDCM). The availability of cost free data should make validation exercises more frequent contributing to our understanding of the qualities and limitations of fire detection products over broader spatial scales and fire regimes. Thanks to this new data policy, the use of Landsat data to validate the GOES fire product will be implemented at the Satellite Analysis Branch (SAB) of the National Environmental Satellite, Data and Information Service (NOAA/NESDIS) in Camp Springs, Maryland. Similar plans are being proposed to validate MODIS Terra *Thermal Anomalies* product at far off-nadir viewing angles

using Landsat 5 data for the Conterminous United States. The use of additional validation data could help identify the major factors leading to the poor overall rate of coincident detections between WF-ABBA and MODIS *Thermal Anomalies* as presented in Section 4.4.2.

Finally, the use of the data integration scheme presented in Chapter 5 should provide a valuable test-bed to assess the implications of fire detection errors for biomass burning emissions modeling as well as for operational fire monitoring in Brazilian Amazonia and elsewhere. Assimilation of the results presented in Chapter 5 into the CATT-BRAMS model will be addressed and is expected to complement the 10+ years fire detection data series being created for Brazilian Amazonia with a biomass burning emissions inventory.

Appendix A

ETM+ Active Fire Mask

In order to improve our sampling capacity of the GOES data, a new 30 m fire mask product was created using Landsat 7 Enhanced Thematic Mapper Plus (ETM+) imagery. Due to similarities in spectral and spatial resolution between the ASTER and ETM+ data, the new ETM+ fire mask product builds on the Giglio *et al*. [2008] algorithm used for producing the ASTER product. Denoting the ETM+ channel 4 and 7 top-of-atmosphere reflectance as ρ_4 and ρ_7, respectively, unambiguous fire pixels are classified using the criteria:

$$R_{74} = \frac{\rho_7}{\rho_4} > 2.5$$
$$D_{74} = \rho_7 - \rho_4 > 0.3$$

Next, candidate pixels are selected based on the following tests:

$$R_{74} > 1.8$$
$$D_{74} > 0.17$$

We apply a fixed 61×61 window centered on the candidate pixel to calculate the background statistics which will be used for the contextual part of the detection code. The mean and standard deviation are calculated for the reflectance ratio ($\overline{R_{74}}$ and σ_{R74}, respectively) and for channel 7 reflectance ($\overline{\rho_7}$ and $\sigma_{\rho 7}$, respectively).

Unambiguous fire pixels and water pixels (pixels for which $\rho_7 < 0.04$) are excluded from the computation. Candidate pixels which satisfy the following conditions are classified as fires:

$$R_{74} > \overline{R_{74}} + Max(3\sigma_{R74}, 0.8)$$
$$\rho_7 > \overline{\rho_7} + Max(3\sigma_{\rho 7}, 0.08)$$

where the *Max* indicates that the maximum value is to be used. The numerical constants appearing in the tests were empirically derived for the scenes used in this study, and the resulting fire masks were visually inspected for consistency.
If needed.

Bibliography

Agresti, A. (1990). *Categorical data analysis*. John Wiley and Sons, 558 pp.

Alencar, A., Nepstad, D., Silva, E., Brown, F. , Lefebvre, P., Mendosa, E., Almeida, D., and Carvalho Jr., O. (1997). O uso do fogo na Amazônia: Estudos de caso ao longo do arco de desmatamento. World Bank, Brasília, Brazil.

Alencar, A., Nepstad, D., and Vera Diaz, M. C. (2006), Forest understory fire in the Brazilian Amazon in Enso and non-Enso years: Area burned and committed carbon emissions, *Earth Interactions, 10***,** Paper 6.

Alencar, A., Solorzano, L., and Nepstad, D. (2004). Modeling forest understory fires in an eastern Amazonian landscape. *Ecological Application*, 14 (4), S139-S149.

Alvalá, R. C. S., Gielow, R., da Rocha, H. R., Freitas, H. C., Lopes, J. M., Manzi, A. O., *et al*. (2002). Intradiurnal and seasonal variability of soil temperature, heat flux, soil moisture content, and thermal properties under forest and pasture in Rondônia. *Journal of Geophysical Research*, 107, doi:10.1029/2001JD000599

Andreae, M.O. (1991). Biomass burning: Its history, use and distribution and its impact on Environmental Quality and Global Climate. In J. Levine (Ed.), *Global biomass burning, atmospheric, climatic, and biospheric implications*, MIT press, 3-21 pp.

Andreae, M. O., and Merlet, P. (2001). Emission of trace gases and aerosols from biomass burning. *Global Biogeochemical Cycles*, 15 (4), 955–966.

Andreae, M. O., Rosenfeld, D., Artaxo, P., Costa, A. A., Frank, G. P., Longo, K. M., and Silva-Dias, M. A. F. (2004). Smoking rain clouds over the Amazon. *Science*, 303, 1337-1342, doi: 10.1126/science.1092779.

Arima, E., Simmons, C. S., Walker, R., and Cochrane, M. A. (2007). Fire in the Brazilian Amazon: A spatially explicit model for policy impact analysis. *Journal of Regional Sciences*, 43 (3), 541-567.

Arkin, P. A. (1979). The relationship between the fractional coverage of high cloud and rainfall accumulations during GATE over the B-array. *Monthly Weather Review*, 107, 1382−1387.

Barbosa, P. M., Stroppiana, D., Grégoire, J. -M., and Cardoso Pereira, J. M. (1999). An assessment of vegetation fire in Africa (1981–1991): Burned areas, burned biomass and atmospheric emissions. *Global Biogeochemical Cycles*, 13, 933−950.

Barlow, J., and Peres, C. A. (2006). Effects of single and recurrent wildfires on fruit production and large vertebrate abundance in a central Amazonian forest. *Biodiversity and Conservation*, 15 (3), 985-1012.

Barlow, J., Peres, C. A., Langan, B. O., and Haugaasen, T. (2003). Large tree mortality and the decline of forest biomass following Amazonian wildfires. *Ecology Letters*, *6* (1), 6-8.

Bellerby, T., Todd, M., Kniveton, D., and Kidd, C. (2001). Rainfall estimation from a combination of TRMM precipitation radar and GOES multispectral satellite imagery through the use of an artificial neural network. *Journal of Applied Meteorology*, 39, 2115−2128.

Betts, A. K., Fuentes, J. D., Garstang, M., and Ball, J. H. (2002). Surface diurnal cycle and boundary layer structure over Rondônia during the rainy season. *Journal of Geophysical Research*, 107 (D20), doi:10.1029/2001JD000356

Boi, P., Marrocu, M., and Giachetti, A. (2004). Rainfall estimation from infrared data using an improved version of the Auto-Estimator Technique. *International Journal of Remote Sensing*, 10, 4657−4673.

Boles, S. H., and Verbyla, D. L. (2000). Comparison of three AVHRR-based fire detection algorithms for interior Alaska. *Remote Sensing of Environment*, 72, 1−16.

Bond T. C., Streets, D. G., Yarber, K. F., Nelson, S. M., Woo, J.-H., and Klimont, Z. (2004). A technology-based global inventory of black and organic carbon emissions from combustion. *Journal of Geophysical Research*, 109, D14203, doi:10.1029/2003JD003697.

Brown, I. F., Schroeder, W., Setzer, A., Maldonado, M. L. R., Pantoja, N., Duarte, A., *et al*. (2006). Monitoring fires in Southwestern Amazonia rain forests. *Eos Transactions of the American Geophysical Union*, 87(26), 253.

Bruno, R. D., Rocha, H. R., de Freitas, H. C., Goulden, M. L., and Miller, S. (2006). Soil moisture dynamics in an eastern Amazonian tropical forest. *Hydrological Processes*, 20, 2477−2489.

Bucini, G., and Lambin, E. (2002). Fire impacts on vegetation in Central Africa: A remote-sensing-based statistical analysis. *Applied Geography*, 22, 27−48.

Cahoon, D. R. Jr., Stocks, B. J., Alexander, M. E., Baum, B. A., and Goldammer, J. G. (2000). Wildland fire detection from space: Theory and application. In Innes, J. L., Beniston, M., and Verstraete, M. M. (Eds.), *Biomass burning and its inter-relationships with the climate system*. Kluwer Academic Publishers, Dordrecht and Boston, 151-169pp.

Calle, A., Casanova, J. L., and Romo, A. (2006). Fire detection and monitoring using MSG Spinning Enhanced Visible and Infrared Imager (SEVIRI) data. *Journal of Geophysical Research*, 111, G04S06, doi:10.1029/2005JG000116.

Cardoso, M. F., Hurtt, G. C., Moore, B., III, Nobre, C. A., and Bain, H. (2005). Field work and statistical analyses for enhanced interpretation of satellite data. *Remote Sensing of Environment*, 96, 212−227.

Cardoso, M. F., Hurtt, G. C., Moore, B., III, Nobre, C. A., and Prins, E. M. (2003). Projecting future fire activity in Amazonia. *Global Change Biology*, 9, 656−669.

Carmona-Moreno, C., Belward, A., Malingreau, J. -P., Hartley, A., Garcia-Alegre, M., Antonovskiy, M., *et al*. (2005). Characterizing interannual variations in global fire calendar using data from Earth observing satellites. *Global Change Biology*, 11, 1537−1555.

Cochrane, M., (2003), Fire science for rainforest. *Nature*, 421, 913-919.

Cochrane, M., Alencar, A., Schulze, M., Souza Jr, C., Nepstad, D. C., Lefebvre, P., and Davidson, E. (1999). Positive feedbacks in the fire dynamic of closed canopy tropical forest. *Science,* 284, 1832-1835.

Cochrane, M., and Laurance, W. F. (2002). Fire as a large-scale edge effect in Amazonia forests. *Journal of Tropical Ecology*, 18, 311-325.

Cochrane, M. A., and Schulze, M. D. (1999). Fire as a recurrent event in tropical forests of the Eastern Amazon: Effects on forest structure, biomass, and species composition. *Biotropica*, 31 (1), 2-16.

Comision Nacional de Actividades Espaciales (CONAE), Geston de Emergencias, Argentina, URL (last visited 24 April 2008): http://www.conae.gov.ar/WEB_Emergencias/Links_de_la_Izquierda/Incendios/incendios.html

Costa, M. H., and Foley, J. A. (1998). A comparison of precipitation datasets for the Amazon basin. *Geophysical Research Letters*, 25, 155−158.

CPC—Climate Prediction Center—National Center for Environmental Prediction (NCEP) — National Weather Service (NWS), Global-merged Infra-red Brightness Temperature data set. URL (last visited 24 April 2008): http://disc.sci.gsfc.nasa.gov/data/datapool/TRMM/01_Data_Products/06_Ancillary/01_Global_MERG_IR/index.html

Centro de Previsão do Tempo e Estudos Climáticos (CPTEC) Projeto Queimadas. URL (last visited 24 April 2008): http://cptec.inpe.br/queimadas

Crutzen, P.J., (1979). The role of NO and NO2 in the chemistry of the troposphere and stratosphere. *Annual Review of Earth and Planetary Science*, 7, 443-472, doi:10.1146/annurev.ea.07.050179.002303.

Crutzen, P. J., and Andreae, M. O. (1990). Biomass burning in the tropics: Impact on atmospheric chemistry and biogeochemical cycles. *Science*, 250, 1669-1678.

Crutzen, P. J., Heidt, L. E., Krasnec, J. P., Pollock, W. H., and Seiler ,W. (1979). Biomass burning as a source of atmospherics gases: CO, H2, N2O, NO, CH3Cl, COS. *Nature*, 282, 253-256.

Csiszar, I., Denis, L., Giglio, L., Justice, C. O., and Hewson, J. (2005). Global fire distribution from MODIS. *International Journal of Wildland Fire*, 14, 117−130.

Csiszar, I., Morisette, J. T., and Giglio, L. (2006). Validation of active fire detection from moderate-resolution satellite sensors: the MODIS example in Northern Eurasia. *IEEE Transactions on Geoscience and Remote Sensing*, 44(7), 1757−1764.

Csiszar, I., and Schroeder, W. (2007). Fire observations from ETM+ and ASTER imagery and implications for active fire product validation from coarse resolution sensors. *Proceedings of the 6th International Workshop of the EARSeL Special Interest Group on Forest Fires*, 27–29 September 2007 Thessaloniki, Greece, 155-159pp.

da Rocha, H. R., Goulden, M. L.,Miller, S. D., Menton, M. C., Pinto, L. D. V. O., de Freitas, H. C., *et al*. (2004). Seasonality of water and heat fluxes over a tropical forest in eastern Amazonia. *Ecological Applications*, 14(4), S22−S32.

Delany, A. C., Haagensen, P., Walters, S., Wartburg, A. F., and Crutzen, P.J. (1985). Photochemically produced ozone in the emission from large-scale tropical vegetation fires. *Journal of Geophysical* Research, 90, 2425-2429.

Di Bella, C. M., Jobbágy, E. G., Paruelo, J. M., and Pinnock, S. (2006). Continental fire density patterns in South America. *Global Ecology and Biogeography*, 15, 192−199.

Direccion de Manejo de Recusos Naturales (DIMARENA), Gobierno Departamental Prefectura Santa Cruz, Bolivia, URL (last visited 24 April 2008): http://servicios.santacruz.gov.bo/forestal/index.php?option=com_mamboezine&Itemid=36

Dozier, J. (1981). A method for satellite identification of surface temperature fields of subpixel resolution. *Remote Sensing of Environment*, 11, 221-229.

Dwyer, E., Pinnock, S., Gregoire, J. -M., and Pereira, J.M. C. (2000). Global spatial and temporal distribution of vegetation fire as determined from satellite observations. *International Journal of Remote Sensing*, 21, 1289−1302.

Ebert, E. E., Janowiak, J. E., and Kidd, C. (2007). Comparison of near-real-time precipitation estimates from satellite observations and numerical models. *Bulletin of the American Meteorological Society*, 88, doi:10.1175/BAMS-88-1-47.

Elvidge, C. D., Kroehl, H. W., Kihn, E. A., Baugh, K. E., Davis, E. R., and Hao, W. M. (1996). Algorithm for the retrieval of fire pixels from DMSP Operational Linescan System Data. In J. S. Levine (Ed.), *Remote Sensing, Modeling and Inventory Development, and Biomass Burning in Africa - Biomass Burning and Global Change*, Vol. 1, MIT Press, pp. 73−85.

Eva, H., and Fritz, S. (2003). Examining the potential of using remotely sensed fire data to predict areas of rapid forest change in South America. *Applied Geography*, 23, 189-204.

Eva, H., and Lambin, E. F. (1998). Remote sensing of biomass burning in tropical regions: Sampling issues and multisensor approach. *Remote Sensing of Environment*, 64, 292−315.

Ferreira, N. C., Ferreira, L. G., and Miziara, F. (2007). Deforestation hotspots in the Brazilian Amazon: Evidence causes of as assessed from remote sensing and census data. *Earth Interactions*, 11 (1), 1-16.

Ferreira, L. V., de Sá, R. M. L., Buschbacher, R., Batmanian, G., Bensuran, B. R., and Costa, K. L. (1999). Áreas protegidas ou espaços ameaçados? World Wide Fund for Nature, Brasilia.

Freitas, S. R., Longo, K. M., Siva-Dias, M. A. F., Silva-Dias, P. L., Chatfield, R., Prins, E., Artaxo, P., Grell, G. A., and Recuero, F. S. (2005). Monitoring the transport of biomass burning emissions in South America. *Environmental Fluid Mechanics*, 5, 135-167, doi: 10.1007/s10652-005-0243-7.

Giglio, L. (2007). Characterization of the tropical diurnal fire cycle using VIRS and MODIS observations. *Remote Sensing of Environment*, 108(4), 407-421, doi:10.1016/j.rse.2006.11.018

Giglio, L., Csiszar, I., and Justice, C. (2006). Global distribution and seasonality of active fires as observed with the Terra and Aqua Moderate Resolution Imaging Spectroradiometer (MODIS) sensors. *Journal of Geophysical Research*, 111, G02016, doi:10.1029/2005JG000142.

Giglio, L., Csiszar, I., Restas, A., Morisette, J.T., Schroeder, W., Morton, D., *et al*. (2008). Active fire detection and characterization with the Advanced Spaceborne

Thermal Emission and Reflection Radiometer (ASTER). *Remote Sensing of Environment*, in press.

Giglio, L., Descloiters, J., Justice, C. O., and Kaufman, Y. (2003a). An enhanced contextual fire detection algorithm for MODIS. *Remote Sensing of Environment*, 87, 273−282.

Giglio, L., and Kendall, J., (2001). Application of the Dozier retrieval to wildfire characterization: A sensitivity analysis. *Remote Sensing of Environment*, 77, 34-49.

Giglio, L., Kendall, J. D., and Justice, C. O. (1999). Evaluation of global fire detection algorithms using simulated AVHRR infrared data. *International Journal of Remote Sensing*, 20, 1947−1985.

Giglio, L., Kendall, J. D., and Mack, R. (2003b). A multi-year active fire dataset for the tropics derived from the TRMM VIRS. *International Journal of Remote Sensing*, 24, 4505−4525.

Giglio, L., Kendall, J. D., and Tucker, C. J. (2000). Remote sensing of fires with the TRMM VIRS. *International Journal of Remote Sensing*, 21, 203−207.

Global Climate Observing System (GCOS) (2006). World Meteorological Organization, Systematic Observation Requirements for Satellite-Based Products for Climate. GCOS-107, WMO/TD No. 1338. September 2006.

Global Observation of Forest Cover – Global Observation for Forest and Land Cover Dynamics (GOFC/GOLD) (2006). Fire Monitoring and Mapping Implementation Team. 2nd Workshop on Geostationary Fire Monitoring and Applications, Darmstadt Germany, 4-6 December 2006. URL (last visited 24 April 2008): http://gofc-fire.umd.edu/products/pdfs/Events/2nd_GOFC_Geo_Workshop_Report%20final.pdf

Global Observation of Forest Cover – Global Observation for Forest and Land Cover Dynamics (GOFC/GOLD) (2004). Report on the Joint GOFC/GOLD Fire and CEOS LPV Working Group Workshop on Global Geostationary Fire Monitoring Applications, Darmstadt Germany, 23-25 March 2004. URL (last visited 24 April 2008): http://www.fao.org/gtos/gofc-gold/docs/GOLD_19.pdf

Govaerts, Y. M., Wooster, M., Lattanzio, A., and Roberts, G. (2007). MSG/SEVIRI fire thermal anomaly (FTA) characterization ATBD, EUMETSAT, Report EUM/MET/SPE/06/0398 (pp. 32).

Goward, S. N., Masek, J. G., Williams, D. L., Irons, J. R., and Thompson, R. J. (2001). The Landsat 7 mission terrestrial research and applications for the 21st century. *Remote Sensing of Environment*, 78, 3−12.

Hansen, J., Sato, M., Ruedy, R., Lacis, A., and Oinas, V. (2000). Global warming in the twenty-first century: An alternative scenario. *Proceedings of the National Academy of Sciences*, 97, 9875-9880, doi:10.1073/pnas.170278997.

Hansen, M. C., DeFries, R. S., Townshend, J. R., Carrol, M., Dimiceli, C., and Sohlberg, R. A. (2003). Global percent tree cover at a spatial resolution of 500 meters: First results of the MODIS Vegetation Continuous Fields Algorithm. *Earth Interactions*, 7, paper 10.

Hansen, M. C., DeFries, R. S., Townshend, J. R., Sohlberg, R., Dimiceli, C., and Carroll, M. (2002). Towards an operational MODIS continuous fields of percent tree cover algorithm: examples using AVHRR and MODIS data. *Remote Sensing of Environment*, 83, 303−319.

Hao, W.M., and M.-H. Liu (1994). Spatial and temporal distribution of tropical biomass burning. *Global Biogeochemical Cycles*, 8 (4), 495-503.

Hughes, R. F., Kauffman, J. B., and Cummings, D. L. (2000). Fire in the Brazilian Amazon: Dynamics of biomass, C and nutrient pools in regenerating forests. *Oecologia*, 124, 574-588.

Intergovernamental Panel on Climate Change (IPCC) (1995). Climate Change 1995: The science of climate change. Contribution of Working Group I to the Second Assessment of the Intergovernmental Panel on Climate Change, JT Houghton, LG Meira Filho, BA Callender, N Harris, A Kattenberg and K Maskell (Eds), Cambridge University Press, UK, 572 pp.

Justice, C., Giglio, L., Korontzi, S., Owens, J., Morisette, J. T., Roy, D., *et al*. (2002). The MODIS fire products. *Remote Sensing of Environment*, 83, 244−262.

Kasischke, E. S., Hewson, J. H., Stocks, B., Van der Werf, G., and Randerson, J. (2003). The use of ATSR active fire counts for estimating relative patterns of biomass burning - A study from the boreal forest region. *Geophysical Research Letters*, 30(18), 1969, doi:10.1029/2003GL017859

Kasischke, E. S., Williams, D., and Barry, D. (2002). Analysis of the patterns of large fires in the boreal forest region of Alaska. *International Journal of Wildland Fire*, 11, 131−144.

Kaufman, Y. J., Hobbs, P. V., Kirchhoff, V. W., Artaxo, P., Remer, L. A., Holben, B. N., *et al*. (1998a). Smoke, Clouds, and Radiation-Brazil (SCAR-B) experiment. *Journal of Geophysical Research*, 103, 31,783−31,808.

Kaufman, Y. J., Justice, C., Flynn, L., Kendall, J., Prince, E. M., Ward, D. E., *et al*. (1998b). Potential global fire monitoring from EOS-MODIS. *Journal of Geophysical Research*, 103, 32215−32238.

Kaufman, Y. J., Setzer, A., Ward, D., Tanre, D., Holben, B. N., Menzel, P., Pereira, M. C., and Rasmussen, R. (1992). Biomass burning airborne and spaceborne experiment in the Amazonas (BASE-A). *Journal of Geophysical Research*, 97(D13), 14,581-14,599.

Kaufman, Y. J., Tucker, C. J., and Fung, I. (1990). Remote sensing of biomass burning in the tropics. *Journal of Geophysical Research*, 95, 9927−9939.

Koltunov, A., and Ustin, S. L. (2007). Early fire detection using non-linear multitemporal prediction of thermal imagery. *Remote Sensing of Environment*, 110, 18−28.

Koren, I., Kaufman, Y. J., Remer, L. A., Martins, J. V. (2004). Measurement of the effect of Amazon Smoke on Inhibition of Cloud Formation. *Science*, (303), doi:10.1126/science.1089424, 1342-1345.

Korontzi, S., Roy, D. P., Justice, C. O., and Ward, D. E. (2004). Modeling and sensitivity analysis of fire emissions in southern Africa during SAFARI 2000. *Remote Sensing of Environment*, 92, 376−396.

Kummerow, C., Barnes, W., Kozu, T., Shiue, J., and Simpson, J. (1998). The Tropical Rainfall Measuring Mission (TRMM) sensor package. *Journal of Atmospheric and Oceanic Technology*, 15, 809−817.

Laurance, W. F., Albernaz, A. K. M., Fearnside, P., Vasconcelos, H. L., and Ferreira, L. V. (2004). Deforestation in Amazonia. *Science*, 304, 1109-1109.

Laurance, W. F., and Williamson, G. B. (2001). Positive feedbacks among forest fragmentation, drought and climate change in the Amazon. *Conservation Biology*, 15 (6), 1529-1535.

Li, Z., Nadon, S., and Cihlar, J. (2000). Satellite-based detection of Canadian boreal forest fires: development and application of the algorithm. *International Journal of Remote Sensing*, 21 (16), 3057-3069.

Matson, M., and Dozier, J. (1981). Identification of subresolution high temperature sources using a thermal IR sensor. *Photogrammetric Engineering and Remote Sensing*, 47, 1311-1318.

Matson, M., and Holben, B. (1987). Satellite detection of tropical burning in Brazil. *International Journal of Remote Sensing*, 8 (3), 509-516.

Mendonça, M. J. C., Vera-Diaz, M. C., Nepstad, D., Seroa da Motta, R., Alencar, A., Gomes, J. C., and Ortiz, R. A. (2004). The economic cost of the use of fire in the Amazon. *Ecological Economics*, 49, 89- 105.

Menzel, W. P., Cutrim, E. C., and Prins, E. M. (1991). Geostationary satellite estimation of biomass burning in Amazonia during BASE-A. In J. S. Levine (Ed.), *Global Biomass Burning: Atmospheric, Climatic, and Biospheric Implications*, MIT Press, 41−46pp.

Menzel, W. P., and Prins, E. M. (1996). Monitoring biomass burning with the new generation of geostationary satellites. In J. S. Levine (Ed.), *Biomass burning and global change*, MIT Press, 56−64pp..

Menzel, W. P., and Purdom, J. F. W. (1994). Introducing GOES-I: the first of a new generation of geostationary operational environmental satellites. *Bulletin of the American Meteorological Society*, 75(5), 757−781.

Moran, E., Brondizio, E. S., Tucker, J. M., Silva-Forsberg, M. C., McCracken, S., and Falesi, I. (2000). Effects of soil fertility and land-use on forest succession in Amazônia. *Forest Ecology and Management*, 139, 93-108.

Morisette, J. T., Giglio, L., Csiszar, I., and Justice, C. O. (2005a). Validation of the MODIS active fire product over Southern Africa with ASTER data. *International Journal of Remote Sensing*, 26(19), 4239−4264.

Morisette, J. T., Giglio, L., Csiszar, I., Setzer, A., Schroeder, W., Morton, W., *et al*. (2005b). Validation of MODIS active fire detection products derived from two algorithms. *Earth Interactions*, 9, 1−25 (paper no. 9).

Morisette, J.T., Privette, J. L., and Justice, C. O. (2002). A framework for the validation of MODIS Land products. *Remote Sensing of Environment*, 83, 77-96.

Morton, D. C., DeFries, R. S., Randerson, J. T., Giglio, L. Schroeder, W., and van der Werf, G. (2008). Agricultural intensification increases deforestation fire activity in Amazonia. *Global Change Biology*, in press.

Morton, D. C., DeFries, R. S., Shimabukuro, Y. E., Anderson, L.O., Arai, E., del bon Espirito-Santo, F., Freitas, R., Freitas, R., and Morisette, J. (2006). Cropland expansion changes deforestation dynamics in the southern Brazilian Amazon. *Proceedings of the National Academy of Science*, 103 (39), 14637-14641.

Nepstad, D., Carvalho, G., Barros, A. C., Alencar, A., Capobianco, J. P., Bishop, J., Moutinho, P., Lefebvre, P., Silva Jr, U. L., and Prins, E. (2001). Road paving, fire regime feedbacks, and the future of Amazon forests. *Forest Ecology and Management*, 154, 395-407.

Nepstad, D. C., Moreira, A. G., and Alencar, A. (1999a), Flames in the rainforest: Origins, impacts and alternatives to Amazonian fires. The Pilot Program to Conserve of the Brazilian Rainforest, World Bank, Brasilia, Brazil.

Nepstad, D., Moutinho, P., Dias-Filho, M. B., Davidson, E., Cardinot, G., Markewitz, D., *et al*. (2002). The effects of partial throughfall exclusion on canopy processes, aboveground production, and biogeochemistry of anAmazon forest. *Journal of Geophysical Research*, 107, doi:10.1029/2001JD000360.

Nepstad, D. C., Schwartzman, S., Bamberger, B., Santilli, M., Ray, D., Schlesinger, P., Lefebvre, P., Alencar, A., Prinz, E., Fiske, G., and Rolla, A. (2006). Inhibition of Amazon deforestation and fire by parks and indigenous lands. *Conservation Biology*, 20(1), 65-73.

Nepstad, D. C., Veríssimo, A., Alencar, A., Nobre, C., Lima, E., Lefebvre, P., Schlesinger, P., Potter, C., Moutinho, P., Mendonza, E., Cochrane, M., and Brooks, V. (1999b). Large scale impoverishment of Amazonian forests by logging and fire. *Nature*, 398, 505-508.

Pedlowski, M. A., Matricardi, E. A. T., Skole, D., Cameron, S. R., Chomentowski, W., Fernandes, C., and Lisboa, A. (2005). Conservation units: A new deforestation frontier in the Amazonian state of Rondonia, Brazil. *Environmental Conservation*, 32(2), 149-155.

Penner, J. E., Dickenson, R. E., and O'Neill, C.A. (1992). Effects of aerosol from biomass burning on the global radiation budget. *Science*, 256, 1432-1434.

Peres, C. A., Barlow, J., and Haugaasen, T. (2003). Vertebrate responses to surface fires in a Central Amazonian forest. *Oryx*, 37, 97-109.

Prins, E. M., Feltz, J. M., Menzel, W. P., and Ward, D. E. (1998). An overview of GOES-8 diurnal fire and smoke results for SCAR-B and 1995 fire season in South America. *Journal of Geophysical Research*, 103(D24), 31821−31835.

Prins, E. M., and Menzel, W. P. (1992). Geostationary satellite detection of biomass burning in South America. *International Journal of Remote Sensing*, 13, 2783−2799.

Prins, E. M., and Menzel,W. P. (1994). Trends in South American biomass burning detected with the GOES VAS from 1983–1991. *Journal of Geophysical Research*, 99(D8), 16719−16735.

Prins, E. M., Schmidt, C. C., Feltz, J. M., Reid, J. S., Wesphal, D. L., and Richardson, K. (2003). A two year analysis of fire activity in the Western Hemisphere as observed with the GOES Wildfire Automated Biomass Burning Algorithm.

Preprints, 12th Conf. on Satellite Meteorology and Oceanography, Long Beach, CA, Amer. Meteor. Soc., CD-ROM, P2.28.

PRODES Monitoramento da floresta Amazônica brasileira por satélite. URL (last visited 24 April 2008): http://www.obt.inpe.br/prodes/

Reinhardt, T. E., Ottmar, R. D., and Castilla, C. (2001). Smoke impacts from agricultural burning in rural Brazilian Town. *Journal of Air and Waste Manage*, 51, 443-450.

Roberts, G., Wooster, M. J., Perry, G. L. W., Drake, N., Rebelo, L. -M., and Dipotso, F. (2005). Retrieval of biomass combustion rates and totals from fire radiative power observations: Application to southern Africa using geostationary SEVIRI imagery. *Journal of Geophysical Research*, 110, D21111, doi:10.1029/2005JD006018.

Roy, D. P., Jin, Y., Lewis, P. E., and Justice, C. O. (2005). Prototyping a global algorithm for systematic fire-affected area mapping using MODIS time series data. *Remote Sensing of Environment*, 97, 137-162.

Rozumalski, R. A. (2000). A quantitative assessment of the NESDIS Auto-Estimator. *Weather Forecasting*, 15, 397−415.

Rudolf, B., Hauschild, H., Rüth, W., and Schneider, U. (1996). Comparison of raingauge analyses, satellite-based precipitation estimates and forecast model results. *Advances in Space Research*, 18, 53−62.

Rummel, U., Ammann, C., Kirkman, G. A., Moura, M. A. L., Foken, T., Andreae, M. O., and Meixner, F. X. (2007). Seasonal variation of ozone deposition to a tropical rain forest in southwest Amazonia. *Atmospheric Chemistry and Physics*, 7, 5,415-5,435.

Schaaf, C. B., Gao, F., Strahler, A. H., Lucht, W., Li, X., Tsang, T., *et al*. (2002). First operational BRDF, albedo nadir reflectance products from MODIS. *Remote Sensing of Environment*, 83, 135−148.

Scholes, R. J., Ward, D. E., and Justice, C. O. (1996). Emissions of trace gases and aerosol particles due to vegetation burning in southern hemisphere Africa. *Journal of Geophysical Research*, 101, 23677−23682.

Schroeder, W., Csiszar, I., and Morisette, J. (2008a). Quantifying the impact of cloud obscuration on remote sensing of active fires in the Brazilian Amazon. *Remote Sensing of Environment*, 112, 456-470, doi:10.1016/j.rse.2007.05.004.

Schroeder, W., Morisette, J. T., Csiszar, I., Giglio, L., Morton, D., and Justice, C. (2005). Characterizing vegetation fire dynamics in Brazil through multisatellite data: Common trends and practical issues. *Earth Interactions*, 9, Paper 13.

Schroeder, W., Prins, E., Giglio, L., Csiszar, I., Schmidt, C., Morisette, J., and D. Morton (2008b). Validation of GOES and MODIS active fire detection products using ASTER and ETM+ data. *Remote Sensing of Environment*, 112 (5), 2711-2726, doi:10.1016/j.rse.2008.01.005.

Schroeder, W., Ruminski, M., Csiszar, I., Giglio, L., Prins, E., Schmidt, C., and Morisette, J. (2008c). Validation analyses of an operational fire monitoring product: The Hazard Mapping System. *International Journal of Remote Sensing*, submitted.

Seiler, W., and Crutzen, P.J. (1980). Estimates of gross and net fluxes of carbon between the biosphere and the atmosphere from biomass burning. *Climatic Change*, 2(3), 207-247, doi:10.1007/BF00137988, 207-247.

Setzer, A.W., and Pereira, M. C. (1991). Amazonia biomass burnings in 1987 and an estimate of their tropospheric emissions. *Ambio*, 20(1), 19-22.

Shukla, J., Nobre, C., and Sellers, P. (1990). Amazon deforestation and climate change. *Science*, 247, 1322-1325.

Sorrensen, C. (2004). Contributions of fire use study to land use/cover change framework: Understanding landscape change in agricultural frontiers. *Human Ecology*, 32(4), 395-420.

Tucker, C. J., Holben, B. N., and Golf, T. E. (1984). Intensive forest clearing in Rondonia, Brazil, as detected by satellite remote sensing. *Remote Sensing of Environment*, 15 (3), 255-261.

UW Madison Cooperative Institute for Meteorological Satellite Studies (CIMSS) Biomass Burning Monitoring Program, URL (last visited 24 April 2008): http://cimss.ssec.wisc.edu/goes/burn/WF-ABBA.html.

van der Werf, G. R., Randerson, J. T., Collatz, G. J., and Giglio, L. (2003). Carbon emissions from fires in tropical and subtropical ecosystems. *Global Change Biology*, 9, 547−562.

van der Werf, G. R., Randerson, J. T., Collatz, G. J., Giglio, L., Kasibhatla, P. S., Arellano Jr., A. F., Olsen, S. C., and Kasischke, E. S. (2004). Continental-scale partitioning of fire emissions during the 1997 to 2001 El Niño/La Niña Period. *Science*, 303, 73-76.

van der Werf, G. R., Randerson, J. T., Giglio, L., Collatz, G. J., Kasibhatla, P. S., and Arellano Jr., A. F. (2006). Interannual variability in global biomass burning emissions from 1997 to 2004. *Atmospheric Chemistry and Physics*, 6, 3423-3441.

Vicente, G. A., Davenport, J. C., and Scofield, R. A. (2002). The role of orographic and parallax corrections on real time high resolution satellite rainfall rate distribution. *International Journal of Remote Sensing*, 23, 221−230.

Vicente, G. A., Scofield, R. A., and Menzel, W. P. (1998). The operational GOES infrared rainfall estimation technique. *Bulletin of the American Meteorological Society*, 79, 1883−1898.

Vila, D., and Lima, A. (2004). Satellite rainfall estimation over South America: The hydroestimator technique. 14th International Conference on Clouds and Precipitation, Bologna, Italy, 8–23 July, 2004.

Vitousek, P. M., Aber, J. D., Howarth, R. W., Likens, G. E., Matson, P. A., Schindler, D. W., Schlesinger, W. H., and Tilman, D. G. (1997). Technical report: Human alteration of the global nitrogen cycle: Sources and consequences. *Ecological Applications*, 7(3), 737-750.

Watson, C. E., Fishman, J., and Reichle, H. G. Jr. (1990). The significance of biomass burning as a source of carbon monoxide and ozone in the southern hemisphere tropics: A satellite analysis. *Journal of Geophysical Research*, 95(D10), 16,443-16,450.

Wolfe, R. E., Nishihama, M., Fleig, A. J., Kuyper, J. A., Roy, D. P., Storey, J. C., *et al*. (2002). Achieving sub-pixel geolocation accuracy in support of MODIS land science. *Remote Sensing of Environment*, 83, 31−49.

Wooster, M. J. (2002). Small-scale experimental testing of fire radiative energy for quantifying mass combusted in natural vegetation fires. *Geophysical Research Letters*, 29(21), doi:10.1029/2002GL015487.

Wooster, M. J., Roberts, G., and Perry, G. L. W. (2005). Retrieval of biomass combustion rates and totals from fire radiative power observations: FRP derivation and calibration relationships between biomass consumption and fire radiative energy release. *Journal of Geophysical Research*, 110(D24311), doi:10.1029/2005JD006318.

Wooster, M. J., Zhukov, B., and Oertel, D. (2003). Fire radiative energy for quantitative study of biomass burning: Derivation from the BIRD experimental satellite and comparison to MODIS fire products. *Remote Sensing of Environment*, 86, 83-107.

Yamaguchi, Y., Kahle, A. B., Tsu, H., Kawakami, T., and Pinel, M. (1998). Overview of advanced spaceborne thermal emission and reflection radiometer (ASTER). *IEEE Transactions on Geoscience and Remote Sensing*, 36, 1062−1071.

Zhang, P., Li, J., Olson, E., Schmidt, T. J., Li, J., and Menzel, W. P.(2006). Impact of point spread function on infrared radiances from geostationary satellites. *IEEE Transactions on Geoscience and Remote Sensing*, 44 (8), 2176-2183.